ELUCIDATING THE ROLE OF METABOLIC CHANGES IN MODULATING CELL FATE FOLLOWING TREATMENT WITH ANTI-MITOTIC DRUGS

ALEX WONG XING FAH

BSc (Hons.), NTU

INSTITUTE FOR HEALTH TECHNOLOGIES

INTERDISCIPLINARY GRADUATE SCHOOL

A thesis submitted to the Nanyang Technological University in partial fulfilment of the requirement for the degree of doctor of philosophy

2019

Statement of Originality

I hereby certify that the work embodied in this thesis is the result of original research and has not been submitted for a higher degree to any other University or Institution.

27/12/18

. . . . . .
Date

. . . . . .
Alex Wong Xing Fah

Supervisor Declaration Statement

I have reviewed the content and presentation style of this thesis and declare it is free of plagiarism and of sufficient grammatical clarity to be examined. To the best of my knowledge, the research and writing are those of the candidate except as acknowledged in the Author Attribution Statement. I confirm that the investigations were conducted in accord with the ethics policies and integrity standards of Nanyang Technological University and that the research data are presented honestly and without prejudice.

28/12/18

. . . . . .
Date

. . . . . .
Karen Crasta

Authorship Attribution Statement

This thesis contains material from 2 papers published in the following peer-reviewed journal(s) where I was the corresponding first author.

Chapter 1 & 2 are published as:
Jakhar, R., Luijten, M. N., **Wong, A. X.***, Cheng, B., Guo, K., Neo, S. P., ... & Karen C. Crasta (2018). Autophagy Governs Protumorigenic Effects of Mitotic Slippage–induced Senescence. *Molecular Cancer Research*, 16(11), 1625-1640.
*Co-first author.

Chapter 3 is published as:
Alex Wong, Sixun Chen, Lay Kien Yang, Yoganathan Kanagasundaram & Karen Crasta (2018). Lipid Accumulation Facilitates Mitotic Slippage-Induced Adaptation to Anti-Mitotic Drug Treatment. *Cell Death Discovery*, 4:109.

My contributions for the paper are as follows:

- Assoc/Prof Karen Crasta provided the initial project direction and edited the manuscript drafts.
- I prepared and edited the manuscript drafts.
- I assisted in designing the study with Assoc/Prof Karen Crasta and performed the laboratory work at Lee Kong Chian School of Medicine. I also analysed the data.
- Sample preparations and executions of the experiments were conducted by me.
- Guo Ke and I performed the experiments for human tumour xenograft model. Initial cytokine profiling experiments were performed by Au Bijin and John E. Connolly. Zebrafish experiments were performed by Indrajit Sinha. Choroid angiogenesis assay was performed by Madhura Kulkarni and Wang Xiaomeng. Lipidomics were performed by Yang Lay Kien and Yoganathan Kanagasundaram.
- Other experiments not included in the thesis were performed by other first or corresponding authors.

27/12/18

. . . . . .

Date

. . . . . .

Alex Wong Xing Fah

ACKNOWLEDGEMENTS

I would like to express my heartfelt gratitude to my supervisor A/Prof. Karen Crasta for her encouragement, guidance and support throughout the whole of my PhD. I appreciate the freedom given to explore in my study. I would also like to offer my sincere gratitude to my mentor, Dr Ruby Huang, who has given me timely advice and invaluable suggestions throughout my PhD. I also thank Dr Cheng Bing for showing me the ropes when I first started out in the lab. I am extremely grateful to Dr Chen Sixun, whose advice, encouragement, guidance and scientific excellence have made this thesis possible.

I thank my dear lab mates, especially He Qianqian, Jeannie Lee, Zhenbagam, Rekha, Monique and Kelvin, who have kept me sane and made this journey an interesting one. I am thankful to Ms Suraini for helping me out with administrative work.

Thank you, NTU Interdisciplinary Graduate School (IGS), for the generous funding through a research scholarship and wonderful student support.

Finally, I would like to express my special appreciation to my mother, father and brother for their unconditional care and love. And special thanks to my wife, Zheng Han Juan, who has been my constant source of love, strength and faith.

TABLE OF CONTENTS

SUMMARY

Anti-mitotic drugs are the most-commonly utilised class of chemotherapeutic agents that are administered as first-line therapy; however, their clinical success has been impeded by chemoresistance and disease relapse. To formulate a treatment that achieves complete remission of the disease, it is critical to gain a complete understanding of the cellular pathways underlying this escape from antimitotic drug-induced cell death, also known as mitotic slippage. Mitotic slippage describes a phenomenon where cells escape antimitotic drug-induced mitotic arrest/death and "slip" into interphase without proper chromosome segregation and cytokinesis. Post-slippage cells do not replicate and are not affected by repeated anti-mitotic drug treatment. They are known to persist and accumulate *in vitro* and *in vivo,* potentially giving rise to chemoresistance. Despite the association between post-slippage cells and their contribution to chemoresistance, the underlying mechanisms of mitotic slippage contributing to anti-mitotic drug resistance remains unclear.

Here, I elucidate cell fate following mitotic slippage and assess one of its major implication - therapy-induced senescence (TIS), a phenomenon that is known to be also initiated by other chemotherapeutic treatments. I employed slippage-prone human osteosarcoma U2OS cells and observed their cell fate upon anti-mitotic drugs treatment. Consistent with other studies, antimitotic-treated U2OS cells undergo mitotic slippage and subsequently entered the state of senescence. I found that post-slippage senescent cells released pro-tumourigenic senescence associated secretory phenotype (SASP) factors that promoted paracrine *in vitro* and *in vivo* cell migration, invasiveness and angiogenesis. These results show the detrimental effects of post-slippage senescent cells and the need to eliminate them. Further analyses revealed that autophagy is involved in the establishment of post-slippage senescence. Blocking autophagy induction by pharmacological and genetic approaches overrode G1 arrest-senescence, reduced SASP-associated paracrine tumorigenic effects, and increased S-phase dependent DNA damage coupled with a concomitant increase in apoptosis. Consistent with this, our *in vivo* mice xenograft model showed the synergistic inhibition of tumour growth upon treatment with the autophagy inhibitor Chloroquine and Paclitaxel.

Another metabolic alteration observed in post-slippage cells is the accumulation of lipids. I found that TOFA, a lipid biosynthesis inhibitor was able to block lipid accumulation, promote early slippage, reduce cellular stress and enhance survival of antimitotic-treated cells. Modulating lipid biosynthesis in post-slippage cells by TOFA, amplified their inflammatory secretion profiles and accelerated the development of paracrine pro-tumorigenic behavior, particularly in cell migration and invasiveness. Contrary to TOFA, inhibition of lipid accumulation by C75, another drug targeting a different lipid biosynthesis pathway, abrogates the production of pro-tumorigenic factors and their associated effects in post-slippage cells. This suggests that discrete lipid biosynthesis pathways contribute differentially to the regulation of pro-tumorigenic inflammation. Unlike autophagy inhibition, blocking lipid biogenesis in post-slippage cells did not abrogate senescence but control the expression and secretion of post-slippage tumourigenic factors.

Lastly, my preliminary results from the final chapter also identified the overexpression of HK2 upon antimitotic treatment that potentially contributes to the glycolytic phenotype post-slippage as well as the induction of autophagy and its downstream effectors. All in all, this study provides insights into alterations in metabolic processes such as autophagy and lipid metabolism during anti-mitotic drugs treatment that plays a role in governing tumourigenic effects incurred post-mitotic slippage. Understanding cell fate post-slippage provides new avenues and insights into the development of novel therapeutic strategies. Our discovery of eliminating of TIS through autophagy inhibition or limiting tumourigenic SASP production through lipid biosynthesis inhibition can potentially lead to treatments that may circumvent antimitotic drug resistance and enhance the treatment efficacy for cancer patients.

LIST OF FIGURES

LIST OF TABLES

LIST OF ABBREVIATIONS

APC/C	Anaphase-promoting complex/cyclosome
ATG	Autophagy-related protein
ATP	Adenosine triphosphate
BafA1	Bafilomycin A1
BODIPY	Boron-dipyrromethane
BUBR1	Mitotic checkpoint serine/threonine-protein kinase BUB1 beta
BSA	Bovine serum albumin
CDC20	Cell-division cycle protein 20
CM	Conditioned media
CQ	Chloroquine
DAPI	4’,6’-diamidino-2-phenylidole
DCFDA	2',7'–dichlorofluorescin diacetate
DMEM	Dulbecco’s Modified Eagle Medium
DMSO	Dimethyl sulfoxide
DNA	Deoxyribonucleic acid
FASN	Fatty acid synthase
FBS	Fetal bovine serum
GFP	Green fluorescent protein
h	Hour(s)
H-H3	Histone H3
HK2	Hexokinase 2
HRP	Horseradish peroxidase
IB	Immunoblotting

IL-1β	Interleukin 1β
IL-6	Interleukin 6
IL-8	Interleukin 8
IκBα	Nuclear factor of kappa light chain polypeptide gene enhancer in B-cells inhibitor, alpha
kDa	Kilo Dalton
LC3	Microtubule-associated proteins 1A/1B light chain 3B
LD	Lipid droplet(s)
NF-κB	Nuclear factor kappa-light-chain-enhancer of activated B cells
Noc	Nocodazole
Mon	Monastrol
MAD1/2	Mitotic arrest deficient 1/2
min	Minute(s)
mRNA	Messenger Ribonucleic acid
M	Mitosis
MS	Mass spectrometry
mTOR	Mammalian target of rapamycin
MW	Molecular weight
PBS	Phosphate buffer saline
PFA	Paraformaldehyde
PS	Post-slippage
ROS	Reactive oxygen species
RT	Room temperature
s	Second(s)

SA-β-gal	Senescence-associated β-galactosidase
SAC	Spindle assembly checkpoint
SASP	Senescence associated secretory phenotype
SDS-PAGE	Sodium dodecyl sulphate-polyacrylamide gel electrophoresis
s.d.	Standard deviation
siRNA	Small interfering Ribonucleic acid
TIS	Therapy-induced senescence
TMRE	Tetramethylrhodamine, Ethyl Ester, Perchlorate
ZM	Aurora kinase inhibitor (ZM 447439)
5-FU	5-Fluorouracil
2-DG	2-Deoxy-D-glucose
3-MA	3-Methyladenine

LIST OF PUBLICATIONS

1) Jakhar, R.*, Luijten, M. N.*, **Wong, A. X.***, Cheng, B., Guo, K., Neo, S. P., ... & Chong, H. C. (2018). Autophagy Governs Protumorigenic Effects of Mitotic Slippage–induced Senescence. *Molecular Cancer Research*, 16(11), 1625-1640. *Co-first author.
2) Shyu, P.*, **Wong, X. F. A.***, Crasta, K.#, & Thibault, G.# (2018). Dropping in on lipid droplets: insights into cellular stress and cancer. *Bioscience reports*, BSR20180764. *Co-first author. # co-corresponding author.
3) **Alex Wong**, Sixun Chen, Lay Kien Yang, Yoganathan Kanagasundaram & Karen Crasta (2018). Lipid Accumulation Facilitates Mitotic Slippage-Induced Adaptation to Anti-Mitotic Drug Treatment. *Cell Death Discovery*, 4:109.

1. INTRODUCTION

1.1 Background and scope

1.1.1 Cell fate response to antimitotic drug treatment

Antimitotic drugs, such as Taxol and Nocodazole, are used as first-line treatments for cancer [1]. The use of antimitotic drugs in the clinic aims to kill replicating cancer cells by inhibiting their ability to undergo regular mitosis and continue proliferating in the body. Cells undergoing mitosis require proper segregation of chromosomes via microtubule dynamics and successful cytokinesis to produce two daughter cells that contain identical copies of the parental genome. At the molecular level, antimitotic agents specifically target the microtubule dynamics by disrupting its polymerisation or depolymerisation. As such, these drugs affect the cells' ability to properly segregate their chromosomes, leading to improper mitotic spindle formation, chromosome misalignment and missegregation and constitutive activation of the spindle assembly checkpoint (SAC), a surveillance mechanism that monitors proper mitotic progression from metaphase to anaphase transition. The SAC stops the progression of the cell cycle by negatively regulating CDC20 (an activator of anaphase promoting complex), and thereby preventing ubiquitination-related activities of the anaphase promoting complex (APC) [2]. The core components responsible for the SAC signal compose the mitotic checkpoint complex (MCC), which includes MAD1/2 (mitotic arrest deficient), BUBR1 (mitotic checkpoint serine/threonine-protein kinase BUB1 beta) and CDC20. Inhibition of APC/C activities prevents ubiquitination and degradation of securin and cyclin B1. Degradation of securin liberates separase which in turn cleaves the cohesin ring structure allowing sister chromatids to separate (transition to anaphase), whereas degradation of cyclin B1 inactivates Cdk1, leading to mitotic exit [3]. Perturbing these two processes of mitotic progression leads to the arrest of cells at a pro-metaphase arrest. These prolonged mitotically-arrested cells subsequently undergo two possible cell fates; either mitotic death or mitotic exit to G1 phase without cell division also known as mitotic slippage.

1.1.2 **Characteristics of mitotic slippage**

Mitotic slippage cells (hence forth referred to as post-slippage cells) are able to overcome the inherent effect of antimitotic drugs and thus survive [4, 5]. The main phenotypical characteristics of cells that have gone through mitotic slippage is (1) multinucleation that arise from the improper segregation of chromosome and (2) tetraploidisation that arise from failure of cytokinesis. *In vivo* studies have confirmed the persistence and accumulation of multinucleated slippage cells upon antimitotic drugs treatment of tumour xenografts in mice [4, 6]. It was proposed that the occurrence of mitotic slippage resembles a potential source of chemoresistance. This is evident by studies showing the correlation between increased incidence of mitotic slippage and drug resistance. For instance, increased mitotic slippage is shown to reduce sensitivity to paclitaxel-induced cell death [7]. In addition, depletion of $p31^{comet}$, a Mad2-binding protein in cancer cells delays the onset of mitotic slippage and promotes cell death following antimitotic drug treatment [8]. Paclitaxel-resistant ovarian cancer cell line was found to possess a weakened SAC with reduced BubR1 expression [9]. Another study revealed that the inhibition of mitotic slippage by depletion of cell cycle regulator Cdc6 was sufficient to reverse paclitaxel resistance and reduce cell viability [10]. Therefore, the need to eliminate the post-slippage cells becomes apparent.

Although the mechanism of mitotic slippage has yet to be fully elucidated, one appealing model by Gascoigne et al. demonstrated that the decision to undergo mitotic cell death or to exit mitosis and proceed to interphase (mitotic slippage) is dictated by two competing networks; one that involves the activation of cell death pathways and the other that protects cyclin B1 from degradation [5]. During protracted mitotic arrest that leads to mitotic death, cell death signals become more robust while cyclin B1 levels fall. Both networks have designated thresholds that dictated the cell fate by whichever the threshold is breached first. Thus, if cyclin B1 levels fall below the mitotic-exit threshold first, cells exit mitosis and slippage occurs. Likewise, if the death threshold is breached first, then the cells undergo mitotic cell death. Cyclin B1 degradation could thereby be an effective indicator of mitotic slippage. Following mitotic slippage, some cells appear to die at interphase, where others

may proceed to re-replicate their genome or the tetraploid multinucleated cells at G1 will enter senescence (Figure 1).

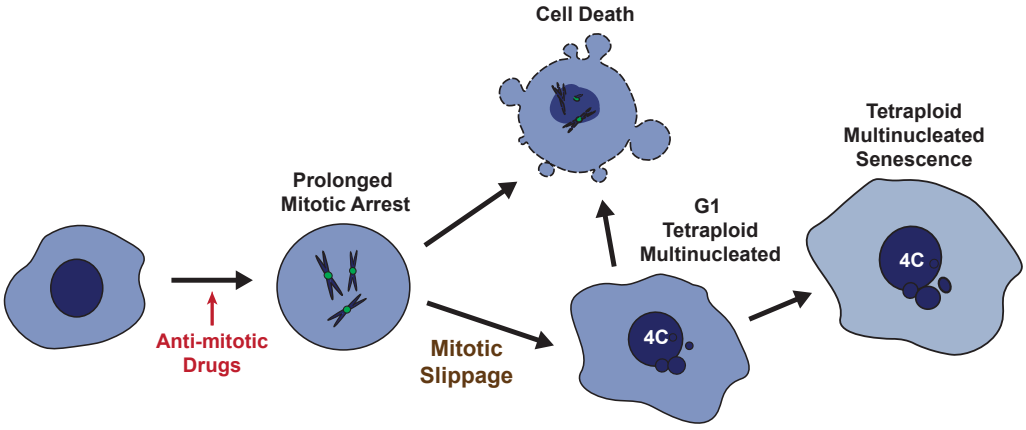

Figure 1. Cell fate upon antimitotic drugs treatment.

Upon treatment with antimitotic drugs, cells will undergo a duration of mitotic arrest and subsequently die during mitosis or undergo mitotic slippage. Post-slippage multinucleated cells can also undergo cell death, or persist and transit into senescence.

1.1.3 Therapy-induced senescence

Cellular senescence is a state of terminal growth arrest inducible by different forms of cellular stress and stimuli such as extensive DNA or oxidative damages [11]. Senescent cells are highly metabolically active and have distinctive characteristics which includes an enlarged, flatten morphology and the increased in senescence-associated β-galactosidase (SA-β-gal) activity [12]. They also encompassed changes in several cellular contents such as the accumulation of dysfunctional mitochondria and the increased in lysosomal content [13]. On the molecular level, senescence is associated with the loss of lamin B1 [14], decreased expression of hypophosphorylated RB (retinoblastoma protein) [15-17] as well as the increased expression of cyclin-dependent kinase inhibitor p21 [18, 19] and tumour suppressor p53 [20, 21]. All these molecular effectors are interconnected and converged towards the establishment of irreversible cell cycle arrest and subsequent senescence. Another distinct hallmark of senescent cells is the acquisition of senescence-associated secretory phenotype (SASP) whereby senescent cells trigger non-autonomous effects through the secretion of cytokines, chemokines and other

soluble factors [13]. Depending on biological events, accumulation of cellular senescence could be beneficial by contributing to wound healing, host immunity and tumour suppression; or detrimental from its implication in diseases particularly aging-related pathology and cancer [22].

Many anticancer therapies have been known to induce cellular senescence commonly term as therapy-induced senescence (TIS) [23-25]. The transformation of cancer cells to terminally growth arrest cells *in vitro* and *in vivo* by TIS have led to several beneficial effects on the management and treatment of cancer. Firstly, cellular senescence is considered a tumour-suppressive mechanism since it impedes cell proliferation which indirectly prevents cancer progression [26]. Also, senescent cells can secrete various factors or exhibit SASP that render dysfunction of neighbouring cancer cells [27]. SASP components can promote the immune surveillance of senescent cells resulting in their eliminated by the host immune system [28]. Lastly, SASP is found to provoke paracrine senescence to surrounding normal cells and tissues that could potentiate the activation of immune surveillance [29]. Paradoxically, TIS cells are also known to acquire tumor-promoting effects. TIS cells could escape from terminal growth arrest and reenter into the cell cycle [30, 31]. Furthermore, the SASP components could trigger the proliferation of neighbouring cancerous and noncancerous cells, making their accumulation undesirable [32-35]. SASP components have also been shown to engender tumor-promoting effects such as cellular motility (invasion, migration and metastasis), epithelial-mesenchymal transition (EMT), angiogenesis as well as inflammation in neighbouring cells [33, 36]. It had been shown that interleukin 8 (IL-8), interleukin 6 (IL-6) and Interleukin 1 (IL-1) are some of the crucial SASP factors that promote tumourigenesis in premalignant cells [32]. In a systemic level, TIS cells could also contribute to the adverse effects of chemotherapies such as fatigue, bone marrow suppression and cardiac dysfunction, potentially undermining the survival rate of cancer patients [37].

The above suggest that TIS or its associated SASP represents a double-edged sword in cancer therapeutics (Figure 2). In the context of antimitotic therapies, the molecular mechanisms underlying senescence following mitotic slippage and their consequential cell fate significance have not been well-

explored. Thus, it is imperative to examine the senescent cell fate following antimitotic-induced mitotic slippage.

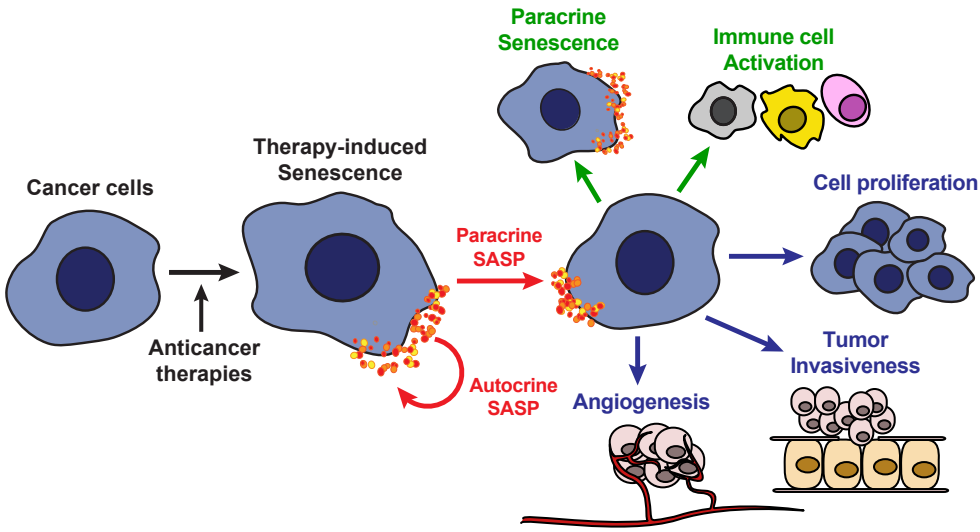

Figure 2. Effects of SASP triggered by therapy-induced senescent (TIS) cells.
Upon anticancer therapies, cancer cells can undergo cell cycle arrest and become senescent. TIS cells acquired SASP that can exert pro-tumourigenic (blue arrow) and/or anti-tumourigenic (green arrow) effects. SASP can promote the reinforcement of senescence in cancer cells or surrounding cells through an autocrine and a paracrine fashion. SASP can also active the immune response and promote the clearance of cancer cells. In respect to the pro-tumourigenic effects, SASP is known to promote cell proliferation, angiogenesis, and tumour migration and invasiveness.

1.1.4 **Autophagy induction upon anticancer therapies**

Autophagy is a highly regulated catabolic process that involves the bulk degradation of intracellular proteins and organelles into macromolecular precursors that are recycled or used for metabolic pathways [38, 39]. The process of autophagy (Figure 3) is regulated by a series of signaling events that occurs at basal level during physiological condition and is inducible by diverse signal and cellular stresses. When cells are exposed to starvation or stressful conditions, class I PI3K or other stimulus triggers the release of mTOR inhibition of Unc-51-like kinase (ULK1) complex, which subsequently induces the activation of class III phosphatidylinositol-3 kinase (PI3K) complex that initiates vesicle nucleation [40]. A group of ATG complexes (ATG5-ATG12) expands the autophagosome membrane whereas the family of microtubule-associated protein 1 (MAB) light chain 3B (LC3) and GABARAP proteins conjugate to lipid phosphatidylethanolamine (PE) and recruit to the membrane [40]. The lipidated form of LC3 (also known as LC3II) is commonly used as a marker of autophagosome [41, 42]. Eventually, the cargo-encapsulated autophagosome fuses with the acidic lysosome where the autophagosome contents are degraded into macromolecular precursors that are recycled or used for metabolic and biosynthetic pathways. The autophagic adaptor protein p62/ sequestosome 1 which specifically target substrates to autophagosomes, and LC3II are degraded with cargo proteins and can be used as an indicator of autophagic flux [43].

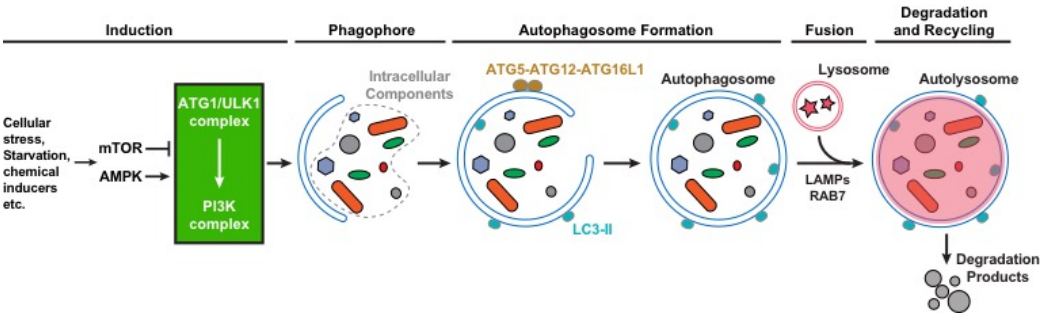

Figure 3. The autophagy process.

On stimulation of autophagy, a series of signaling pathways initiate the synthesis and elongation of phagophores which engulfs intracellular components such as organelles and macromolecules. The membrane completes the encapsulation of cargo materials and matures into a closed doubled-membrane autophagsomes. The outer autophagosomal membrane fuses with a lysosome to form autolysosomes where the autophagic cargo is degraded by lysosomal hydrolases and recycled back into the cytoplasm. Key proteins involved in autophagy are: ATG, autophagy-related proteins; PI3K, phosphatidylinositol-3 kinase; LC3, microtubules-associated protein 1 light chain 3; LAMPs, lysosomal-associated membrane; ULK1, Unc-51-like kinase.

Many anticancer drugs such as doxorubicin, paclitaxel and Imatinib have been shown to induce cellular autophagy in cancer cells [44-46]. Autophagy activation was found to reduce the sensitivity of hepatocellular carcinoma (HCC) to doxorubicin treatment [47]. Ovarian cancer stem cells (CSC) require the activation of autophagy to survive carboplatin treatment [48]. In both studies, inhibition of autophagy in the cancer cells by chloroquine treatment restored their sensitivity to chemotherapies, suggesting that autophagy functions as an adaptive response to cancer treatment. Indeed, high levels of autophagic activity found specifically in a subpopulation of cells that escaped from chemotherapeutic treatment and persisted supports the notion that autophagy underlies the chemoresistance of these cells [49]. Several mechanisms on how autophagy contributes to chemoresistance or tumour reoccurrence had been uncovered. Therapy-induced autophagy has been proposed to confer cell survival through various means such as alleviating cellular stress, reprogramming of cell metabolism or dictating alternative cell fate such as senescence [49-52]. For instance, the work by Hu *et al*. demonstrated that devascularisation induced by antiangiogenic therapy

promotes a hypoxic environment, which in turn activates an adaptive autophagic response to promote tumour cell survival [50].

Apart from the protective mechanism of autophagy, anticancer drugs such as 5-Fluorouracil (5-FU) or Imatinib could trigger autophagy-mediated cell death in certain settings [46, 53]. Autophagic cell death is a caspase-independent form of programmed cell death that is characterised by the large-scale accumulation of autophagosomes [54]. It had been shown that 5-FU treatment induces autophagic cell death in PUMA or Bax-deficient human colon cancer cells but not in wild type (WT) cells [53]. Inhibition of autophagy by 3-Methyladenine (3-MA) reduces the cell death in apoptotic deficient cancer cells. Furthermore, some anticancer drugs such as sorafenib and monofunctional platinum (II) complex could also induce autophagic cell death in human cancer cells [55, 56]. As such, autophagic cell death induced by chemotherapies could functions as an alternative cell death machinery for cancer cells that are resistance to cell death or have apoptotic defects [57]. In this context, the activation of autophagy by chemotherapies or autophagy agonists could trigger autophagic cell death that contributes to the efficacy of anticancer drugs.

Autophagy is also known to be closely associated with senescence [58, 59]. Autophagy is found to be activated upon senescence induction and is essential to facilitate senescence transition [60, 61]. It has been revealed that the inhibition of autophagy via pharmacological and genetic means reduced or delayed senescence response triggered by oncogenic stress or irradiation [62-64]. The process of autophagy is postulated to provide recycled building blocks to support energy homeostasis and cellular biosynthesis (i.e. synthesis and secretion of SASP factors) for the maintenance and establishment of highly metabolically active senescence state [62]. Indeed, it has been shown that therapy-induced senescent lymphomas expressing high level of SASP factors are sensitive to autophagy inhibition [64].

Taken together, autophagy induction upon anticancer therapies resembles a double-edge sword with pro-survival or pro-death potential. Depending on the context, especially the type of cancers and the drugs used, anticancer drugs could induce different effects of autophagy that potentially

enhance their anti-tumour properties or contribute to therapeutic resistance. Understanding the functions of autophagy under specific chemotherapeutic treatment allows the development of a therapeutic strategy (i.e. by inhibiting or activating autophagy) to circumvent resistance and enhance the efficacy of the treatment for cancer patients.

1.1.5 **Lipid accumulation upon anticancer therapies**

Cancer cells frequently exhibit specific changes in their lipid metabolism. The diverse roles of lipids in membrane structure, cellular signaling and protein regulation strongly suggest that lipids are essential components of the cellular machinery that can regulate proliferation, migration and survival of cancer cells [65]. Gene expression profiling of various tumors has shown the upregulation of genes such as Acetyl-CoA carboxylase (ACC), ATP citrate lysate (ACLY) and fatty acid synthase (FASN) that are involved in lipogenesis and cholesterol synthesis pathways [66-68]. As such, excessive lipids and cholesterols in cancer cells are converted and stored as cytoplasmic lipid droplets (LD). In agreement, increased number of LD have been reported in many cancer cells [69, 70]. Furthermore, a positive correlation of lipid droplet accumulation and cell proliferation has been recently established in colon cancer cells, suggesting an involvement of lipid droplets in cell proliferation with potential implications to the pathogenesis of colon adenocarcinoma [71]. Analogous to the role of lipid synthesis in promoting cancer, the presence of reserve LD could function either as primary or an alternative source of energy (ATP produced via fatty acid ß-oxidation) or as part of the structural component of biological membrane (for example, phosphatidylcholine (PC), phosphatidylethanolamine (PE), phosphatidylglycerol (PG) and phosphatidylserine (PS)) for cancer cell proliferation.

Apart from mediating cancer cell development and proliferation, accumulation of lipid or LD has been widely reported to correlate with chemotherapeutic treatments. For example, lipid accumulation has been shown to be a consequence of metabolic changes during etoposide-induced apoptosis,

where the inhibition of FA β-oxidation in defective mitochondria, re-directs FFAs toward lipid storage [72]. Indeed, inhibition of β-oxidation or oxidative phosphorylation is sufficient to drive lipid droplet formation in cancer cells. Treatment of N-Myc proto-oncogene protein-amplified neuroblastoma cells with 10058-F4, an inhibitor of c-Myc/Max protein, a member of the basic helix-loop-helix leucine zipper family of transcription factors, triggers the accumulation of intracellular LD as an outcome of mitochondrial dysfunction [73]. The chemotherapeutic drugs doxorubicin and 5-fluorouracil (5-FU) in human colon carcinoma cells induce the accumulation of LD as a result of upregulated TG biosynthesis [74, 75]. Hence, this points to a potential role for LD as part of a general stress response to different classes of chemotherapeutic treatments. Increased LD formation during chemotherapy may also be a consequence of non-apoptotic cell death (NCD) as ferroptosis-induced NCD perturbed FA metabolism [76, 77]. Lipid biosynthesis stimulated the accumulation of FA and initiated NCD in fibrosarcoma HT1080 cell lines [78]. Suppression of either LD or lipid accumulation by the lipid biosynthetic inhibitor, 5-(tetradecyloxy)-2-furoic acid (TOFA), reduced lipid dysregulation-associated cell death [79]. All above point out to lipid accumulation as a generic stress response, a marker of apoptotic induction or a contributor to cell death upon chemotherapeutic treatment.

Apart from assisting cell death, lipid is also known to accumulate in cancer cells surviving chemotherapeutic treatments. Conventional anticancer treatments in tumour cells may induce a stable cell cycle arrest, a cytostatic phenotype known as “therapy-induced senescence” (TIS) as described above. Irreparable DNA damage, chemotherapeutics or ionizing radiation could potentially contribute to the induction of TIS. TIS cells from etoposide treatment were found to contain LD that are numerous and larger in size than their proliferating counterparts [80, 81]. The accumulation of LD in TIS from enhanced lipid import was found to contribute to the onset and maintenance of senescence. Excess lipids that could not be stored in overloaded LD may promote the generation of lipotoxic diacylglycerol and ceramides that potentially trigger stress-induced cellular senescence [80]. This is further supported by the notion that triglyceride or ceramide alone is sufficient to

induce senescence in cancer cells. Other than TIS cells, residual breast cancer cells surviving oncogene-inactivation were found to harbor increased lipid accumulation that were used as an energy source from β-oxidation [82]. Similar phenomena have also been established in oncogene ablation-resistant pancreatic cancer cells [83]. Therefore, therapy-induced lipid accumulation could promote survival of cells through supplying energy demand and promoting apoptosis-resistant senescence.

Taken together, therapy-induced lipid accumulation not only contributes to cell death phenotype but could also play a pro-survival role following drug treatment. Although it is indisputable that cellular lipid accumulation can be induced by certain chemotherapeutics treatment, limited studies had been performed to define the mechanisms and functions of such accumulation. Understanding the functions of LD or lipid accumulation under specific chemotherapeutic treatment allows the development of a therapeutic strategy (i.e. by inhibiting lipid biosynthesis) to circumvent resistance and enhance the efficacy of the treatment for cancer patients.

1.1.6 **Metabolic reprogramming upon anticancer therapies**

One of the stipulated hallmarks of cancer which was originally described by Otto Warburg is the "Warburg effect"; where most cancer cells reprogram energy metabolism by favouring the utilisation of glycolysis instead of oxidative phosphorylation for bioenergetics demands despite the availability of oxygen [84]. This unique metabolic switch adopted by cancer cells was later revealed to be essential to both provide high rate of ATP production and glycolytic intermediates (e.g. nucleosides and amino acids) for biosynthesis of proliferating cancer cells [85, 86]. Although glycolysis only produced 2 ATP per glucose consumed as compared to 36 ATP produced by mitochondrial oxidative phosphorylation, the low ATP produced by glycolysis can be compensated by the increase in glucose uptake by cancer cells [87]. As such, tumours are shown to upregulate the expression of numerous glycolytic-related enzymes such as glucose transporter 1 (Glut1), hexokinase 2 (HK2), lactate dehydrogenase A (LDHA), phosphofructokinase 1 (PFK1) and others [88, 89].

Interestingly, metabolic reprogramming is not only a consequence of malignant transformation but also observed in response to chemotherapy; particularly in chemoresistant cells. It has been recently reported that cisplatin treatment promotes glycolysis through inducing the accumulation of cytoplasmic 6-phosphofructo-2-kinase/fructose-2,6-biphosphatase 3 (PFKPB3), subsequently preventing DNA damage and apoptosis [90]. Elevated glycolysis is also observed in glioblastoma cells treated with radiotherapy [91]. Dichloroacetate, a glycolytic inhibitor sensitizes glioblastoma cells to radiotherapy by inducing a glycolytic shift towards oxidative phosphorylation. Furthermore, it has been revealed that glycolysis is essential for the chemoresistance of colorectal cancer [92]. 5-fluorouracil (5-FU) resistant colorectal cancer cells were sensitive to glycolytic inhibitors such as 3-bromopyruvate (3-BP) and 2-Deoxy-D-glucose (2DG). The production of ATP derived from glycolysis could be crucial for chemoresistant cancer cells to cope with chemotherapeutic stress and bioenergetics demand, which includes maintaining the function of ATP-dependent efflux transporter P-glycoprotein 1 (P-gp), repairing and replicating of DNA/RNA, increasing the expression of anti-apoptotic genes, and activating of intracellular survival signaling [93-96].

These studies suggest that metabolic alteration upon chemotherapeutic treatment is context-dependent and that such alteration may provide a survival advantage for chemoresistant cells.

In the context of antimitotic drug treatment, the transition of cancer cells from its highly proliferative to predominantly senescent state is perceived to be metabolic dynamic and bioenergetically demanding. Firstly, the prolonged mitotic arrest from the activation of SAC requires continuous transcription of mitotic regulators. The prolonged mitotic arrest was very recently found to be dependent on glycolysis instead of mitochondrial oxidative phosphorylation (OXPHOS) for survival [97]. Secondly, the 'exit from mitotic arrest to slippage' phenotype by disassembly of the mitotic checkpoint complex (MCC) is ATP-dependent [98]. Lastly, therapy-induced senescent cells remain metabolically active despite the lack of growth and proliferation [99]. Therefore, similar to the above mentioned chemotherapy-induced resistant cells, it is highly plausible that antimitotic-induced post-slippage cells display alteration in their metabolic pathway to mediate cellular survival.

1.2 Research Objectives

This study was initiated with the notion that post-slippage cells are a subpopulation of cells that escape mitotic cell death and survive antimitotic drugs treatment. Despite the putative association of post-slippage cells and chemoresistance, limited studies have focused on elucidating mitotic slippage and the subsequent cell fates following slippage. Chapter 1 of this thesis aims to investigate cell fates and their impact on the tumor microenvironment following antimitotic drugs-induced mitotic slippage, particularly on post-slippage senescence. It is hypothesised that post-slippage senescent cells possess pro-tumourigenic potential that contributes to chemoresistance or tumour recurrence.

Chapter 2 and Chapter 3 of this thesis aim to elucidate the molecular mechanism(s) underlying post-slippage cell fate; specifically, on autophagy and lipid metabolism. The second chapter describes experiments undertaken to determine the activation of autophagic pathway in post-slippage cells and the role of the pathway in modulating mitotic slippage-induced senescence. The third chapter describes the findings on lipid accumulation upon antimitotic drug treatment and the role of lipid metabolism in mediating cell fate post-slippage.

Lastly, the fourth and final chapter will briefly describe my efforts in delineating the effects on other metabolic alterations (e.g. glycolysis) induced by cancer cells in response to antimitotic drugs treatment and determining if the identified metabolic pathways mediates cell fate response to antimitotic drugs treatment.

1.3 Rationale and Significance of Study

The characterisation of mitotic slippage and subsequent cell fates in this study provides an insight into pathways and molecular mechanisms underlying the escape from cell death that may be responsible for antimitotic drug resistance in patients. Understanding the mechanisms involved in dictating cell fate post-antimitotic drug treatment, such as dependence on autophagy and lipid metabolism found in this study, opens up opportunities for the development of novel therapeutic strategies circumventing antimitotic drug resistance and enhancing treatment efficacy for cancer patients.

2. MATERIALS AND METHODS

2.1 Cell Cultures and Reagents

Human osteosarcoma U2OS, colorectal carcinoma HCT116, breast adenocarcinoma MCF-7 and MDA-MB-231 cancer cell lines were purchased from American Type Culture Collection (ATCC). Cells were maintained in Dulbecco's Modified Eagle's Medium (DMEM) (Gibco) supplemented with 10% Fetal Bovine Serum (Hyclone GE) and 100 units/mL penicillin (Gibco) at 37^{o}C in a humidified atmosphere of 5% CO2. Chemicals and the concentration used are listed in Appendix Table 1.

2.2 Generation of stable cell lines

The stable cell lines were generated through the courtesy of fellow Lab members. To establish stable expression of GFP-H2B and GFP-LC3, U2OS cells were infected with viral particles produced from HEK293T cells transfected with pBabe-puro-H2B-GFP (#26790), pBabe-puro-Omi-mCherry (#48685) or pBabe-puro-LC3 (#22405) (Addgene) along with retroviral packaging plasmids. To generate stable knockdown of autophagy-related genes (ATG5), U2OS cells were infected with viral particles produced from HEK293T cells transfected with targeting plasmids along with lentiviral packaging plasmids. Two days after infection, cells were selected with puromycin (1 μg/mL) for two weeks. The shRNA plasmids used in this study were as follows: shATG5-pLKO.1-puro was cloned using the following target sequence (sense): 5'-GACAAGAAGACATTAGTGA-3'. PLKO.1-puro (#19119) and pLKO.1-empty vector (control shRNA) (#10878) were purchased from Addgene.

2.3 Cell Cycle Synchronization

Cells were serum starved for 24 h to synchronize cells in G0/G1 phase, followed by 24 h of 3 mM thymidine treatment to synchronize cells in S phase. Cells were then released in drug-free media for 3 h to enter G2 phase before commencing the respective drug treatments.

2.4 BODIPY 493/503 Staining

BODIPY 493/503 (D3922) (Thermoscientific) was purchased from Life Technologies. Live cells were trypsinised and washed twice in PBS before incubating in 2 μg/mL BODIPY (in PBS) for 15 min at 37°C. After staining, cells were washed twice in PBS and analysed on an Accuri C6 flow cytometer (BD Biosciences) under FL-1 channel. Data analysis was performed using FlowJo software.

2.5 Cell Viability Assay

For relative cell viability analyses, 7,500 cells were seeded in a 96-well plate and treated for the respective duration. Cell viability was assessed using CellTiter96® One Solution Proliferation Assays kit (G3580) (Promega) according to manufacturer's instructions. For absolute cell viability analysis, cells were seeded in 10 cm dish and treated for the respective duration. Cells were then trypsinised, stained with 0.4% trypan blue solution and counted using an automated cell counter (Luna™). The number of viable cells = Total number of cells – Number of blue cells.

2.6 Clonogenic Survival Assay

U2OS cells were plated at 7,500 cells per well in 6-wells plates. Cells were synchronised before the addition of respective drugs for the desired duration. The medium was then removed, the wells were washed twice with PBS and fresh medium was added. Plates were incubated for 5-10 days until macroscopic colonies formed. For quantification of colonies, the wells were washed twice with ice-cold PBS and fixed for 10 min with 4% paraformaldehyde (PFA). Colonies were stained with a 0.4 % crystal violet/20 % methanol solution for 10 min. The crystal violet solution was removed, the wells were washed with water to remove excess dye, and dried at room temperature overnight. Colonies were quantified by solubilisation in 1 mL of 100% methanol followed by spectrophotometric analysis at 570nm. The survival of treated cells was normalized relative to non-treated cells and statistical significance was determined by two-tailed Student's *t*-tests.

2.7 Cellular ROS Measurement

Treated cells were trypsinised and washed twice in PBS before being incubated in 20 μM of 2',7'–dichlorofluorescin diacetate (DCFDA) (ab113851) (Abcam) working solution for 25 min at 37°C. After staining, cells were washed in PBS and analysed on an Accuri C6 flow cytometer (BD Biosciences) under FL-1 channel. Data analysis was performed using FlowJo software. Fluorescence intensities were normalised against untreated cells.

2.8 Extracellular Lactate Measurement

1.2 x 10^6 U2OS cells were grown in 10 cm dishes and treated with nocodazole and Taxol for 48 h. After treatment, cells were washed with PBS to remove dead cells or debris and 7 mL of fresh culture media were added. After 12 h incubation, respective cell culture media were collected and deproteinised using 10K Nanosep® Centrifugal Devices (Pall Corporation). Lactate from deproteinised samples was measured using Lactate Assay kit (MAK064) (Sigma) as per manufacturer's instructions. Cell counts were performed for normalisation. Lactate concentration is determined by measuring the absorbance at 570 nm using BioTek Cytation^{TM} 3 microplate plate reader.

2.9 Human Cytokine and Chemokine Array

150 μL of conditioned media (CM) were collected per condition for the assay. 64 cytokine/chemokine/growth factor biomarkers were quantified simultaneously by using a Discovery Assay® called the Human High Sensitivity T-Cell Discovery Array 64-Plex (Eve Technologies Corp, Calgary, AB, Canada). The multiplex assay was performed by Eve Technologies using the Bio-Plex™ 200 system (Bio-Rad Laboratories, Inc., Hercules, CA, USA), and a Milliplex Human High Sensitivity T-Cell panel (Millipore, St. Charles, MO, USA) according to their protocol. The assay sensitivities of these markers range from 0.11 – 3.25 pg/mL. The concentration of individual cytokines was determined based on the standard curve plotted from the determined concentration of a set standards and median fluorescent Intensity value. The cytokine profiling in Chapter 2 was carried out by Dr. John Connolly's lab, Agency for Science, Technology and Research (A*STAR), Institute of Molecular and Cell Biology (IMCB).

2.10 **Human Tumour Xenografts**

All animal studies were approved by the Institutional Animal Care and Use Committee (IACUC No. 151103) of the Biological Resource Centre and were carried out under the policies from the Animal Facility Centre of the Agency 1 for Science, Technology and Research (A*STAR), Singapore. 2 x 10^6 HCT116 colon cancer cells were mixed with 20% BD Matrigel and 200 - 300 μL of mixtures were injected subcutaneously into both dorsal flanks of female BALB/c athymic nude mice (nu/nu) (InVivos) (n = 5 mice in each treatment group). 10 days later, when tumour volume reached around 300 mm^3, mice were injected intraperitoneally with respective treatment every three days for two weeks (vehicle control - 10% DMSO, 12.5% Cremophor, 12.5% ethanol, and 65% saline based diluent; Noc - 10 mpk; Taxol - 10 mpk; chloroquine, CQ - 30 mpk; Noc + CQ - 10 mpk:30 mpk; Taxol + CQ - 10 mpk:30 mpk). Tumour volume was measured every three days from start of treatment by using the formula: (Length x $Width^2$)/2. Mice were sacrificed at the end of the treatment schedule and all tumours (n = 10 tumours per treatment group) were harvested for weight measurement, immunohistochemistry and immunofluorescence. Tumour tissue was fixed in 10 % buffered neutral formalin solution for histological studies. After fixation, tissues were embedded in paraffin wax and solid sections were cut at 4 μm. The sections were deparaffinised in xylene, hydrated using graded series of alcohol and blocked using 3% BSA in PBS for 1 h at room temperature and then stained according to immunofluorescence protocol described above.

2.11 **Intracellular ATP Measurement**

U2OS cells were treated with nocodazole and Taxol for 48 h. After treatment, cells were counted and plated at 10,000 cells per well in white opaque, clear flat bottom 96-wells plates (Perkin Elmer). Intracellular ATP levels were measured using Luminescent ATP Detection Assay kit (ab113849) (Abcam) as per manufacturer's instructions. Measured ATP levels were normalised against the control (untreated samples).

2.12 **Mitochondria Staining**

Tetramethylrhodamine, Ethyl Ester, Perchlorate (TMRE) (T669) and MitoSox Red Mitochondrial superoxide indicator (M36008) were purchased from Life Technologies (Thermoscientific). For TMRE staining, live cells were trypnised and washed twice in PBS before incubating in 200 nM TMRE working solution (in PBS) for 20 min at 37°C. After staining, cells were immediately analysed on an Accuri C6 flow cytometer (BD Biosciences) under FL-2 channel. Data analysis was performed using FlowJo software. For MitoSox staining, live cells were trypnised and washed twice in PBS before counting. 1 $x10^5$ cells per condition were incubated with 5 μM MitoSox reagent working solution (in PBS) for 10 min at 37°C. After staining, cells were washed in PBS and plated in a 96-well microplate for analysis using BioTek Cytation™ 3 microplate plate reader (Ex: 549nm, EM: 575nm). Fluorescence intensities were normalised against control non-treated cells.

2.13 **Microarray and Data Analysis**

Synchronised U2OS cells were treated with DMSO or Noc for 48 h, followed by total RNA extraction using RNeasy plus Mini Kit (QIAGEN) according to manufacturer's instructions. RNA yield quantity and quality were assessed using NanoDrop Spectrophotometer (NanoDrop Products, ThermoFisher Scientific, Inc., Wilmington, DE, USA) and Agilent Bioanalyzer with Agilent 6000 Nano RNA kit (Agilent Technology, Santa Clara, CA, USA). Samples were considered acceptable for testing when 28S and 18S rRNA bands resolved into two discrete bands that had no significant smearing below each band with RIN value more than 8.0. Double stranded cDNA was generated from the RNA sample using the GeneChip® WT PLUS Reagent Kit according to the manufacturer protocol. Fragmentation and end-terminus labeling of cDNAs were done using the same kit according to the manufacturer protocol. The quality and concentration of cDNAs were measured using NanoDrop Spectrophotometer and only 5.5 μg of cDNA will be used for microarray analysis. The samples were then hybridized to GeneChip® Human Transcriptome Array 2.0 at 45°C for 16 h overnight, following manufacturer procedures. GeneChips post-processed were done on the AFX Fluidics 450 Station, according to all AFX protocols and procedures defined for the Human

Transcriptome Array 2.0 (FS450_0001), as outlined in the kit manual. GeneChips were scanned on the GC3000 G7 Scanner. Data were extracted and processed using Partek® Genomics Suite™ (Partek Incorporated, St. Louis, MO, USA). For microarray data analysis, raw microarray. cel files were imported into Partek Genomic Suite (v7.0) (Partek Inc., St. Louis, MO) with the core meta-probe set. The configuration consisted of a pre-background adjustment for GC content and probe sequence, Robust Multiarray Analysis (RMA) for background correction, quantile normalization and probe set summarization using median computation from the raw data of each file. All signals were log2 transformed. Library files were specified by Affymetrix (Human Gene 2.0 AGCC library file) and the annotation file version was HTA-2_0.na36.hg19.transcript.csv. For determination of differential expression, probe set information is summarized into gene level information. The ANOVA was performed for all samples with contrasts set to type of drug treatment. Genes differentially expressed by >2.5 and <-2.5 folds between two biological replicates of Noc versus DMSO with an unadjusted p-value of less than 0.05 were selected and examined. Hierarchical clustering was created based on all annotated genes from the selected differential gene expression gene list.

2.14 **Mitochondrial DNA Quantification**

Total DNA (nuclear and mitochondrial DNA) was isolated using the Blood & Cell Culture DNA Mini Kit (Qiagen) as per manufacturer's instructions. Mitochondrial DNA (mtDNA) / nuclear (nDNA) ratios were determined by analysing the levels of mitochondrial DNA encoded cytochrome oxidase II subunit (COXII) using StepOnePlus™ Real-Time PCR system (Thermoscientific). The expression level of COXII gene was normalised to the expression of nuclear encoded and housekeeping gene β-globin.

2.15 **Oil Red O Staining**

A working oil red O solution was generated by diluting a 3.5 mg/mL stock solution (O0625) (Sigma) (in 100% isopropanol) with distilled water (6:4 ratio by volume). This solution was incubated at room temperature for 30 min and filtered through 0.22 μm pore size syringe filter unit (Pall Corporation) before use. Fixed cells were incubated in 60 % isopropanol for 1 min, dried at room

temperature, and incubated in oil red O staining solution for 1 min. Cells were rinsed with distilled water for 2-5 times and counterstained with Hoechst 33342 before being mounted in ProLong Gold Antifade (P36935) (Life Technologies). Bright field images were captured using Nikon High Speed Live Cell Microscope (C11578-22C) with 40X objective.

2.16 Preparation of Conditioned Media

Cells were treated with the respective drugs for 48 - 72 h followed by culture with drug-free media containing 0.5 - 1% FBS for an additional 48 h. After collection, the media were centrifuged at 5,000 × g, filtered through a 0.22 μm pore size syringe filter (Pall Corporation) and mixed with fresh culture media containing 40% FBS in a proportion of 3:1 to obtain CM containing 10% FBS.

2.17 Quantification of Cellular Migration and Metastasis in Zebrafish (ZgraftTM)

Synchronised H2B-GFP U2OS cells were incubated with the respective CM for 48 h and stained with DiI (Vybrant, Life Technologies) before being injected into zebrafish embryos. Embryos were imaged 48 h after injection to determine the metastatic tumour foci position relative to injection site. The Zebrafish assay was carried out at Dr. Indrajit Sinha's lab, Acenzia Inc, Windsor, Ontario, Canada.

2.18 RNA extraction and RT-qPCR

Total RNA was extracted using RNeasy plus Mini Kit (QIAGEN) according to manufacturer's instructions. cDNA was reverse transcribed using iScript™ RT supermix (Bio-Rad), subjected to SYBR Kit (#4472942) (Life Technologies) and analysed using StepOnePlus™ Real-Time PCR system (Thermoscientific). The relative expression values of each gene were normalised to expression of GAPDH. Primers used are listed in Appendix Table 2.

2.19 Senescence-associated β-galactosidase Staining

U2OS cells were plated at 2 x10^5 per cells per well in 6-wells plates. Cells were synchronised before the addition of respective drugs for the desired duration. The medium was then removed and the wells were washed twice with PBS. Cells were fixed and stained using the Senescence β-Galactosidase (SA-β-gal)

Staining Kit (#9860) (CST) according to manufacturer's instructions. Bright field images were captured using Nikon High Speed Live Cell Microscope (C11578-22C) with 40X objective.

2.20 **Time-lapse Imaging**

Cells are seeded in 6-well MatTek glass bottom plate at 4 $x10^5$ per well in a volume of 1.5 mL culture media. Twenty-four hours later, FBS-free DMEM media was substituted for 24 h to starve the cells. Twenty-four hours later, 3 M thymidine was added and cell incubated for 24 h. Synchronised cells were then washed with 1x PBS and released in 1.5 mL fresh media before addition of the respective drugs. Imaging was performed using Nikon High Speed Live Cell Microscope (C11578-22C) with 40X objective, with image collected every 15 min using 25 ms and 50 ms exposures for Differential Interference Contrast (DIC) and GFP channels respectively. Captured image sequences were viewed and analysed using MetaMorph software.

2.21 **Tumourigenic Phenotypic Assays**

For scratch wound migration assay, cells were seeded onto a 6-well plate to 90% confluency and a p200 pipet tip was used to create a scratch on cell monolayer. 2 mL of CM were added and the wound closure rate was tracked. For cell invasion assay, 5 $x10^5$ cells were incubated with CM and plated on the top surface of transwell filter chambers pre-coated or uncoated with Matrigel (BD Biosciences). After 24 h of incubation, non-invasive cells on the top chamber were removed by swapping the surface with cotton buds and washed twice with PBS. Invaded cells at the bottom chamber were fixed with 4% PFA and stained with 0.05% crystal violet. The percentage of invasive cells was quantified by cell counting. For choroid angiogenesis assay, segments of the peripheral choroid layer from eyes of P3 mice were incubated with CM 1:3 diluted with EGM2 media (Lonza) over four days and imaged under phase contrast. The choroid assay was performed by A/P Wang Xiaomeng's lab, NTU, LKCMedicine.

2.22 **Immunoblotting**

Whole-cell lysates were prepared in Pierce RIPA Buffer with Halt^{TM} Protease & Phosphatase Inhibitor Cocktail (Thermoscientific). Protein concentration was

measured using Bradford assay (Bio-Rad). An appropriate volume of Laemmli sample buffer was added to equal amounts of total proteins followed by boiling for 5 min. Protein samples were resolved by TRIS-glycine SDS PAGE gels (Bio-Rad) and transferred onto nitrocellulose membranes, which were incubated with blocking buffer (5% milk in PBST (PBS with 0.1% Tween® 20)) for 1 h. After which, the respective antibodies (3% milk in PBST) were incubated overnight at 4°C. The blots were washed with PBST for 3 times and incubated with HRP-conjugated anti-mouse or -rabbit antibodies (Amersham Biosciences) for 1 h. Blots were washed with PBST for 3 times before detection by ChemiDoc MP system (Bio-Rad) using ECL substrates (Thermoscientific). Antibodies used are listed in Appendix Table 3.

2.23 **Lipidomic analysis by mass spectrometry**

Six control cell samples (DMSO-treated) and six Nocodazole-treated cell samples (3 x 10^6 cells each) were freeze-dried to obtain the dry weight. Cells were extracted with a methanol/dichloromethane (DCM)/water (1:2:0.2) mixture. Water was subsequently added to obtain a lower phase DCM layer enriched with lipids. Dried lipid extracts were then reconstituted in 300 µL of methanol. A quality control (QC) sample was created by combining 10 µl aliquot from each extract. A dilution series of the QC sample and IS (internal standard) were first analysed to ensure the MS responses were linear over the concentration range of the analytes. The twelve lipid extracts and QC samples were diluted to appropriate concentration and then mixed with pre-determined concentration of IS which contains 14 deuterated standards representative for 14 lipid classes. The extracts and QC sample spiked with IS were then analysed in triplicates in randomized order. Data were acquired in full scan mode in both positive and negative ionization mode. A separate HRMS/MS data were acquired on the QC sample using “auto MS/MS” mode for the identification of the lipid species. The mass spectrometry analysis was carried out by Dr. Yoganathan Kanagasundaram ’s lab, A*STAR, Bioinformatics Institute (BII).

2.24 **Statistical Analysis**

GraphPad Prism software was used for the statistical analyses. Two-tailed, unpaired Student's *t*-test was used to access the statistical differences between the control and the drug-treated groups. *p*-values of <0.05 were considered statistical significant.

3. CHAPTER 1: MITOTIC SLIPPAGE-INDUCED SENESCENCE PROMOTES PARACRINE TUMOURIGENIC EFFECTS THROUGH SASP

3.1 Background and Rationale

One apparent outcome of mitotic slippage that potentially contributes to chemoresistance is cellular senescence. As mention earlier, therapy-induced senescent (TIS) cells could elicit a tumour-suppressive or tumour-promoting mechanism. Although paclitaxel treatment has been reported to induce cellular senescence in various cancer cell lines [37, 100, 101], the functional role of antimitotic-induced senescent cells remains elusive. Thus, in this chapter, I will elucidate the consequences of mitotic slippage and their associated mechanisms that could contribute to chemoresistance. Understanding the cell fate upon antimitotic drug treatment allows the development of a therapeutic strategy to circumvent resistance and enhance the efficacy of the antimitotic therapies.

3.2 Results

3.2.1 Cells undergo mitotic slippage upon antimitotic drugs treatment.

Previous studies have shown that cell lines such as U2OS osteoscarcoma cells and hTERT-RPE1 telomerase-immortalised non-transformed retinal pigment epithelial cells are prone to mitotic slippage instead of mitotic cell death when treated with antimitotic drugs [5, 102]. As a first step to confirm that U2OS cells indeed undergo mitotic slippage upon Noc treatment, live cell-imaging was performed to track chromosomally-labeled GFP-tagged Histone 2B (H2B-GFP) U2OS cells. Following treatment with Nocodazole (Noc), cells were observed by time-lapse microscopy. The cells arrested in mitosis as visualised by their round shape and condensed chromosome morphology (Figure 4a). The mitotically-arrested cells then underwent a series of morphological changes (i.e. cell blebbing, Figure 4a) before flattening and entering interphase (G1) without proper chromosome segregation and cytokinesis. These cells were observed to be multi-nucleated, a typical characteristic of post-slippage cells, due to the improper chromosome segregation. The live-cell imaging results correlated to the microscopic

evaluation and time-course immunoblotting analysis as shown in Figure 4b and Figure 4c respectively. The immunoblot analysis of synchronised U2OS cells treated with Noc or Taxol showed degradation of cyclin B1 (indicating exit from mitosis), and the reduction in phosphorylated BubR1 (a spindle assembly checkpoint marker) and Histone-H3 (H-H3) (a mitotic marker) following the onset of mitotic slippage (Figure 4c). I also observed that post-slippage cells induced activation of cell cycle arrest proteins p53 (tumour suppressor protein) and p21 (cyclin-dependent kinase inhibitor 1); indicating that cells arrested at G1 phase of the cell cycle may possibly be entering senescence. Being chromosomally unstable and polyploid, post-slippage cells activated a G1 checkpoint via p53-dependent pathway [103, 104]. All in all, the above data confirmed that U2OS cells undergo mitotic slippage and hence can be utilized as a model to investigate metabolic changes or survival mechanisms governing post-slippage cells.

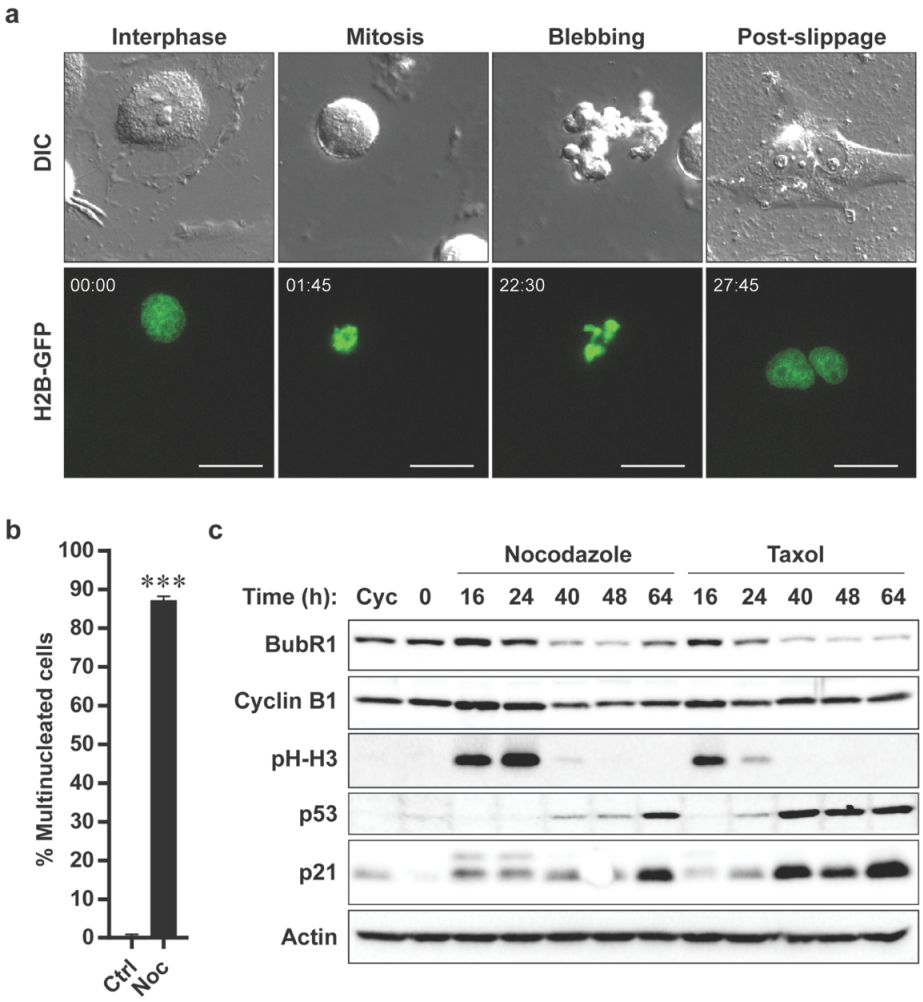

Figure 4. U2OS cells undergo mitotic slippage upon prolonged Nocodazole treatment.

(a) Frames taken from time-lapse imaging of U2OS cell expressing H2B-GFP (green) undergoing mitotic slippage upon Nocodazole (Noc) treatment. A single U2OS cell transits from interphase toward mitosis (cell rounding and condensed chromosomes). After a duration of mitotic arrest, cell undergo blebbing (onset of mitotic slippage) before reattaching to surface as multinucleated post-slippage cells. Top panel: DIC; Bottom: GFP-H2B. Time stamp = hh:ss. Scale bar: 25 µm. (b) Synchronised U2OS cells were treated with and without Noc for 48 h, stained using DAPI and quantified for multinucleated cells. Plot shows percentage of multinucleated cells. 50 cells per condition. Data are mean ± s.d. of 3 independent experiments. (c) Immunoblot analysis of synchronised U2OS cells treated with 100 ng/mL Noc (Left) and 150 nM Taxol (Right) throughout the time course. ***p<0.001 by Student's t-test.

3.2.2 **Induction of cellular senescence by prolonged antimitotic drugs treatment**

Following treatment of U2OS cells with Noc for prolonged duration, I observed that cells displayed large and flattened morphology reminiscent of senescence. To confirm that antimitotic drugs treatment indeed induces senescence, I stained the cells for senescence-associated beta-galactosidase (SA-β-gal) activity. SA-β-gal is an endogenous lysosomal enzyme that accumulates in senescent cells [105]. As shown in Figure 5a, after 3 days of Noc treatment, approximately 45% of U2OS cells stained positive for SA-β-gal, indicating entry into senescence. To confirm that this was a *bona fide* permanent cell cycle arrest that is expected of a stable senescence phenotype, Noc was removed after 3 days and cells were then cultured in fresh media for another six days. I observed a progressive increase in the percentage of cells that entered senescence (Figure 5a), confirming that cells underwent a permanent cell cycle arrest. Senescence establishment at Day 3 was further confirmed by immunoblotting analysis with other senescence-associated markers such as lamin B1, RB, p21 and p53 (Figure 5b). Consistent with literature, my data showed reduction in lamin B1 levels, decreased phosphorylation of RB Ser780, and an increased expression of p21 and p53 in post-slippage cells as compared to the control untreated cells. Interestingly, we observed a reduced expression of total RB in cells post-slippage. Although RB is a known effector of senescence [11], many studies have reported the reduction of total RB in senescent cells [106-109]. This could be explained by a report showing that the loss of RB could triggers a p53/p21 dependent checkpoint that sustains senescence induction [109]. Nevertheless, all this confirmed that cells post-slippage indeed entered senescence.

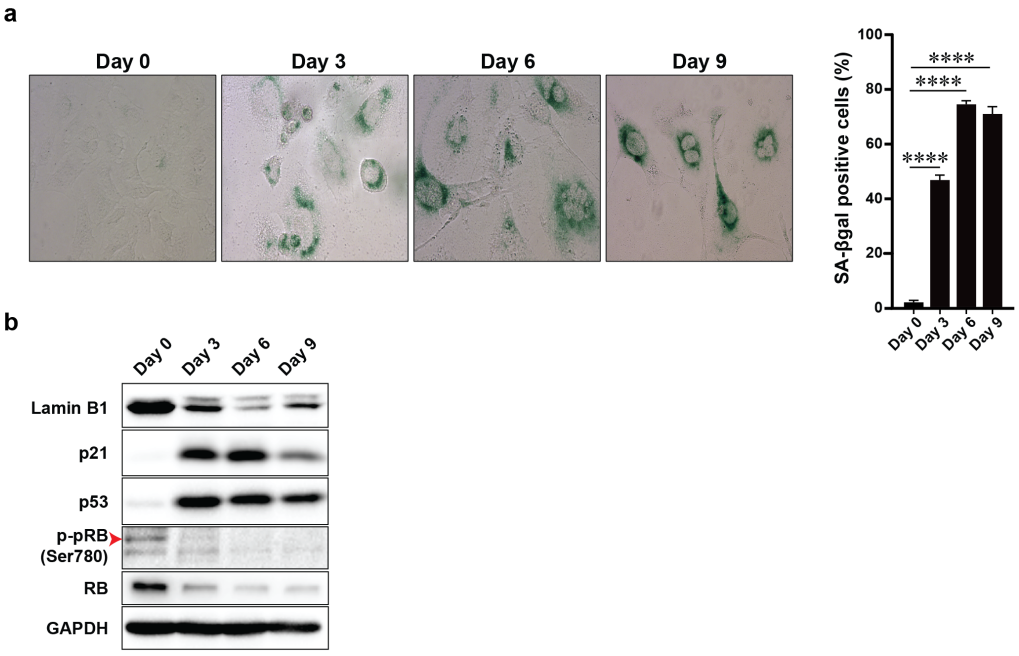

Figure 5. Antimitotic-treated U2OS cells display hallmarks of senescence.

(a) Left: Representative images of U2OS cells treated with Nocodazole for 72 h (as depicted by Day 3), release into fresh media for another 3 and 6 days (as depicted by Day 6 and Day 9 respectively) and stained for SA-β-gal. Right: Plot shows percentage of SA-β-gal positive cells. 100 cells per condition. Data are mean ± s.d. of 2 independent experiments. Scale bar: 10 μm. (b) Immunoblot analysis of senescence-associated markers as per conditions from (a). Red arrow indicates the band corresponding to p-pRB. ****$p<0.0001$ by Student's t-test.

Another phenotypic characteristic of senescence is the accumulation of dysfunction mitochondria [110-112]. To examine mitochondrial content in post-slippage cells, I first visualised mitochondria using U2OS cells expressing H2B-GFP and mCherry-labelled mitochondrial serine protease HtrA/Omi (Omi-mCherry). An increased mitochondrial mass was observed in Noc-treated post-slippage cells (Figure 6a). This observation is consistent with the increased mitochondrial DNA (mtDNA) when cells were treated with Noc for 48 h and 72 h (Figure 6b). Hydrogen peroxide (H_2O_2), a known inducer of oxidative stress was used as a positive control to induce degradation of mitochondrial DNA [113]. Next, I determined the functional status of mitochondrial permeabilisation by evaluating mitochondrial membrane potential. Healthy mitochondria create an electrochemical gradient essential to drive the synthesis

of ATP and generate mitochondrial membrane potential [114]. To measure mitochondrial membrane potential, I stained cells with tetramethylrhodamine ethyl ester (TMRE) followed by analysis using BD Accuri C6 flow cytometry. TMRE is a positively-charged dye that is readily sequestered in negatively-charged healthy mitochondria (approximately -180 mV) and emits a red fluorescence (FL2 channel) [115]. A reduction in TMRE intensity ($TMRE^{Low}$) indicates mitochondrial depolarization. I observed that even though post-slippage cells showed increased number of mitochondria, a higher percentage of $TMRE^{Low}$ cells was detected in post-slippage cells compared to control cells (Figure 6c). I also detected increased levels of reactive oxygen species (ROS) and mitochondrial superoxide that correlate with mitochondrial dysfunction in these post-slippage cells (Figure 6d). The above findings suggest that post-slippage cells accumulate dysfunctional mitochondria.

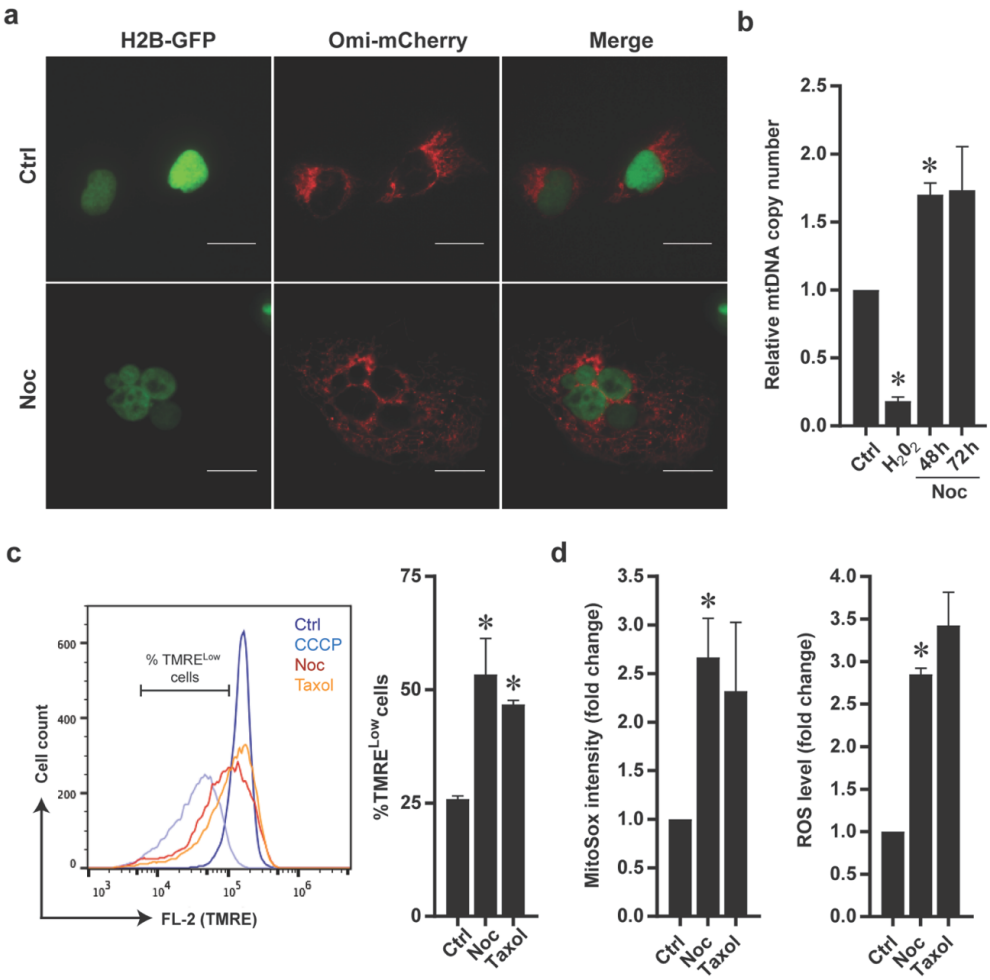

Figure 6. Antimitotic-treated U2OS cells accumulate dysfunctional mitochondria. (a) Representative images of H2B-GFP/Omi-mCherry U2OS cells treated with Nocodazole for 72 h. Scale bar: 25 µm. (b) RT-qPCR analysis shows relative expression of COXII (mitochondrial DNA) normalised to β-globin (nucleus DNA) in U2OS cells treated with Nocodazole for 48 h and 72 h. 100 µm H_2O_2 was used as a positive control to induce degradation of mitochondrial DNA. (c) Left: FACS profile of U2OS cells treated with Noc or Taxol for 72 h and stained with TMRE. FCCP was used as a positive control to induce mitochondrial depolarisation. Right: Plot shows percentage of $TMRE^{Low}$ cells. (d) Plots show the relative MitoSox intensity (left) and ROS level (right) of Noc- and Taxol-treated U2OS cells. Experiments were performed at least twice. *p<0.05 by Student's t-test.

One of the defining hallmarks of senescence is the acquisition of SASP [13]. This phenotype distinguishes senescent cells from non-senescent cells and encodes specific protein expression and secretion resulted in autocrine or

paracrine effects on the surrounding microenvironment [116]. SASP factors such as chemokines, cytokines, and proteases secreted by senescent cells could positively or negatively affects the therapeutic outcomes of anticancer therapies, such as by promoting tumour or senescent cells clearance or mediating tumor progression [23, 32, 117]. Therefore, I performed gene expression microarray on U2OS cells treated with DMSO (control) or Noc for 48 h and scrutinised the expression of SASP-related factors (Figure 7a-b). The microarray data revealed the upregulation of several factors, including cytokines and chemokines IL-1α, IL-1β, CXCL8 and CCL3 in Noc-treated U2OS cells (Figure 7a-b). In addition, the results from quantitative real-time qPCR and Multiplex cytokine assays confirmed the upregulated expression and secretion of various SASP-related factors in Noc-treated U2OS cells as compared to DMSO-treated control cells (Figure 7c). Taken together, the above findings confirmed that post-slippage cells enter senescence and express multiple hallmarks of cellular senescence.

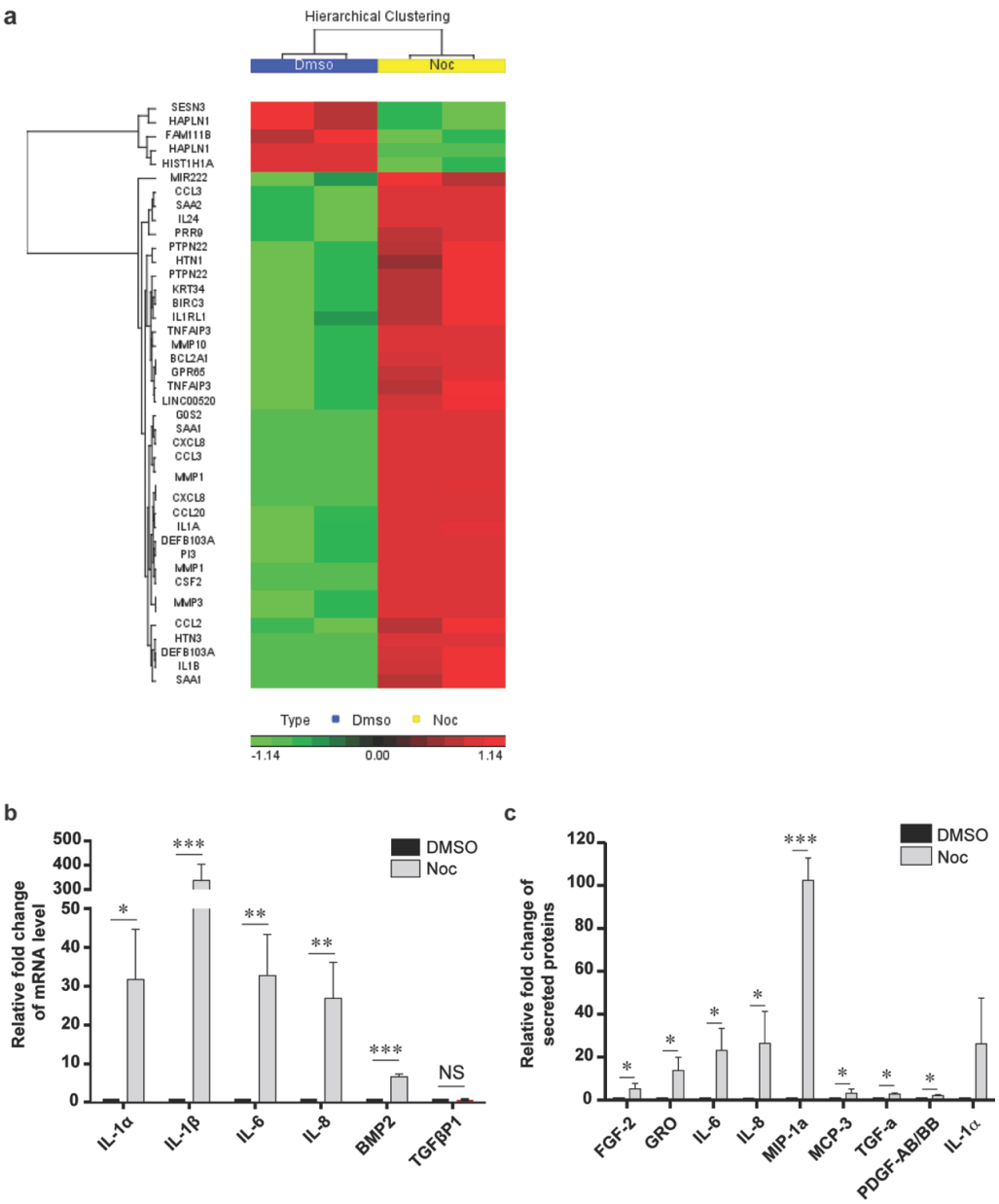

Figure 7. Antimitotic-treated U2OS cells display SASP.

(a) Total mRNA extracted from U2OS cells treated with Nocodazole (Noc) or DMSO for 48 h was subjected to microarray. Top hits are shown for genes that are at least 2.5-fold upregulated (red) or downregulated (green) after treatment. (b) RT-qPCR analysis shows relative mRNA expression of SASP components in DMSO-treated or Noc-treated U2OS cells for 72 h. mRNA levels were normalised to GAPDH and DMSO control. (c) Plot shows relative fold change of secreted cytokines from U2OS cells treated with DMSO or Noc for 72 h using Multiplex cytokine array. Data are mean ± s.d. of 3 independent experiments. *p<0.05, **p<0.005, ***p<0.001 and NS=not significant by Student's t-test.

3.2.3 **Pro-tumorigenic effects induced by post-slippage cells through SASP**

It has been reported that chemotherapy-induced senescent cells and its associated SASP factors promote chemoresistance and tumourigenesis [32, 33, 37]. The significant increase in the secretion of post-slippage SASP factors prompted us to investigate whether the factors mediate tumorigenic phenotypes such as cell migration, invasion and angiogenesis. As shown by the experimental scheme in Figure 8a, CM derived from DMSO- or Noc-treated U2OS cells were obtained to perform various phenotypic assays. To assess cell migration, U2OS cells expressing H2B-GFP were incubated with CM from their respective treated cells and subjected to the classical scratch wound healing assay. As shown in Figure 8b, CM derived from post-slippage cells promoted a faster rate of wound closure as compared to control CM. Detection of cell proliferation by cell counting do not show any significant difference in cell proliferation between the control and post-slippage CM, suggest that the increased rate of wound closure was not affected by proliferation. To evaluate cell invasiveness, H2B-GFP U2OS cells incubated with either control or post-slippage CM were subjected to transwell invasion assays. An increased number of cells incubated with post-slippage CM invaded the bottom of the filter chamber compared to control CM (Figure 8c). To evaluate angiogenic potential, choroid angiogenesis assay, an *ex vivo* model of angiogenesis was used. Increased growth of vascular sprouting from choroid explants incubated with post-slippage CM compared to control CM was observed after four days (Figure 8d), indicated that the angiogenic capability was conferred by factors derived from the post-slippage cells. Taken together, it was concluded that post-slippage factors confer paracrine pro-tumorigenic behavior through the induction of cell migration, invasiveness and angiogenesis.

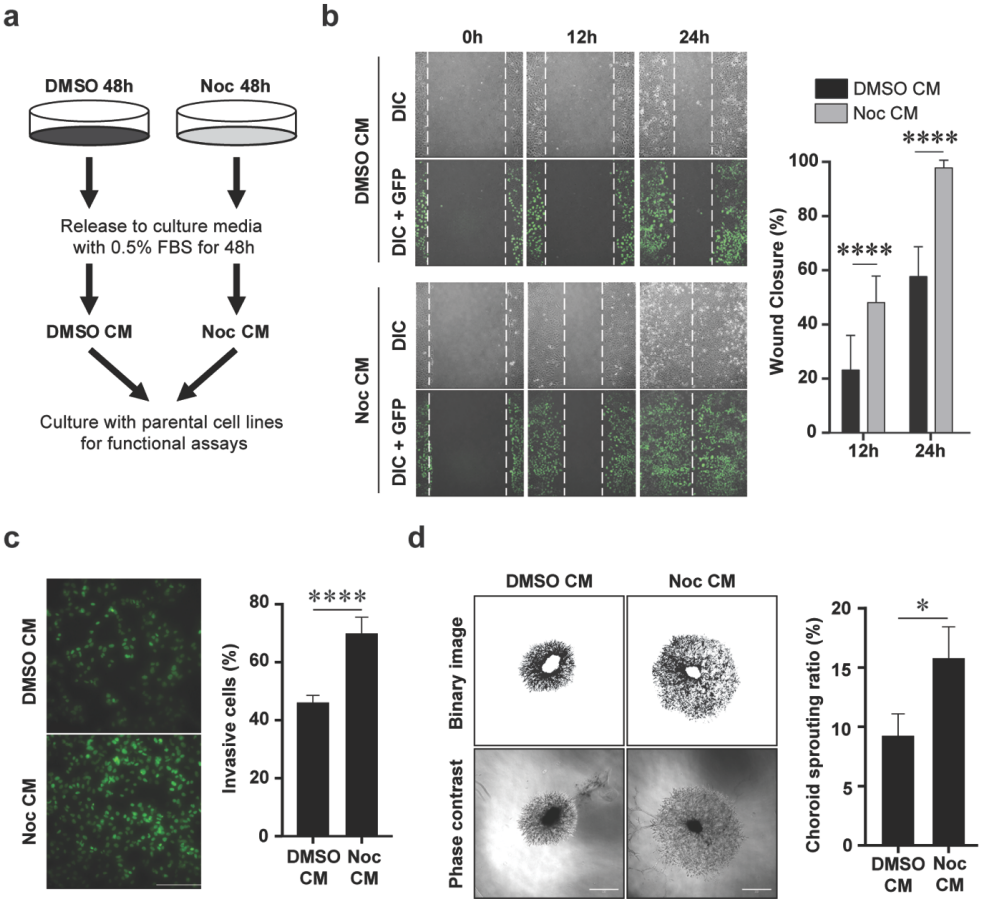

Figure 8. SASP factors release from post-slippage cells promote paracrine tumorigenic effects.

(a) Experimental scheme describes the preparation of CM for determining paracrine tumorigenic effects. (b) H2B-GFP U2OS cells were incubated with their respective CM for 48 h and performed the scratch wound healing assay. Left: Representative images of CM-treated H2B-GFP U2OS cells taken at t= 0 h (immediately after scratching), 12 h and 24 h. Right: Plot shows rate of wound closure in DMSO CM- or Noc CM-treated U2OS cells. Data are mean ± s.d. of 3 independent experiments. Scale bar: 200 µm. (c) H2B-GFP U2OS cells were treated as per (b). Invasive ability was assessed by Transwell Matrigel assay. Scale bar: 200 µm. Plot shows percentage of invasive cells. n=5 random fields were taken per condition and data are mean ± s.d. of 3 independent experiments. (d) Representative images of choroidal sprouts formed after culturing with respective CM for 48 h. Plot shows choroid sprouting ratio (Area of vascular sprouting / Area of the explant). Minimum of 6 explants analysed per treatment. Data are mean ± s.d. of 3 independent experiments. *p<0.05 and ****p<0.0001 by Student's t-test.

3.3 Discussion

In this chapter, I studied the consequences of mitotic slippage and its subsequent cell fate in response to antimitotic drugs treatment. When cells are exposed to antimitotic drug such as Nocodazole, they arrest in mitosis and eventually die or undergo mitotic slippage. Majority of the cells also die after slippage, whereas a remaining population of cells survive and transit into senescence - a phenomenon widely known as therapy-induced senescence (TIS) [24]. Although TIS cells encompass several key features common among most senescent cells, their effects and consequences of senescence induction may vary depending on the nature of the drug used and the cancer cell type in question [24]. My results indicate that antimitotic-induced post-slippage cells display several hallmarks of senescence: (1) increased in cell size and activity of SA-β-gal, (2) loss of lamin B1 protein, (3) accumulation of dysfunctional mitochondrial and (4) induction of SASP.

The role of TIS in mediating therapeutic outcomes remains controversial, with studies showing the tumor-suppressive function of TIS in stimulating immune-mediated clearance of senescent or remaining tumor cells [118], while other studies described tumor-promoting effects for TIS [23, 32, 33, 37]. In this study, I found that SASP factors released by post-slippage senescent cells elicit paracrine pro-tumorigenic effects such as cell migration, invasiveness and angiogenesis (Figure 3.5). My result complements the study showing induction of pro-inflammatory cytokines and metastasis in breast cancer cells treated with paclitaxel [119]. Although post-slippage SASP factors conferred paracrine pro-tumourigenic phenotypic effects such as migration, invasion and vascularisation on neighbouring cells, the proliferation of cells incubated with CM from post-slippage cells remains unaffected. This could be explained by the high heterogeneity of SASP composition and quantity that is dependent on cell type and mode of senescence induction [36]. Therefore, post-slippage SASP may function as a secondary role in promoting tumourigenesis in cells where migration, invasion and angiogenesis are uncoupled from cell proliferation thereby leading to the development of a more malignant phenotype in cancer cells [120]. It is conceivable that once surrounding cells transit toward malignancy, post-slippage SASP will be involved in potentiating

the tumourigenic capabilities of these cells, demonstrating that mitotic slippage-induced senescence could serve as a conduit for malignant transformation and antimitotic therapy resistance.

With the detrimental effects of post-slippage senescent cells, elimination of senescent cells could potentially enhance the efficacy of antimitotic therapies. Clearing therapy-induced senescent cells also reduces the detrimental side-effects of the drugs such as bone marrow suppression, cardiac dysfunction and even cancer recurrence [37, 116]. It is anticipated that the elimination of senescent cells overall will prevent toxicity of anticancer treatment and enhance therapeutic benefit. In this regard, several approaches are available to eliminate senescent cells or blocking deleterious SASP induction [116]. Senolytic compounds could be used to specifically induce cell death in senescent cells. Reprogramming of SASP factors not only prevent the adverse effects of senescence but also promote anti-tumour inflammation for the clearance of tumour or tumour-associated senescence cells [28].

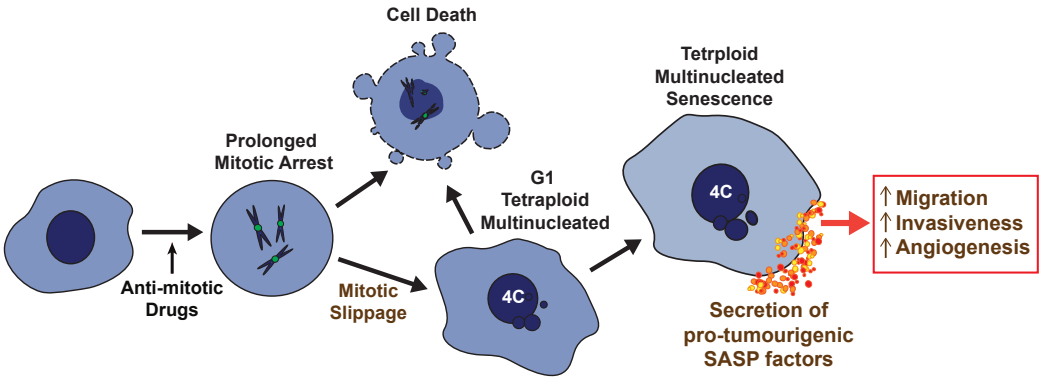

Figure 9. Proposed model depicting the pro-tumorigenic effects triggered by soluble factors release from multinucleated senescent cells.

Upon treatment with antimitotic drugs, mitotic-arrested cells can die in mitosis or undergo mitotic slippage. Post-slippage multinucleated cells can persist and transit into senescence. The cells secrete SASP factors that promote paracrine tumorigenic effect such as cell migration, invasiveness and angiogenesis.

4. CHAPTER 2: AUTOPHAGY GOVERNS PRO-TUMORIGENIC EFFECTS OF MITOTIC SLIPPAGE-INDUCED SENESCENCE

4.1 Background and Rationale

Autophagy is known to be activated during senescence induction and could facilitate the process of senescence [60, 61]. It is highly plausible that autophagy is involved in mediating cell fate post-slippage as defined in the previous chapter. Here, this chapter determines whether antimitotic-treated post-slippage cells activate autophagy and whether autophagy plays a role in mediating post-slippage senescence and its associated tumour-promoting effects. Understanding the functions of autophagy under specific chemotherapeutic treatment allows the development of a therapeutic strategy (i.e. by inhibiting or activating autophagy) to circumvent resistance and enhance the efficacy of the treatment for cancer patients.

4.2 Results

4.2.1 Enhanced autophagic activity following mitotic slippage

To determine whether autophagy is triggered upon treatment with antimitotic drugs, I first visualised the subcellular localisation pattern of microtubule-associated protein 1 (MAB) light chain 3B (LC3) using GFP-LC3 expressing U2OS cells. LC3 is widely used as a marker for autophagy. During basal activity of autophagy, LC3 will appear as a diffused staining throughout the cytoplasm. Upon elevated autophagic induction, LC3 is processed post-translationally into cytoplasmic LC3-I and then converts into LC3-II that specifically associates with autophagosome membrane. The accumulation of GFP-LC3 on the autophagosome will appear as fluorescent puncta in the cell [121]. As shown in Figure 10a, I observed a higher percentage of post-slippage cells harboring GFP-LC3 puncta foci as compared to DMSO-treated control cells, indicating autophagosome accumulation (Figure 10a). The induction of autophagy upon Noc treatment was further verified by immunoblotting analysis showing the conversion of cytosolic LC3 (LC3-I) to autophagosome membrane-bound LC3 (LC3-II) as well as the degradation of the ubiquitin-

binding autophagic adaptor protein p62/SQSTM1 (Figure 10b) in post-slippage (PS) cells (t= 36 h and 48 h). To confirm the increased autophagy flux in post-slippage cells, I used Bafilomycin A1 (BafA1), a pharmacological inhibitor of autophagy that blocks the acidification of autolysosome and the fusion of autophagosome and lysosome. Co-treatment of Noc and BafA1 induced an increased in LC3-II at t= 36 h and 48 h (Figure 10b) compared to Noc control, suggesting that LC3-II accumulation post-slippage to be due to autophagosome accumulation and not the dysfunction in downstream autophagic processes such as autophagosome-lysosome fusion or autolysosomes degradation. LC3-II accumulation in post-slippage cells was also suppressed by inhibiting autophagy using stable expression of short hairpin RNA targeting ATG5 (shATG5), a protein essential for the elongation of phagophoric membrane into autophagic vesicles [122] (Figure 10c).

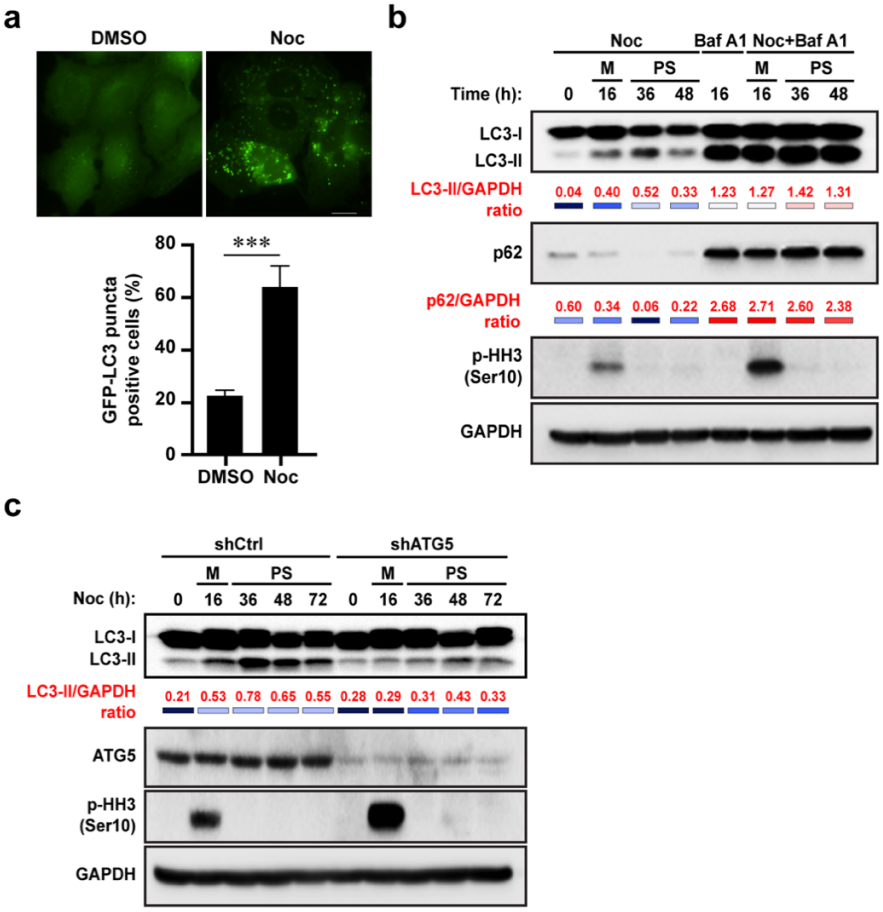

Figure 10. Autophagy is induced during mitotic slippage.

(a) U2OS cells stably expressing GFP-LC3 were assessed for GFP puncta formation following 48 h Nocodazole (Noc) treatment. Plot shows percentage of GFP-LC3 puncta positive cells (>5 puncta per cell) following indicated treatments. 50 cells per condition. Scale bar: 20 µm. (b) U2OS cells were treated with Noc in the presence and absence of autophagy inhibitor, Bafilomycin A1 (BafA1) for the indicated time point and probed for autophagic proteins. M: mitotic; PS: post-slippage. (c) U2OS cells stably expressing shCtrl or shATG5 were treated with Noc for the indicated time probed for autophagic proteins. ***p<0.001 by Student's t-test.

Autophagic induction occurs via numerous pathways that ultimately converge towards the regulation of AMPK/ULK/mTOR axis, which integrates growth factor and nutrient signals to regulate cellular metabolism and maintain energy homeostasis [123]. Phosphorylation of AMP-activated protein kinase (AMPK) on Thr172 activates autophagy by directly activating Unc-51 Like Autophagy Activating Kinase (ULK1) through phosphorylation of Ser317 and Ser777. In contrast, high activity of the mammalian target of rapamycin (mTOR)

negatively regulates autophagy by preventing ULK1 activation via ULK1 Ser757 phosphorylation and disrupting the interaction between of ULK1 and AMPK [124]. To assess whether the autophagy induction in post-slippage cells was mediated via the AMPK/ULK/mTOR axis, U2OS cells were treated with Noc and subjected to immunoblotting. Both mTOR and AMPK were activated in mitotic cells 16 h post-Noc treatment as shown by increased phosphorylation of the mTOR substrate p70 S6K, conversion of total ULK1 to phosphorylated ULK1 (Ser757) as well as increased phosphorylated AMPK (Thr172) (Figure 11). This corresponds with the increased autophagy, and was consistent with an observed elevation of LC3-II (Figure 11). As it was previously reported that autophagy can be activated via a mTOR-independent manner (23,24), our findings suggest presence of autophagic activity despite mTOR activation during mitosis. On the other hand, reduced levels of phosphorylated-p70 S6k indicating decreased mTOR activity with concomitant decrease in ULK1 phosphorylated on Ser757 residue was observed in post-slippage cells (Figure 11). These findings together with the observed increase in phosphorylated AMPK (Thr172) and LC3-II levels, strongly suggested that the AMPK/ULK/mTOR axis promotes autophagy induction post-slippage.

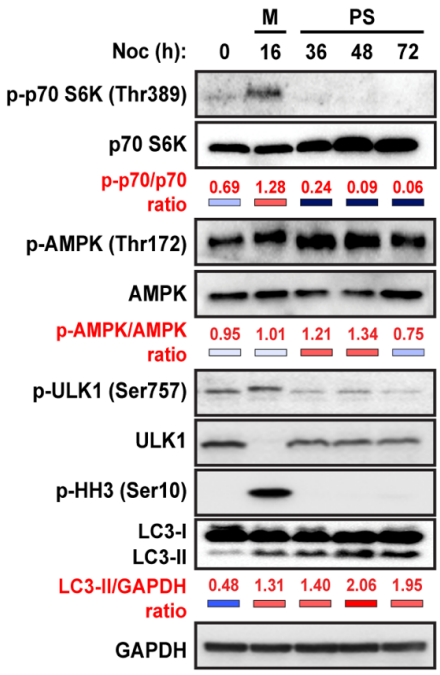

Figure 11. Autophagy is induced via AMPK/ULK1/mTOR axis.

U2OS cells were treated with Nocodazole for the indicated time point probed for AMPK/ULK1/mTOR-related proteins. The LC3-II/GAPDH and p62/GAPDH signal intensity ratios are shown at the bottom of the relevant lanes.

4.2.2 **Autophagy inhibition in post-slippage cells leads to senescence bypass and cell death**

Since autophagy is enhanced in post-slippage cells, I sought to investigate whether the senescence cell fate could be affected by autophagic inhibition. Inhibition of autophagy by BafA1 resulted in senescence bypass as observed by decreased percentage of cells stained with SA-β-gal (Figure 12a). Similar reduction in SA-β-gal staining was detected in Noc-treated U2OS shATG5 cells (Figure 12a). Concomitantly, a corresponding increase in cells entering S-phase was suggested by the increased BrdU-labelling upon inhibition of autophagy by siRNA targeting of ATG5 (Figure 12b). The efficiency of autophagy inhibition by siATG5 was shown by the suppressed induction of LC3-II level upon Noc treatment (Figure 12c). This unequivocally confirmed that post-slippage senescence was dependent on autophagy.

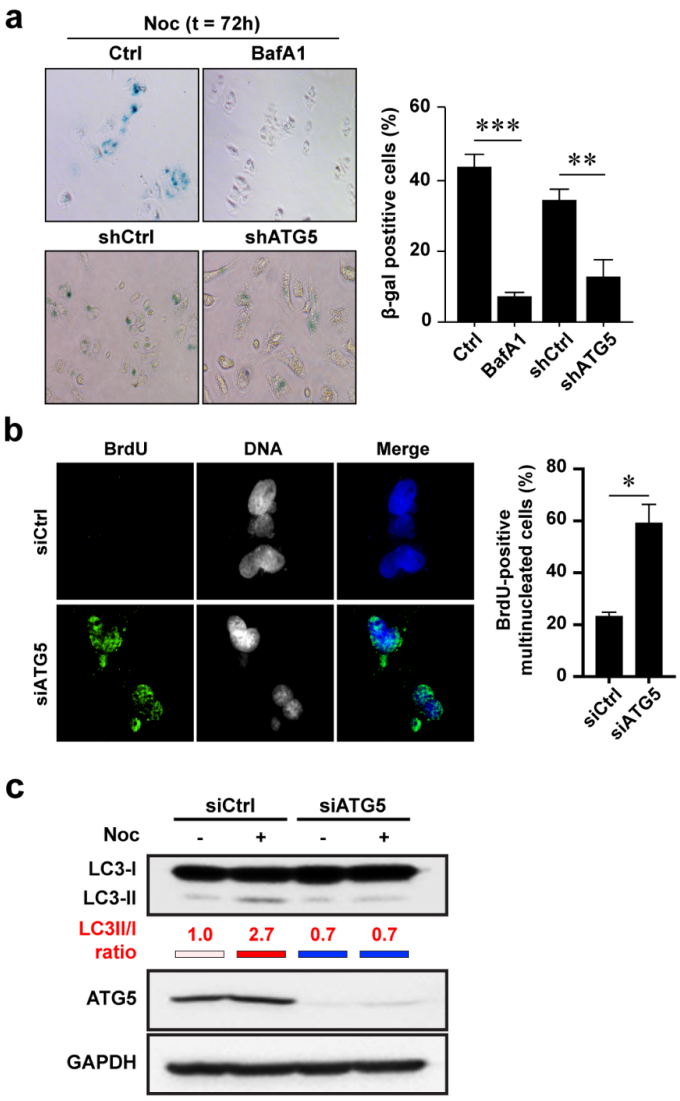

Figure 12. Autophagy inhibition abrogates post-slippage senescence.

(a) Representative images of U2OS cells stained with SA-β-gal after the respective treatments. Plot shows percentage of SA-β-gal positive cells. 100 cells per condition. Data are mean ± s.d. 3 of independent experiments. Scale bar: 10 μm. (b) U2OS cells were transfected with siCtrl or siATG5 followed by Noc treatment for 72 h. Proliferation was assessed by the BrdU incorporation assay. Plot shows percentage of BrdU-positive multinucleated cells. 100 cells per condition. Data are mean ± s.d. 3 independent experiments. Scale bar: 20 μm. (c) IB shows efficiency of ATG5 knockdown in U2OS cells transfected with siCtrl or siATG5 followed by 72 h of Noc treatment. *p<0.05, **p<0.005 and ***p<0.001 by Student's t-test.

The inhibition of post-slippage senescence by autophagy might inevitably drive cells toward post-slippage death. Our time-lapse imaging revealed that autophagy inhibition in Noc-treated U2OS cells showed an

increased cell death post-slippage (Figure 13a). Co-treatment of cells with Noc and BafA1 showed an overall reduction in cell viability as compared to Noc treatment alone (Figure 13b). Consistent with this, clonogenic survival assays showed reduction of long-term cell survival following autophagic inhibition (Figure 13c-d).

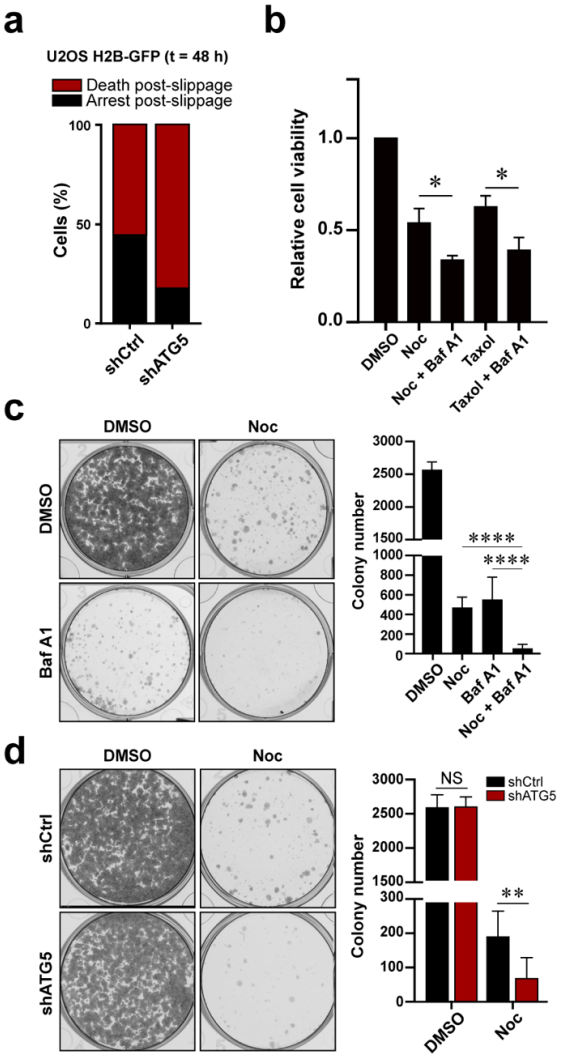

Figure 13. Autophagy inhibition potentiates post-slippage cell death.

(a) H2B-GFP U2OS shCtrl or shATG5 cells were treated with Nocodazole (Noc) for 48 h. Post-slippage multinucleated cells were tracked individually by time-lapse imaging for another 48 h. Red: Cells that undergo post-slippage death. Black: Cells that arrest post-slippage. 50 cells per condition. Data are mean ± s.d. of 2 independent experiments. (b) U2OS cells were treated with Noc or Taxol in absence or presence of BafA1 for 72 h. Cell viability was assessed by CellTiter96® One Solution Proliferation assay. (c) For clonogenic survival assay, synchronised U2OS cells were treated the

respective drugs for 72 h. Surviving cells were re-plated and culturing for another 10 days. Left: Representative images of U2OS cells treated with the indicated drugs followed by crystal violet staining. Right: Plot shows number of colonies counted using GelCount software. 8 wells per condition of 2 independent experiments. (d) U2OS shCtrl or shATG5 cells were treated with Noc for 72 h and subjected to clonogenic assay as in (c). *p<0.05, **p<0.005, ****p<0.0001 and NS=not significant by Student's t-test.

To determine whether these findings could be extrapolated to other types of antimitotic drugs, cells treated with Noc, Taxol, Mon and ZM for 72 h and detected for the apoptotic marker cleaved PARP following ATG5 knockdown. Interestingly, the increased in cell death was restricted to microtubule-targeting drugs Noc and Taxol (Figure 14). Additionally, autophagy inhibition increased DNA damage (as determined by γH2AX foci and 53BP1 protein levels) compared to control (Figure 14). Enhanced replication stress was shown by increased RPA32 phosphorylation at 72 h post-Noc treatment as compared to control (Figure 14). These cells then undergo increased replication stress and DNA damage, culminating in cell death. Taken together, our findings suggest that autophagy mediates cell survival upon anti-mitotic drug treatment and that inhibition of autophagy engenders cells to bypass senescence post-slippage and enter S phase.

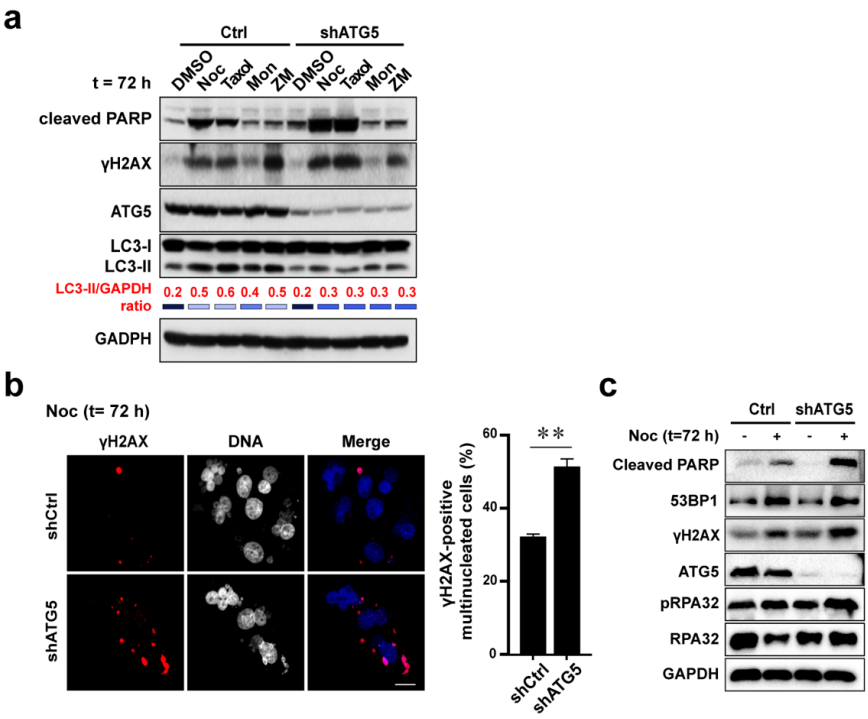

Figure 14. Autophagy inhibition potentiates DNA damage and replicative stress. (a) U2OS shCtrl or shATG5 cells were treated with indicated drugs for 72 h and subjected to IB analysis. (b) U2OS shCtrl or shATG5 cells were treated with Noc for 72 h and subjected to IF. Plot shows percentage of γH2AX positive multinucleated cells. 100 cells per condition. Data are mean ± s.d. of 2 independent experiments. Scale bar: 20 μm. (c) U2OS shCtrl or shATG5 cells were treated with Noc for 72 h and subjected to IB analysis. **P<0.005 by Student's t-test.

4.2.3 **Autophagy confers paracrine pro-tumourigenic effects through regulating SASP**

Earlier on, it had been shown that autophagy regulates the establishment of post-slippage senescence. Next, I determined whether autophagy could also regulate SASP and its associated pro-tumourigenic effects. U2OS cells were treated with Noc in the presence or absence of BafA1 and analysed the media for the secretion of post-slippage SASP factors. A discernible decreased in the expression of SASP cytokines CXCL3, IL-1β, IL-6, IL-8 and CCL7, coupled with increased expression of BMP2 post-slippage was observed following autophagy inhibition compared to control (Figure 15a). This suggests that autophagy is involved in the activation of senescence and consequently modulates SASP following mitotic slippage. Since autophagy modulates the

secretion of SASP factors, it is plausible that SASP-induced tumourigenic function will also attenuated following autophagic inhibition. Transwell migration assays using cells incubated with CM from post-slippage U2OS cells expressing shATG5 showed a significant reduction in the percentage of cells capable of invasion compared to control CM (Figure 15b). With regards to angiogenic potential, post-slippage CM promoted increased vascular sprouting compared to control CM from cycling cells in choroid explants, whereas autophagic inhibition significantly reduced the sprouting activity (Figure 15c). To further examine if the in vitro migratory and invasive reduction following autophagic inhibition could be extrapolated to metastatic inhibition in vivo, the zebrafish model of malignancy was used to evaluate metastatic potential [125]. The transparency of the zebrafish embryo provides the unique ability to visualise the real time *in vivo* migratory changes of fluorescently labeled tumour cells. U2OS H2B-GFP-expressing cells were incubated with CM from either cycling or post-slippage cells expressing shATG5 or control for 48 h before injection into zebrafish embryos. H2B-GFP-expressing cells incubated with post-slippage CM were observed to migrate out from the injection site and metastasise further than cells incubated with control CM (Figure 15d). This metastatic potential was significantly reduced in post-slippage CM derived from U2OS shATG5 cells (Figure 15d). All these observations support the role of autophagy-dependent SASP secretion in promoting *in vivo* paracrine migration, invasion and angiogenesis.

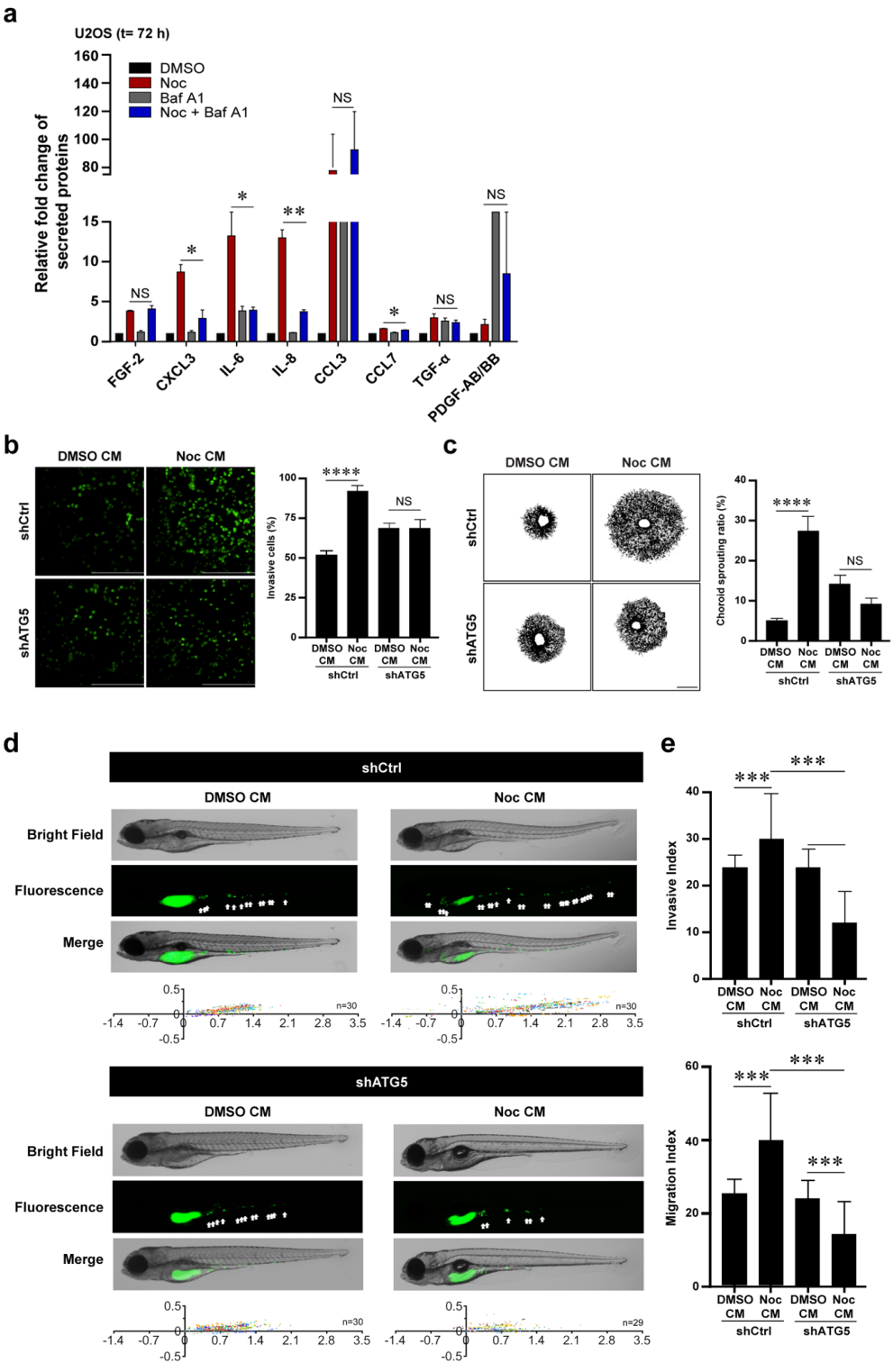

Figure 15. Autophagy inhibition attenuates SASP production and the associated pro-tumorigenic effects.

(a) Multiplex cytokine assays of supernatant derived from U2OS cells treated with Nocodazole (Noc) in absence or presence of BafA1 for 72 h. (b) Representative images of choroidal sprouts formed using indicated CM generated from U2OS shCtrl or shATG5 cells. Plot shows the ratio of choroid sprouting. Minimum 6 explants analysed

per treatment. (c) U2OS cells expressing H2B-GFP were cultured with indicated CM generated from U2OS shCtrl or shATG5 for 48 h. Invasive ability was assessed by transwell invasion assay. Scale bar: 200 μm. Plot shows percentage of invasive cells. 5 random fields were taken per condition. Data are mean ± s.d. of 3 independent experiments. (d) H2B-GFP U2OS cells were cultured with indicated CM generated from U2OS shCtrl or shATG5 cells, followed by injection into zebrafish embryo. All tumour foci observed in all tested larvae belonging to each treatment group (represented as n on the graph), is presented as a scatter plot. Foci in one larva is represented by one colour. "n" denotes number of injected embryos from 3 biological replicates. (e) Quantitative determination of metastatic ability upon indicated treatments was measured by Invasive Index (top) and Migration Index (bottom). *p<0.05, **p<0.005, ***p<0.001, ****p<0.0001 and NS=not significant by Student's t-test.

4.2.4 **Combination treatment of antimitotic drugs and autophagy inhibitor arrest tumour growth**

To assess whether the findings mentioned above could be extrapolated to an in vivo model, HCT116 xenograft tumours were treated with combination treatment of either Noc or Taxol and autophagic inhibitor Chloroquine (CQ). Similar to BafA1, CQ blocks autophagic flux and cargo degradation through the disruption of lysosome function [126]. Our results showed that combination treatment (Noc+CQ or Taxol+CQ) significantly decreased tumour growth and final tumour weight as compared to control Noc or Taxol alone (Figure 16a-c), suggesting that the tumours were most sensitive to combination treatment. Because LC3 and p62 is constantly degraded during autophagy process, autophagy inhibition will lead to the accumulation of LC3 and p62 (as shown previously in Figure 10b). Indeed, molecular assessment of tumour sections derived from the mice xenografts showed more robust LC3 and p62 puncta accumulation in the combination drug-treated mice compared to Noc or Taxol treatment alone (Figure 16d-e), indicating the efficient inhibition of autophagy by CQ. These results support the notion that autophagy inhibition potentiates the cell death induced by anti-mitotic drugs treatment.

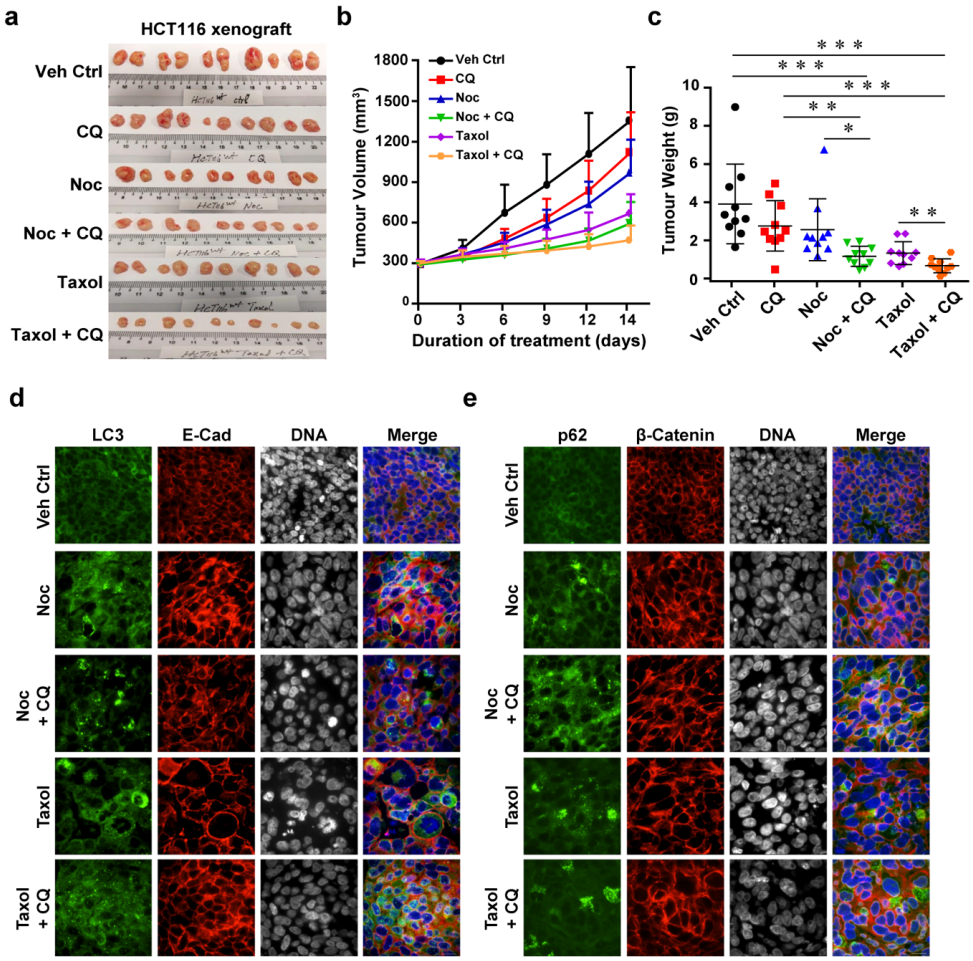

Figure 16. Synergistic inhibition of tumour growth by antimitotic drugs and autophagy inhibitors.

(a) Representative images of xenograft tumours harvested from nude mice after two weeks of indicated treatment. Drug dosage used: Chloroquine (CQ): 30 mg/kg, Noc: 10 mg/kg and Taxol: 10 mg/kg. (b) Effect of combinatorial treatment on the growth of xenograft tumours generated by subcutaneous injection of HCT116 cells in nude mice. Data are mean of ± s.d. (n=10 tumours per group). (c) The weight of tumour after two weeks of indicated treatment. Dots represent individual tumour weight, n=10 tumours per group. Scale bar 20 µm. (d-e) Immunofluorescence analysis of tumour sections from single and combination drug-treated xenograft mice probed against autophagy-related antibodies LC3 and p62. *P<0.05, **P<0.005 and ***P<0.001 by Student's t-test.

4.3 Discussion

In this chapter, I propose the model outlined in Figure 17. In response to the prolonged mitotic arrest induced by anti-mitotic drugs, cells undergo either mitotic cell death or mitotic slippage. After mitotic slippage, autophagy is induced via the AMPK/mTOR/ULK1 axis. Multinucleated tetraploid cells that persist post-mitotic slippage can undergo senescence and drive paracrine tumourigenic effects both *in vitro* and *in vivo* in an autophagy-dependent manner. The inhibition of autophagy by pharmacological and genetic means in post-slippage cells abrogate the senescence and SASP induction, and subsequently promotes cell death.

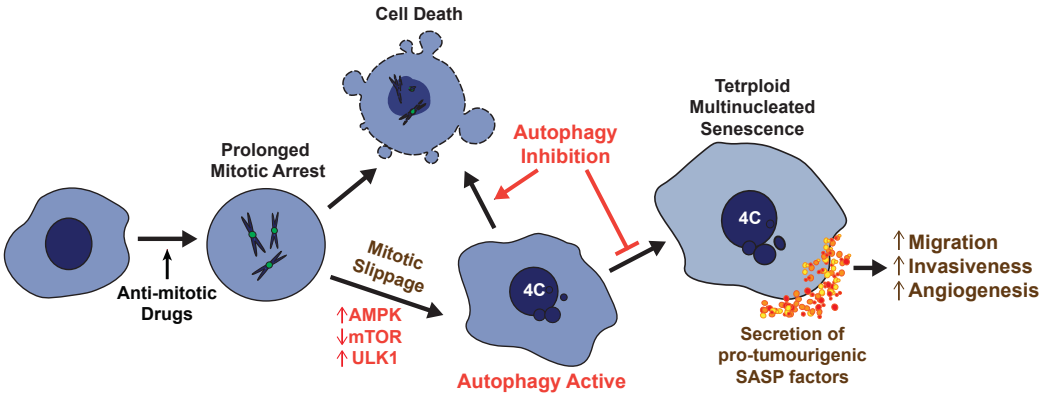

Figure 17. Proposed model of autophagy-mediated tumourigenesis upon antimitotic treatment.

Upon treatment of cancer cells with anti-mitotic drugs, autophagy is activated via AMPK/mTOR/ULK1 axis. The increased autophagic activity in post-slippage cells promotes senescence and the associated SASP production. The secreted SASP factors confer pro-tumourigenic potential that promotes *in vitro* and *in vivo* migration, invasiveness and angiogenesis. Conversely, following autophagy inhibition, senescence is abrogated and post-slippage cells undergo death.

Although prior work by Young et al. showed that autophagic inhibition delayed the senescence phenotype following oncogene activation [60], this study demonstrates that inhibition of autophagy post-slippage results in the bypass of senescence and transit towards cell death. The most compelling evidence for senescence bypass after autophagy inhibition was the increased

entry into S-phase, induction of DNA damage and replication stress, and reduction in cell viability in post-slippage cells collaterally. The attenuation of senescence by autophagic inhibition has been described to be mediated by autophagy-dependent degradation of lamin B1 [127]. The loss of lamin B1, as described before [14] and also shown in our study, is a senescence-associated marker. Inhibition of autophagy or LC3-lamin B1 interaction prevented oncogene-induced lamin B1 loss and attenuated senescence [127]. Since similar blockage of lamin B1 degradation upon autophagy inhibition was observed in this study, it will be worth exploring whether LC3-lamin B1 interaction contributes to autophagy-induced senescence. Nevertheless, autophagy has also been known to be a potential inhibitory regulator of senescence [58, 128]. It has been shown that selective autophagy could regulate the degradation of transcription factor GATA4 [128]. Unlike general autophagy, selective autophagy is highly regulated whereby the cargo are specifically selected for degradation [129]. During non-senescent condition, GATA4-p62 complex is constantly degraded by selective autophagy. However, upon senescence induction, selective autophagy is suppressed resulting in GATA4 stabilisation due to decreased GATA4-p62 interaction. Subsequently, the non-degraded GATA4 triggers a series of events which ultimately leads to activation of NF-kB-induced SASP production, thus facilitating senescence [128]. Therefore, this study led to the suggestion that the differential regulation of senescence may be dependent on type of autophagy induced.

This study establishes a key mechanism underlying post-slippage cell fate and propose a novel strategy of combining cytotoxic drugs with autophagy inhibition to tackle undesired effects of mitotic slippage-induced senescence. It is conceivable that high metabolic nature of senescent cells may depend on autophagy for nutrient source to support cellular metabolism and survival [130]. This dependence could render them selectively vulnerable to autophagic inhibition. Indeed, *in vivo* zebrafish and mice xenograft tumour models showed the reduction in metastatic potential and the arrest of tumour growth respectively, upon synergistic autophagy inhibition and antimitotic drug treatment (Figure 15 & 16). Currently, the autophagy inhibitors Chloroquine (CQ) and Hydroxychloroquine (HCQ), clinically approved for treatment of malaria, and other newly discovered, more potent autophagy-modulating

compounds are showing promising results in clinical trials in tackling chemotherapeutic resistance [38, 57, 131].

One potential limitation of this study was that no immune regulatory cells or responses were taken into considerations when elucidating the effectiveness of combination treatment using antimitotic therapies and autophagy inhibition. Indeed, it had been proposed that autophagy activation in malignant cells could potentiate the effectiveness of immunogenic chemotherapy and radiation therapy [132]. The beneficial effects of autophagy inducers had been implied by the increased effectiveness of cisplatin or radiation treatment in breast carcinoma when treated in combination with starvation or caloric restriction [133, 134]. Both starvation and caloric restriction are well-known potent inducers of autophagy [39, 135, 136]. Furthermore, autophagy-deficient tumours from melanoma had been shown to be non-responsive to immunogenic chemotherapy [137]. As such, these studies show that promoting autophagy, rather than inhibiting autophagy might be a more clinically relevant strategy. It remains uncertain whether the autophagy-mediated SASP factors triggered by post-slippage cells could reactivate tumour-specific immune response. In post-slippage settings, one could speculate that since there is no significant upregulation of cytokines such as interleukin 2 (IL-2), interleukin (IL-12) and interferon gamma (IFNγ) that are responsible for pro-tumour immunity [138, 139]. More work will be needed to determine the role of post-slippage senescence and SASP in mediating cancer immunosurveillance.

5. CHAPTER 3: LIPID ACCUMULATION FACILITATES MITOTIC SLIPPAGE-INDUCED ADAPTATION

5.1 Background and Rationale

Aberrant lipid accumulation in cancer cells has emerged as a possible diagnostic and therapeutic target. As mentioned earlier, lipid build-up during chemotherapy treatment could be a stress response that precedes death, or promotes cell survival through supplying energy demand or inducing cellular senescence [72, 80, 82, 83, 140]. During the investigation on post-slippage cell fate, it was unexpectedly discovered that lipid droplets (LD) were present in antimitotic-treated U2OS cells. Using a differential interference contrast (DIC) microscope with 40x objective magnification, the label-free LD appear as relative large and highly refractive round droplets [141]. These findings prompted us to investigate the mechanisms and functional consequences of lipid or LD accumulation in post-slippage cells.

5.2 Results

5.2.1 Antimitotic drugs induce lipid accumulation in mitotic-arrested and post-slippage cells.

To determine the effects of antimitotic drugs in modulating lipid metabolism, I treated mitotic slippage-prone osteosarcoma U2OS cells with Nocodazole (Noc), an antimitotic drug targeting microtubule polymerization, and assessed lipid accumulation in these cells. Post-slippage U2OS cells stained with Oil Red O (ORO), a dye that stains neutral triglycerides and lipids, displayed an increase in cytoplasmic lipid droplets (LD) compared to DMSO-treated control (Figure 18a-b). Combinatorial treatment of cells with Noc and Triascin C (TC), a potent inhibitor of long fatty acyl CoA synthetase (ACS) were able to significantly reduce LD accumulation in post-slippage cells. ACS is an essential enzyme involved in the biogenesis of lipid droplet [142, 143]. A corresponding induction of LD accumulation was also observed upon treatment of Noc in HCT116 human colon carcinoma and MDA-MB-231 breast adenocarcinoma cell lines treated with Noc (Figure 18c-d). Flow cytometric analysis of LD by BODIPY 493/503 staining also confirmed the accumulation

of LD in post-slippage cells (Figure 18e). Consistent with the above observations, induction of mitotic slippage by various classes of antimitotic drugs such as Taxol, Monastrol (Mon) and ZM447439 (ZM) also showed build-up in LD formation (Figure 18f). Monastrol is an inhibitor of mitotic kinesin, Eg5 that arrests cells in mitotic with monoastral spindles [144]. ZM447439 is an inhibitor of Aurora-B kinase that functions in the attachment of mitotic spindle to the centromere during mitotic transition [145].

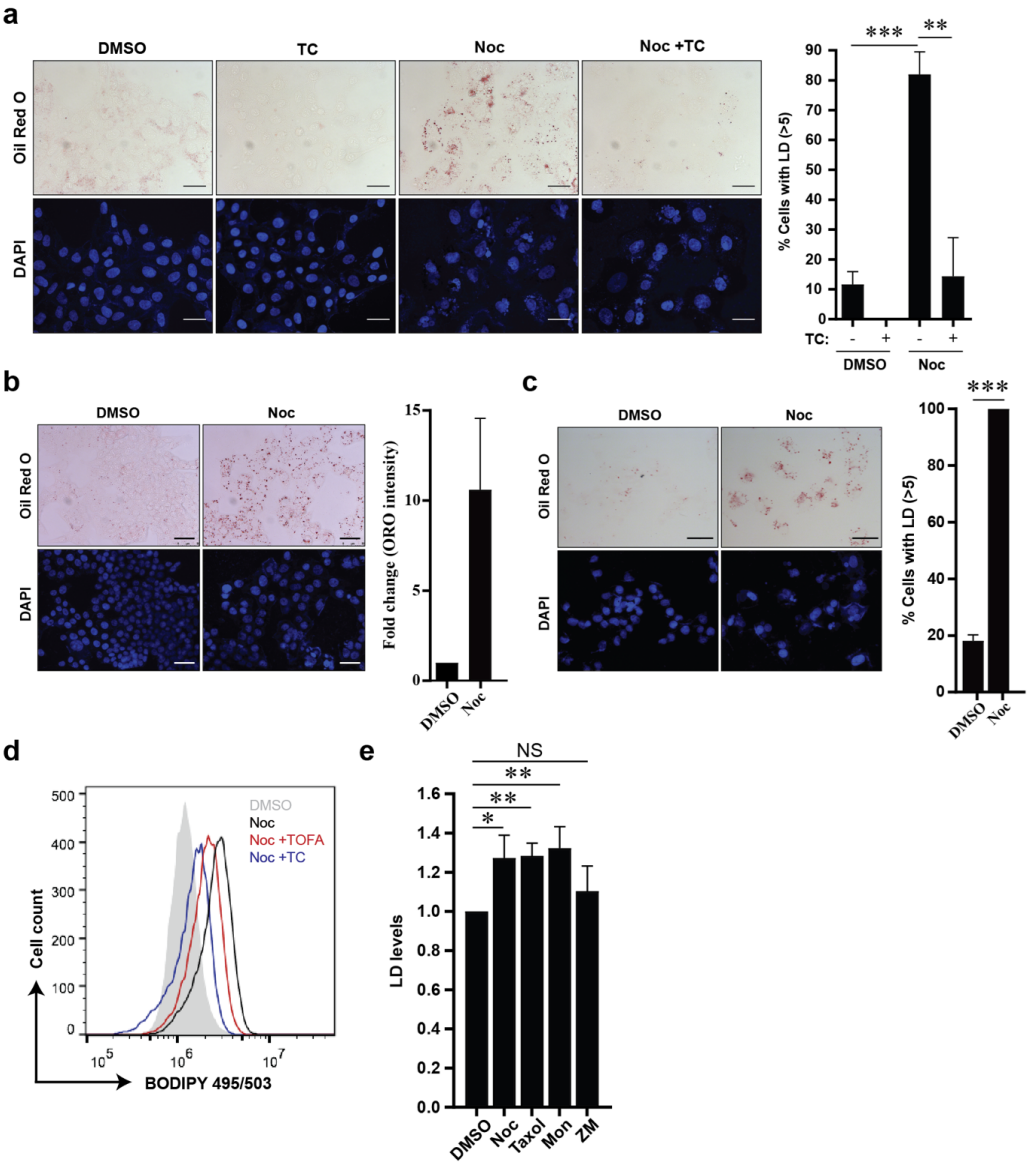

Figure 18. Antimitotic drugs induce lipid accumulation in post-slippage cells.

(a) Representative images of U2OS cells treated with DMSO or Noc in the presence or absence of Triascin C (TC) for 48 h before staining with Oil Red O. Scale bar: 50 µm. (b) Quantification of cells with >5 LDs from (a). Data are mean ± s.d. of 3 independent experiments. (c) Left: Representative images of HCT116 cells treated with DMSO or Noc for 48 h before staining with Oil Red O (ORO). Scale bar: 50 µm. Right: Quantification of ORO intensity by ImageJ software. Data are mean ± s.d. of 2 independent experiments. (d) Left: Representative images of MDA-MB-231 cells treated with DMSO or Noc for 48 h before staining with Oil Red O (ORO). Scale bar: 50 µm. Right: Quantification of cells with >5 LDs. Data are mean ± s.d. of 2 independent experiments. (e) Flow cytometry analysis of U2OS cells treated with Noc alone or in combination with 1µM TC or 10µM TOFA. Cells are stained for LD using BODIPY 493/503. (f) LD levels in cells treated with different classes of anti-mitotic

drugs for 48 h and analyzed using flow cytometry. The mean fluorescence intensity values of the total cell population for each sample were converted to ‘‘LD levels’’ in the graphs. Data are mean ± s.d. of 3 independent experiments. *p<0.05, **p<0.005, ***p<0.001 and NS=not significant by Student’s t-test.

To unbiasedly quantitate the accumulation of lipid in post-slippage cells, I performed mass spectrometry analysis on DMSO-treated (control) and Noc-treated U2OS cells. MS data revealed that post-slippage cells induce significant upregulation of the lipid species triglycerides that constitute the major components of LD (Figure 19) (Table 4).

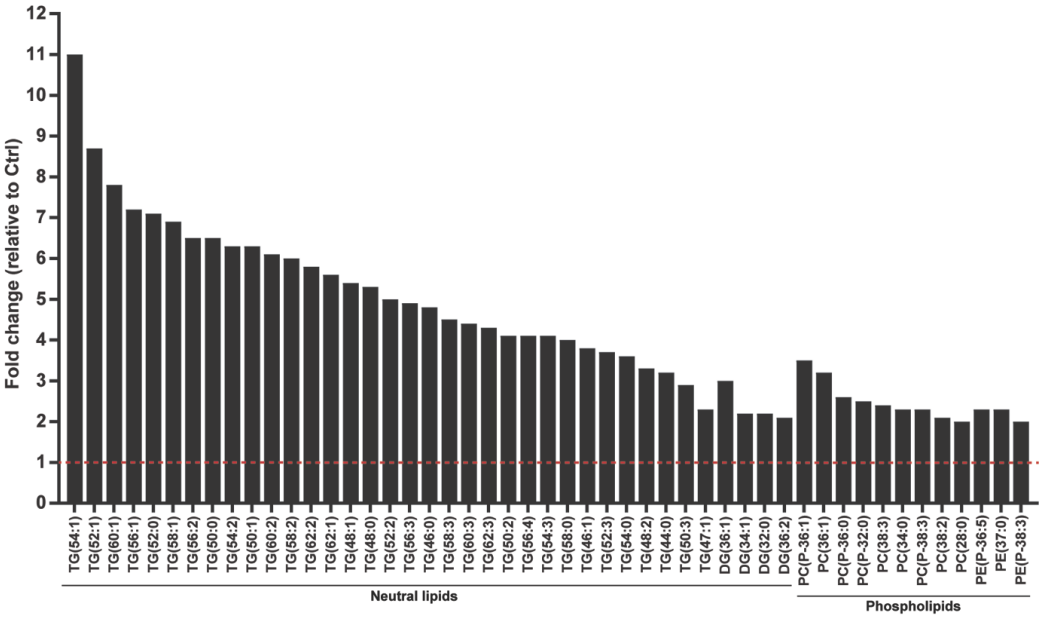

Figure 19. Nocodazole-induced post-slippage cells contain elevated level of triglycerides.

U2OS cells were treated with Noc for 48 h and collected for lipidomic analysis by liquid chromatography and mass spectrometry. Each class of lipids was normalised with internal standard. Lipids identified were matched by Lipid Maps and confirmed with MS/MS data. Lipids shown were greater than 2-fold change (p>0.05) with respect to DMSO-treated (Ctrl) cells. The lists of lipid species with the specific fold change are shown in table 4.

Prior to mitotic slippage, cells treated with antimitotic drugs undergo mitotic arrest that may trigger the onset of lipid accumulation [102, 146]. A

rapid mitotic slippage with shorter mitotic arrest as shown by treatment with ZM447439 – a drug that has the ability to overcome the SAC, do not induce significant LD in post-slippage cells (Figure 18e). To determine if post-slippage lipid accumulation originates from mitotic arrest, I analysed mitotically-arrested U2OS cells for the presence of LD and observed that over 50% of mitotic-arrested cells were observed to contain LD (Figure 20). Combinatorial treatment of cells with Noc and TC were able to significantly reduce LD accumulation in mitotic-arrested cells. Furthermore, mitotic-arrested cells cultured in serum-depleted medium (-FBS) also deplete LD. All these findings suggest that antimitotic drug-induced lipid accumulation do originate from mitotic arrest.

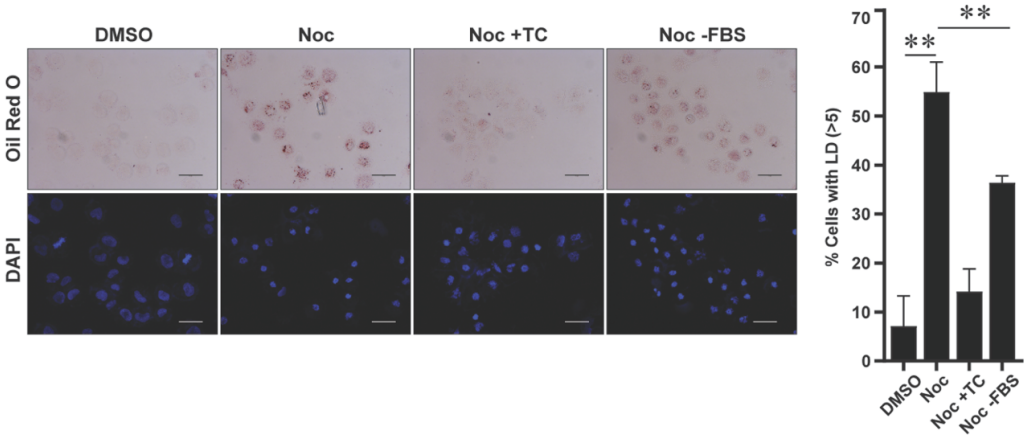

Figure 20. Nocodazole-induced lipid accumulation in mitotic-arrested cells.
Left: Representative image of U2OS cells treated with Noc alone or in the presence of TC for 24 h and stained for Oil Red O (red) and DAPI (blue). Scale bar: 50 μm. Right: Quantification of cells with >5 LDs. Data are mean ± s.d. of 3 independent experiments. **p<0.01 by Student's t-test.

5.2.2 **Fatty acid uptake contributes to lipid accumulation in post-slippage cells.**

Accumulation of lipid induced by anticancer drugs such as bevacizumab was shown to be due to the increased uptake of fatty acid (FA) from the surrounding environment [147]. As such, I hypothesised that extracellular FA may contribute to lipid accumulation in our context. To this end, I investigated the effect of Noc treatment on FA uptake in U2OS cells. Significant

upregulation in the rate of fatty acid uptake was observed in Noc-treated U2OS cells as compared to DMSO-treated control (Figure 21a-b). The microarray analysis of gene expression in Noc-induced post-slippage cells revealed a significant enrichment of FABP4 mRNA as compared to DMSO-treated cells (Accession number: GSE114515) (Table 5). Fatty acid-binding proteins (FABPs) belong to a family of cytoplasmic proteins known to be involved in FA uptake and transport [147, 148]. I assessed the expression of FABPs in our post-slippage cells and as expected, the mRNA expression of FABP4 is significantly elevated in post-slippage U2OS cells (Figure 21c). To determine if FABP4 promotes Noc-induced LD accumulation, I co-treated cells with Noc and the small molecule inhibitor of FABP4 (BMS309403) and observed that inhibition of FABP4 resulted in a modest reduction in LD level in Noc-treated cells (Figure 21d). All the above suggest that FABP4 mediates enhanced FA uptake that partly contributes to LD accumulation in post-slippage cells.

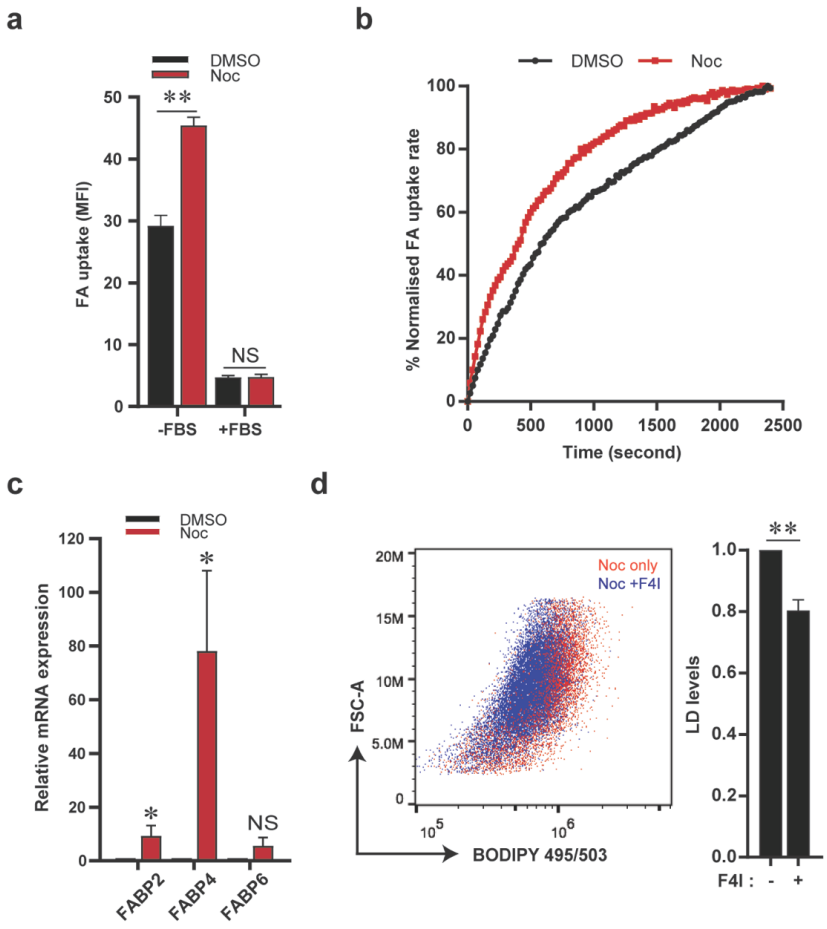

Figure 21. Enhanced fatty acid uptake in post-slippage cells contributes to LD accumulation.

(a) FA uptake in U2OS cells treated with DMSO or Noc for 48 h. Serum starvation (SS) is performed after drug treatment to stimulate FA uptake. Negative control of FA uptake assay in full serum (FBS) condition. Measurement of FA uptake in cells was quantified by mean fluorescence intensity (MFI). Data are mean ± s.d. of 3 independent experiments. (b) Representative plot of fatty acid uptake kinetic performed as per (a). (c) Synchronised U2OS were treated with DMSO or Noc for 48 h and analysis for FABP mRNA expression. (d) Flow cytometry analysis of U2OS cells treated with Noc alone or in combination with different concentration of FABP4 inhibitor (F4I). Cells are stained for LD using BODIPY 493/503. Data are mean ± s.d. of 3 independent experiments. *p<0.05, **p<0.005 and NS=not significant by Student's t-test.

5.2.3 **Blocking lipid biosynthesis suppresses cellular stress and promotes survival of post-slippage cells.**

It remains unclear as to whether LD accumulation upon antimitotic drug treatment promotes survival or drives cell death. To ascertain this, I evaluated the sensitivity of U2OS cells treated with various classes of antimitotic drugs to assess correlation with their respective LD level post-drug treatment. The augmented accumulation of LD observed in cells treated with more potent antimitotic agents (Figure 22a) suggests that LD accumulation is associated with cell death post-antimitotic treatment. To further characterise the link between LD accumulation and antimitotic-induced cell death, I blocked lipid accumulation with pharmacological inhibitor of lipid biosynthesis, 5-tetradecyl-oxy-2-furoic acid (TOFA). TOFA inhibits the rate-limiting enzyme of fatty acid biosynthesis pathways, Acetyl-CoA carboxylase (ACC) which converts Acetyl-CoA to Malonyl-CoA. Co-treatment of Noc and TOFA were able to further reduce the accumulation of LD (Figure 18d) and promote the short- and long-term survival of post-slippage cells (Figure 22b-d).

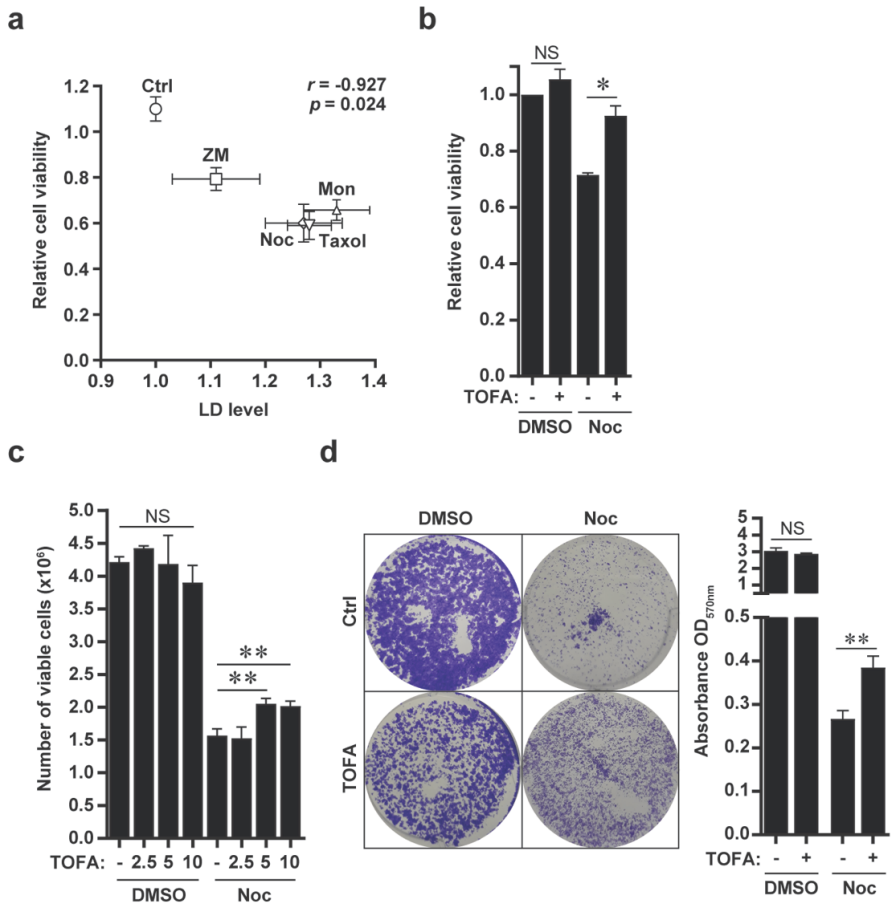

Figure 22. Lipid biosynthesis inhibitor TOFA promotes the survival of post-slippage cells.

(a) Cell viability and LD level of U2OS cells after 48 h of treatment with the respective antimitotic drugs. Cell viability was compared to the LD level and Pearson correlation coefficients were calculated. (b) Synchronised U2OS cells were treated with DMSO or Noc in the presence or absence of TOFA for 48 h, followed by reseeding for 24 h before performed Celltitre®96 one aqueous assay (Promega). Data are mean ± s.d. of 2 independent experiments. (c) Synchronised U2OS cells were treated with DMSO or Noc alone or in combination with TOFA for 48 h before quantifying the number of viable cells. Data are mean ± s.d. of 3 independent experiments. (d) Left: Long-term clonogenic assay of U2OS cells treated with DMSO or Noc in the presence or absence of TOFA. Cells were treated with indicated drugs for 48 h, followed by replacing cells with fresh media for another 5 days before performing crystal violet staining. Right: Plot shows the absorbance (OD570nm) derived from quantification of crystal violet staining. Data are mean ± s.d. of 3 independent experiments. *p<0.05, **p<0.01 and NS=non-significant by Student's t-test.

It is known that post-slippage cells often acquired extensive DNA damage from prolonged mitotic arrest and multinucleation [149]. I observed that TOFA-treated post-slippage cells have a dramatic reduction in DNA damage and ROS levels in TOFA-treated post-slippage cells as compared to the LD-laden post-slippage cells (Figure 23a-b).

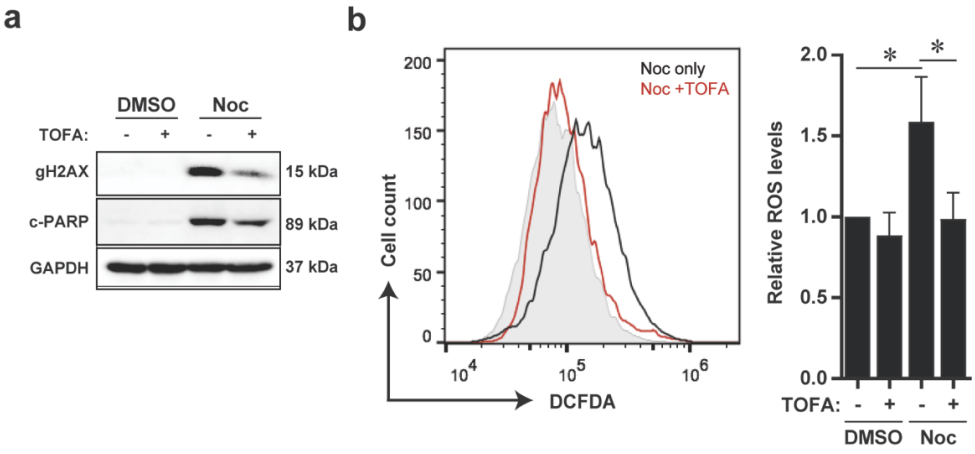

Figure 23. Lipid biosynthesis inhibitor TOFA suppresses DNA damage and ROS production of post-slippage cells.

(a) Western blot of U2OS cells treated with the respective drugs for 48 h (b) Left: Flow cytometry analysis of synchronized U2OS cells treated with the indicated drugs for 48 h, followed by DCFDA staining. Right: Quantification of ROS level in U2OS cells treated with the indicated drugs for 48 h. Data are mean ± s.d. of 3 independent experiments. *p<0.05 by Student's t-test.

Previous studies have shown that the duration of mitotic arrest dictates the extent of post-slippage multinucleation and DNA damage [150]. As such, it is hypothesised that lipid inhibition by TOFA may reduce the duration of mitotic arrest and promotes early slippage upon nocodazole treatment. Our results showed an increased degradation of cyclin B1, a trigger of mitotic exit [5] and the reduction of pH-H3 levels when cells are co-treated with Noc and TOFA (Figure 24a-b); where mitotic exit is known to be triggered by the rapid degradation of cyclin B1. I validated our observations using live cell imaging microscopy to discern the duration of mitotic arrest in the cells by measuring the time between cell rounding to mitotic slippage. A significant reduction in the duration of mitotic arrest was observed when cells were co-treated with

TOFA and Noc (Figure 24c-d). All the above suggest that blocking lipid biosynthesis by TOFA reduces the duration of Noc-induced mitotic arrest which in turn decreased DNA damage and ROS levels in post-slippage cells possibility leading to their subsequent survival.

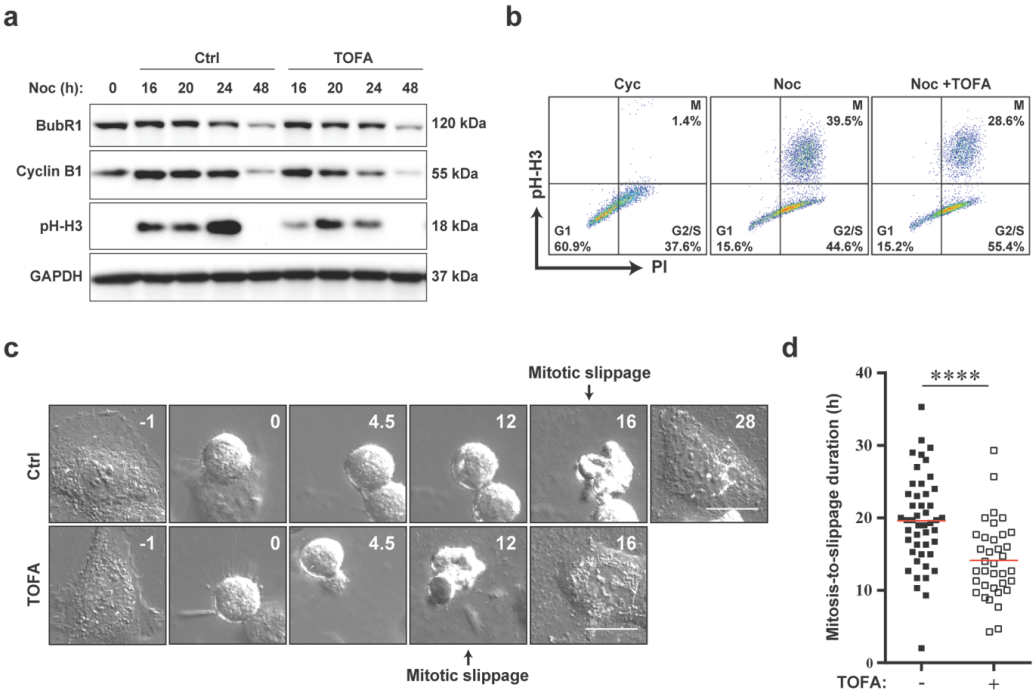

Figure 24. TOFA reduces the duration of Noc-induced mitotic arrest.

(a) Synchronised U2OS cells were treated with Noc in the presence or absence of 10 μM TOFA for the indicated time point before performing western analysis. (b) Flow cytometry analysis of mitotic cells using pH-H3/PI. Representative plots of U2OS cells treated with DMSO (Control) or Noc in the presence or absence of TOFA for 24 h. G1: G1 phase of cell cycle; M: Mitosis; G2/S: G2/S phase of cell cycle. (c) Frame of individual U2OS cells entering mitosis and undergoing mitotic slippage. Cells were treated with Noc in the presence or absence of TOFA. Numbers represent time relative to mitotic entry in hours. Scale bar: 25 μm. (d) A single representative experiment is plotted measuring the duration of mitotic arrest in U2OS cells treated with Noc in the presence or absence of TOFA. n=47 without TOFA, n=36 with TOFA. ****p<0.001 by Student's t-test.

5.2.4 **Lipid biosynthesis regulates the production of post-slippage inflammatory factors and its effect on cell migration and invasiveness.**

It has been shown that post-slippage cells enter senescence, exhibit SASP and secrete pro-inflammatory factors such as IL-6, IL-8 and IL-1β which promote paracrine pro-tumourigenic effects such as migration, invasiveness and angiogenesis [151]. With regards to lipid metabolism, it has recently been revealed that therapy-induced senescent cells promote the build-up of lipids that potentially contribute to senescence induction [80]. To determine whether lipid biosynthesis regulates post-slippage senescence, TOFA-treated post-slippage cells were stained with senescence-associated marker beta-galactosidase (SA-β-gal). SA-β-gal staining revealed no discernible difference in senescence establishment when post-slippage cells were treated with TOFA (Figure 25a). In addition, no discernable changes were observed in the expression of senescence-associated lamin B1 and p21 between control and TOFA-treated post-slippage cells were observed (Figure 25b), confirming that TOFA treatment did not affect post-slippage senescence induction.

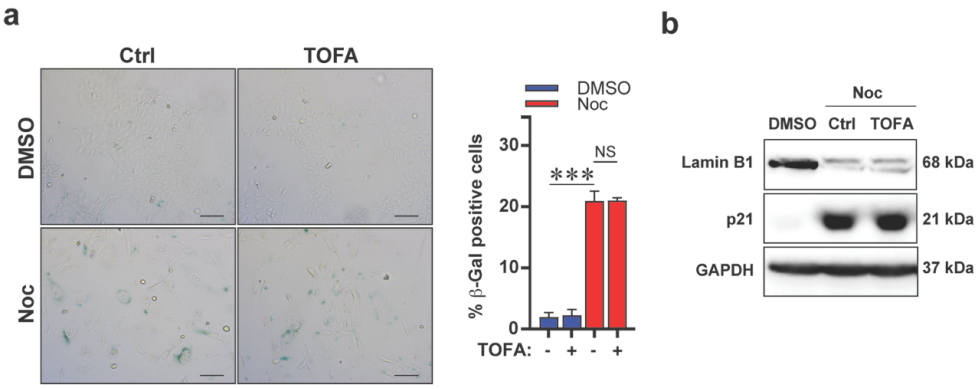

Figure 25. TOFA treatment does not affect post-slippage senescent cells.

(a) Left: Representative images of control or post-slippage cells treated with TOFA for 48 h before performing b-gal assay. Scale bar: 100 μm. Right: Plot shows percentage of cells stained positively for β-gal. Data are mean ± s.d. of 3 independent experiments. (b) Representative blot of synchronized U2OS cells treated with Noc for 48 h before subjecting the cells with various concentration of TOFA for another 48 h. ***p<0.001 and NS=non-significant by Student's t-test.

Next, I determined whether lipid biosynthesis regulates the production of pro-tumorigenic factors in post-slippage cells by treating Noc-induced post-slippage cells with TOFA for the analysis of pro-inflammatory factor secretion (Figure 26a). Consistent with previous findings, post-slippage cells showed increased secretion of several cytokines and chemokines such as IL-6, IL-8 and IL-1β (Figure 26b). However, treatment of TOFA in post-slippage cells also showed an amplified secretion of pro-tumourigenic factors such as IL-6 and IL-8 as compared to DMSO-treated post-slippage cells (Figure 26b). A dose-dependent increase in the expression of IL-8 and IL-1β is detected upon treatment of post-slippage cells with TOFA (Figure 26c). Treatment of TOFA in U2OS cells did not induce the expression of IL-8 and IL-1β, suggesting that TOFA specifically regulates pro-inflammatory factors post-slippage. To assess whether TOFA affects the migratory and invasiveness induced by post-slippage secretory factors, CM from control or TOFA-treated post-slippage cells were collected and performed scratch wound healing assay and transwell invasion assays. CM obtained from DMSO-treated post-slippage cells promoted the rate of wound closure and transwell invasiveness validating the ability of Noc-induced post-slippage cells in promoting migratory and invasiveness in the tumor microenvironment (Figure 26d-e). Interestingly, CM from TOFA-treated post-slippage cells containing elevated pro-tumourigenic factors further potentiated the migratory and invasive capabilities compared to DMSO-treated post-slippage cells (Figure 26d-e).

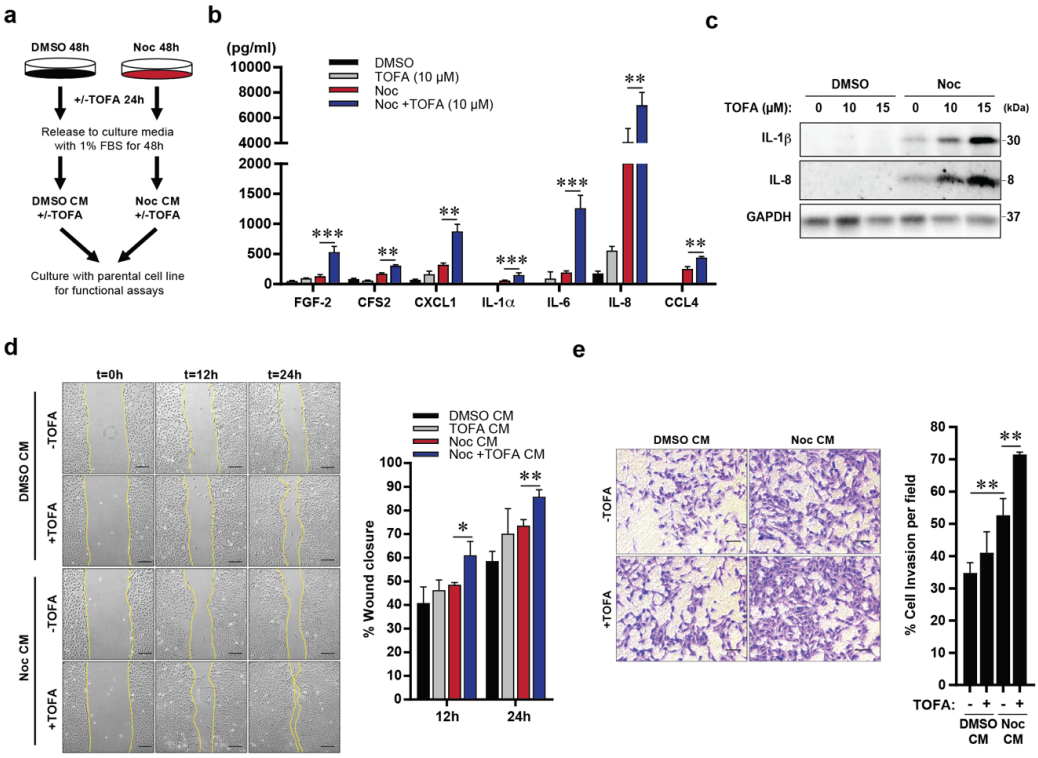

Figure 26. TOFA enhances motility and invasiveness induced by post-slippage secretion.

(a) Scheme depicts the preparation of CM for Human cytokine/chemokine multiplex array and for determination of paracrine tumorigenic effects. (b) The concentrations of various cytokines/chemokines in the CM derived from the respective treatments using Human cytokine/chemokine array. Data are mean ± s.d. of 3 independent experiments. (c) Representative blot of synchronised U2OS cells treated with Noc for 48 h before subjecting the cells with various concentration of TOFA for another 24 h. (d) U2OS cells were incubated with their respective CM and subjected to scratch wound healing assay. Left: Representative images of CM-treated U2OS cells taken at 0 h and the indicated time intervals. Scale bar: 100 μm. Right: Plot shows percentage of wound closure. (e) Right: Invasive ability was assessed by Transwell Matrigel assay. Scale bar: 100 μm. Left: Plot shows percentage of invasive cells. Representative data from 3 independent experiments. *p<0.05, **p<0.01 and ***p<0.001 by Student's t-test.

To confirm the effect of lipid inhibition on post-slippage inflammatory factors, Noc-induced post-slippage cells were treated with another inhibitor of lipid biosynthesis, C75 and analysed their expression and secretory profiles of several cytokines and chemokines. C75 inhibits fatty acid synthase (FASN) activity that are direct downstream of Acetyl-CoA carboxylase (ACC) [68].

Surprisingly, contrary to TOFA, co-treatment with C75 suppressed the secretion of several cytokines and chemokines such as IL-6, IL-8 and IL-1β (Figure 27). In addition, CM derived from post-slippage cells co-treated with C75 attenuated the migratory and invasive capabilities (Figure 27). Our data suggests that lipid biosynthesis pathways in post-slippage cells differentially regulate the production of inflammatory factors that leads to associated pro-tumourigenic effects such as invasion and migration.

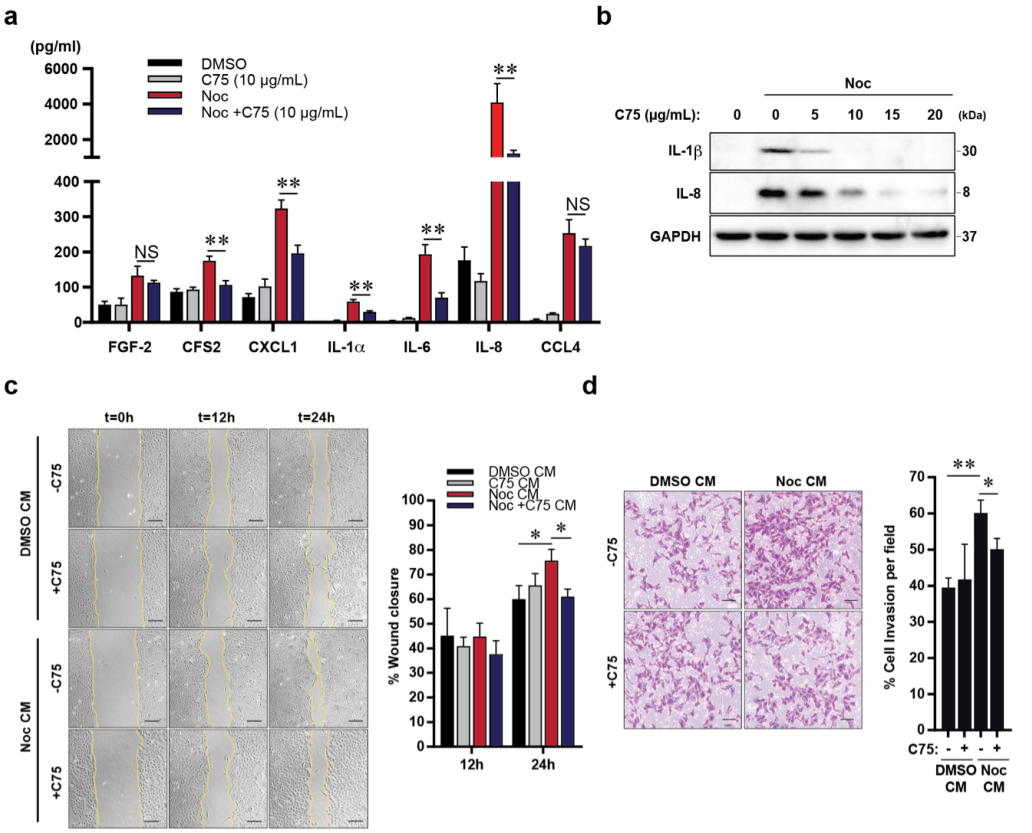

Figure 27. C75 abrogates motility and invasiveness induced by post-slippage secretion.

(a) The concentrations of various cytokines/chemokines in the CM derived from the respective treatments using Human cytokine/chemokine array. Data are mean ± s.d. of 3 independent experiments. (b) Representative blot of synchronised U2OS cells treated with Noc for 48 h before subjecting the cells with various concentration of C75 for another 24 h. (c) U2OS cells were incubated with their respective CM and subjected to scratch wound healing assay. Left: Representative images of CM-treated U2OS cells taken at 0 h and the indicated time intervals. Scale bar: 100 μm. Right: Plot shows percentage of wound closure. (d) Right: Invasive ability was assessed by Transwell Matrigel assay. Scale bar: 100 μm. Left: Plot shows percentage of invasive cells.

Representative data from 3 independent experiments. *p<0.05, **p<0.01 and NS=non-significant by Student's t-test.

5.2.5 **Lipid inhibition by C75 modulates post-slippage induced NF-κB activation.**

The production of pro-tumourigenic cytokines such as IL-1, IL-6 and IL-8 are known to be induced by NF-kappaB family of transcriptional factors [152]. Previous reports have also described activation of NF-κB dependent inflammatory response upon paclitaxel treatment in multiple cancer cells [153-155]. Hence, one could predict that the suppression of pro-tumourigenic inflammation by C75 in post-slippage cells could be due to the suppression of NF-κB activation. In agreement with other reports, western blot analysis revealed the enhanced phosphorylation of IκBα and p65 in Noc-treated post-slippage cells, suggesting that NF-κB pathway is activated in post-slippage cells (Figure 28a). Interestingly, treatment of post-slippage cells with C75 suppressed NF-κB activation as shown by reduced IκBα and p65 phosphorylation compared to untreated post-slippage cells (Figure 28b). This was further confirmed by the modest reduction of nuclear p65 in C75-treated post-slippage cells as compared to the untreated control (Figure 28c). These results suggest that lipid inhibition by C75 suppressed the expression of inflammatory factors via NF-κB inactivation and subsequently perturbed the pro-tumorigenic effects induced by post-slippage cells.

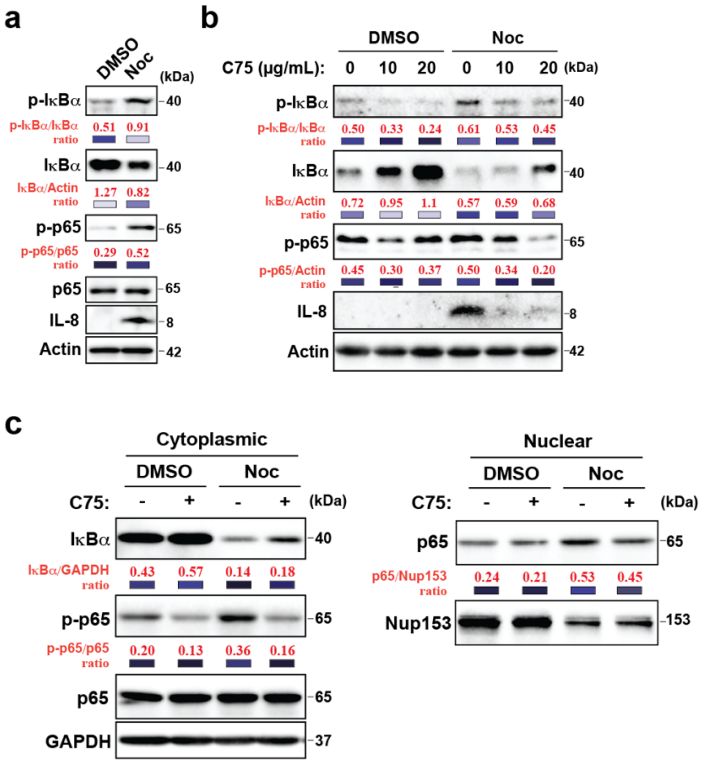

Figure 28. C75 inhibits Noc-induced NF-kB activation.

(a) Representative blot of synchronized U2OS cells treated with DMSO or Noc for 48 h and release into drug-free media for another 24 h. (b) Representative blot of synchronised U2OS cells treated with Noc for 48 h before subjecting the cells with various concentration of C75 for another 24 h. (c) Representative blot of synchronised U2OS cells treated with Noc for 48 h before subjecting the cells with 15 μg/mL of C75 for another 24 h. Collected cells were subjected to nuclear/cytoplasmic extraction followed by IB. GAPDH and Nup153 function as control markers for cytoplasmic and nuclear extraction respectively.

5.3 **Discussion**

Although many anticancer drugs could induce lipid accumulation in cancer cells [73, 74, 80, 146, 156, 157], the consequences of this phenomenon remain uncertain and could affect the efficacy of anticancer drugs. In this study, I explored the role of lipid metabolism in regulating cell fate upon antimitotic drugs treatment. Our results revealed that antimitotic drug treatment induced the accumulation of lipid in both mitotic-arrested and post-slippage cells. Lipid accumulation upon chemotherapy can be triggered by several mechanisms such as enhanced lipogenesis, increased uptake of lipids and inhibition of fatty acid (FA) oxidation [158]. The accumulation of lipid content in post-slippage cells was partly contributed by an increase in FABP4-mediated FA uptake. FABP4 is known to be upregulated in many aggressive cancers as well as recurrent tumours to facilitate the uptake and transport of extracellular FA from adipocytes to mitochondria for β-oxidation [159-161]. More work will have to be done to delineate the role of FABP4 in mediating post-slippage cell fate. Nevertheless, lipid accumulation upon antimitotic drugs treatment can also occur from the defective or loss of mitochondria during mitotic arrest [97]. As such, impairment of mitochondrial β-oxidation promotes LD formation by diverting fatty acid (FA) toward storage [72, 73].

The duration of mitotic arrest is known to be tightly linked to the extent of multinucleation and DNA damage following mitotic slippage [149]. I did not observe any significant increase in LD level in cells treated with ZM447439, a drug that shorten the duration of mitotic arrest by overcoming the spindle assembly checkpoint. Blocking lipid biosynthesis by TOFA promoted early mitotic slippage, suggesting a role for lipids in ensuring proper mitotic progression. Support for this can be garnered from the finding that siRNA-mediated depletion of lipid biosynthesis enzymes such as DGAT2 (a TAG synthesizing enzyme) resulted in defective cell division, reminiscent of mitotic slippage [162]. Incidentally, secreted factor(s) from tumour-associated macrophages (TAMs) were recently found to suppress the cytotoxicity effects of antimitotic agents by promoting early mitotic slippage and cancer cell survival following paclitaxel treatment [163]. It will be of interest to investigate

whether TAMs engender mitotic slippage via modulation of lipid biosynthetic pathways.

Several inflammatory signaling pathways had been proposed to be activated by multinucleated cells [164]. Our previous study had shown that pro-tumorigenic inflammatory factors were secreted by post-slippage senescent cells [165]. Inhibition of autophagy abrogates the induction of post-slippage senescence and its associated secretion of inflammatory factors. Although the inhibition of lipid biosynthesis did not affect the establishment of post-slippage senescence, we observed an alteration in the secretory profile of post-slippage cells. The inhibition of ACC and FASN by TOFA and C75 respectively, promote opposing effects on the production of post-slippage secretory factors and the subsequent tumour-promoting effects (Figure 8). This disparity could result from the regulation of mitochondrial fatty acid (FA) oxidation by the different lipid inhibitors used in post-slippage cells. FA oxidation is known to regulate the expression and secretion of cytokines in various cell types such as in oncogene-induced senescent cells, tumour-associated macrophages and myeloid-derived suppressor cells [166-169]. It was speculated that TOFA treatment decreases the level of Malonyl-COA which prevents inhibition of FA oxidation [170]. On the contrary, inhibition of FASN by C75 promotes the accumulation of Malonyl-COA, further suppressing FA oxidation and the subsequent production of pro-tumorigenic factors [79, 171]. Alternatively, pro-tumorigenic factors could be altered by FA levels and saturation. It has been shown that fatty acids induce the expression and secretion of inflammatory cytokines such as IL-6, IL-8 and IL-1β via activation of nuclear factor-kappaB (NF-kB) pathway in normal and cancer cells [172-174]. Indeed, our data revealed that C75 suppressed the activation of NF-κB in post-slippage cells supports the notion that increased lipid or FA promotes the induction of post-slippage secretory factors. Another plausible inflammatory pathway involved could be through the lipid mediators such as prostaglandin that are produced through conserved lipid biosynthesis pathways involving specific enzymes such as ACC and FASN. Collectively, our data suggests that lipid biosynthesis is involved in the modulation of pro-tumorigenic factors induced by post-slippage cells.

Apart from the enhanced cell migration and invasiveness induced by post-slippage secretory factors, a distinct inflammatory response could also influence immune cells infiltration and the subsequent clearance of post-slippage cells [151]. On the contrary, the pro-tumorigenic cytokines secreted can also stimulate the polarization of M1 macrophages into M2 tumour-associated macrophage (TAMs) that further enhance the pro-tumorigenic properties of surrounding tumour cells [168]. Furthermore, paclitaxel treatment induces the infiltration of TAMs into mammary adenocarcinoma and suppresses antitumor T-cell response [154]. Therefore, more studies will be needed to be determine the effect of antimitotic-induced pro-tumourigenic factors on immune cells or the tumour microenvironments and whether lipid metabolism mediates the tumourigenic effects.

In conclusion, it was demonstrated that the alterations of lipid biosynthesis in antimitotic-treated cells by pharmacological inhibitors had implications on the survival and tumour-promoting effects of post-slippage cells (Figure 29). Inhibition of lipid accumulation could promote early mitotic slippage and contributes to the survival of post-slippage cells. Post-slippage secretory factors can be fine-tuned by modulation of lipid biosynthesis through NF-κB-dependent manner. Our study highlights the potential of targeting lipid biosynthesis in post-slippage cells to reprogram its secretory profile that not only could negate the tumour-promoting effects, but may also promote anti-tumour inflammation for the clearance of tumour or post-slippage cells.

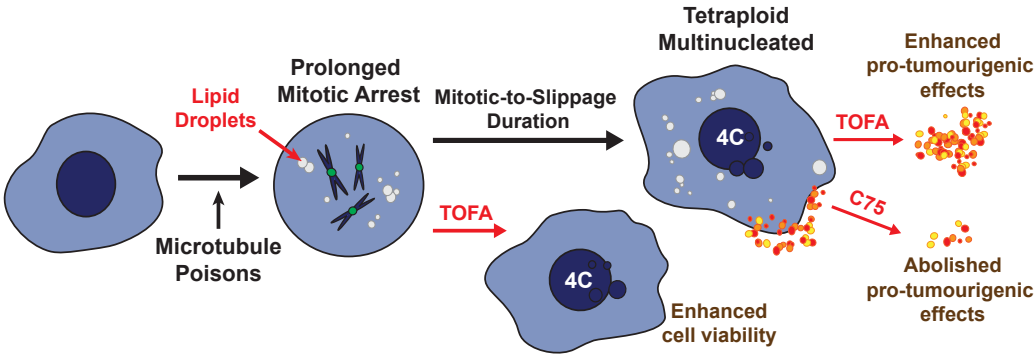

Figure 29. Proposed model depicting the role of lipid biosynthesis in the regulation of cell fate upon antimitotic drugs treatment.

Upon treatment with antimitotic drugs, mitotic-arrested cells accumulate lipid droplets (LDs) that persist throughout mitotic slippage. Co-treatment of lipid biosynthesis inhibitor, TOFA and antimitotic drugs shorten the duration of mitotic arrest resulting in LD-depleted post-slippage cells. Treatment of TOFA in post-slippage cells amplifies the secretion of tumour-promoting inflammatory factors and its associated effects, whereas an opposing phenomenon was observed upon treatment with another lipid inhibitor, C75.

6. CHAPTER 4: ANTI-MITOTIC DRUG TREATMENT INDUCED THE EXPRESSION OF HEXOKINASE 2 IN CANCER CELL LINES

6.1 Background and Scope

Metabolic reprogramming is not only a consequence of malignant transformation but also observed in response to chemotherapy; particularly in chemoresistant cells. It is highly plausible that anti-mitotic drug induced post-slippage cells display alterations in their energy metabolism pathway to mediate cellular survival or cell fate post-slippage. Here, I delineate the bioenergetics change, specifically on glycolysis induced by cancer cells in response to antimitotic drugs treatment.

6.2 Results

6.2.1 Enhanced glycolysis upon treatment of cells with antimitotic drugs

Alteration in glucose metabolism has been widely reported in drug-resistant cancer cells [175-177]. A metabolic shift from oxidative phosphorylation to glycolysis is detected in paclitaxel-resistant Hela cells that are generated from prolonged exposure to non-toxic dose of paclitaxel. These cells exhibit increased expression of glycolysis-related proteins such as pyruvate kinase isozymes M1/M2 (PKM1/2), fructose-bisphosphate aldolase C (ALDOC) and lactate dehydrogenase A (LDHA) when compared to their parental cells [176]. Therefore, I first determine the glycolytic potential of antimitotic-induced post-slippage cells by analyzing the glucose consumption and lactate production. Increased aerobic glycolysis leads to more glucose consumption and lactic acid being converted from pyruvate and secrete into the microenvironment [178, 179]. Our results show the increased glucose uptake and accumulation of extracellular lactate in both Noc- and Taxol-treated U2OS cells (Figure 30a-b). The enhanced glycolysis induced by antimitotic drugs treatment was paralleled to the significant increase in intracellular ATP content in antimitotic-treated cells (Figure 30c).

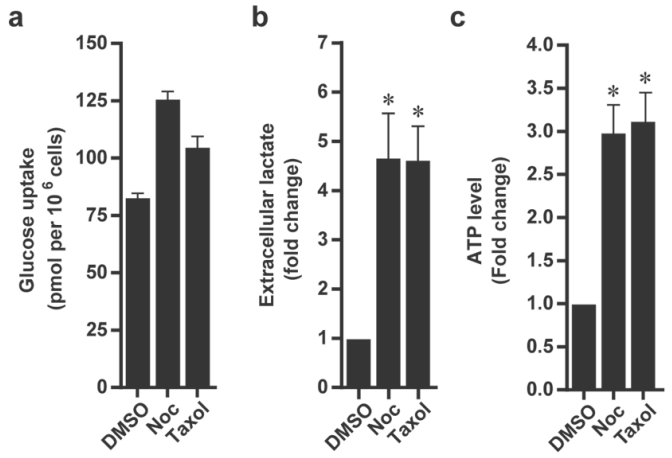

Figure 30. Antimitotic-treated cell lines exhibit enhanced glycolysis.

U2OS cells treated with Noc or Taxol and the levels of glucose uptake (a), extracellular lactate (b) and intracellular ATP (c) were determined. Experiments are performed at least twice. *$p<0.05$ by Student's t-test.

6.2.2 **Induction of HK2 expression in antimitotic-treated cells**

To further delineate the glycolysis induction, I screened the treated cells for a panel of glycolytic-related genes by real-time qPCR. Consistent with the microarray analysis of Noc-induced post-slippage cells (Table 1), I detected the significant upregulation of hexokinase 2 (HK2) in Noc- and Taxol-treated U2OS cells (Figure 31a). HK2 is the rate-limiting enzyme that mediates the first step of glycolysis and is crucial for Warburg effect in cancer cells. Next, I analysed the protein expression of HK2 in antimitotic-treated cells. 72 h treatment of U2OS cells with Noc and Taxol results in the significant induction in HK2 expression (Figure 31b). Furthermore, I detected a time-dependent increase in HK2 expression upon Noc treatment (Figure 31c). To exclude any cell-specific effects, I confirm the expression of HK2 in antimitotic drugs treated breast cancer cell lines, MCF-7 and MDA-MD-231 cells. Both breast cancer cell lines showed an appreciable increase in HK2 expression upon Noc and Taxol treatment (Figure 31d).

Gene	Fold change	*P*-value	Description
ALDOC	1.12	0.986	Fourth step of glycolysis, involved in gluconeogenesis
PDK1	-1.04	0.201	Convert pyruvate to Acetyl-CoA
HK2	1.89	0.003	Rate-limiting, first step of glucose metabolism
PFKFB3	1.16	0.038	Allosteric activator of PFK-1, stimulate glycolysis
PGK1	-1.08	0.902	First step of ATP generation in glycolysis
LDHA	-1.04	0.778	Interconversion of pyruvate and lactate

Table 1. Microarray analysis of glycolysis gene expression in post-slippage U2OS cells (Nocodazole-treated) versus control cells (untreated). Accession number: GSE114515.

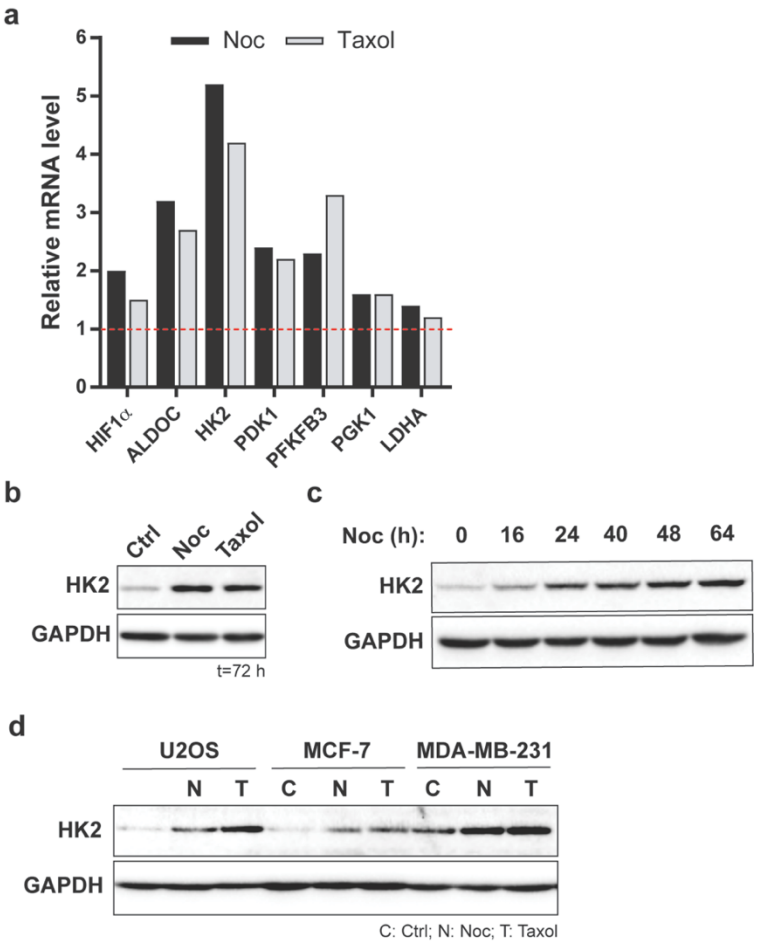

Figure 31. Antimitotic-treated cell lines induce upregulation of HK2.

(a) RT-qPCR analysis of glycolysis-related genes in U2OS cells treated with Nocodazole (Noc) or Taxol for 72 h. (b) Immunoblot analysis of U2OS cells treated with Noc or Taxol for 72 h or with Noc only in a time-dependent manner (c) and analysed for HK2 expression. (d) Immunoblot analysis of U2OS, MCF-7 and MDA-MB-231 cell lines treated with Noc or Taxol for 48 h.

6.2.3 **Effects of HK2 depletion in antimitotic-treated cells**

To delineate the role of HK2 induction upon antimitotic drug treatment, I performed a siRNA knockdown of HK2 in U2OS cells and treated the cells with Noc. I managed to obtain a strong HK2 knockdown efficiency in vehicle-treated (DMSO) and Noc-treated cells (Figure 32a). Next, I determine whether HK2 overexpression is essential for the viability of Noc-treated cells by performing a cell counting analysis. Our preliminary results showed a modest reduction in the number of HK2 knockdown cells surviving Noc treatment

(Figure 32b). However, in the absence of Noc treatment, HK2 knockdown per se also reduced the number of surviving cells suggests that HK2-dependent viability is not specific to post-slippage cells. More work will be needed to validate the effect of HK2 depletion on cell fate post-slippage.

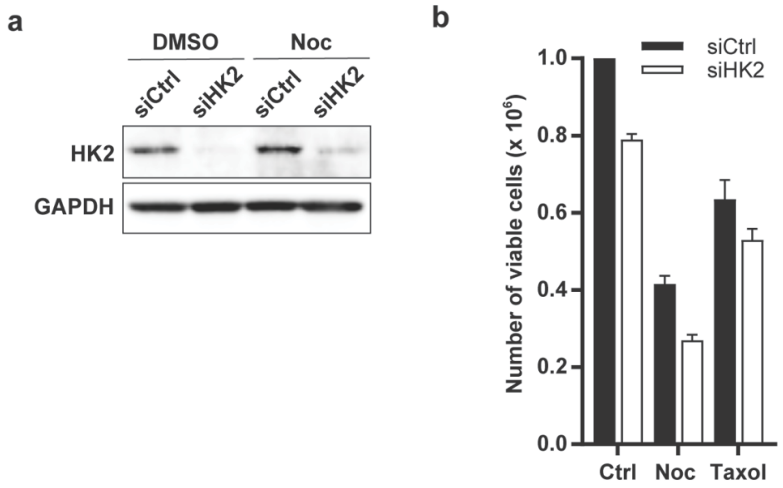

Figure 32. Antimitotic-treated cell lines induce upregulation of HK2.

(a) Immunoblot analysis of U2OS cells transfected with HK2 targeting or non-targeting control siRNA before treatment with Noc for 48 h and analysed for HK2 expression. (b) Cell viability analysis of U2OS cells pre-treated with the respective siRNA as in (a) before treatment with Noc or Taxol for 48 h. The number of viable cells were quantified using trypan blue exclusion method. Number of viable cells = Number of total cells – Number of blue cells.

6.3 Discussion

One of the key hallmarks of cancer is the elevated glycolysis essential to provide energy and carbon sources for cell growth and proliferation [178]. Thus far, few studies have reported the enrichment of glycolytic pathways upon chemotherapeutic treatment. Our data showed that antimitotic drugs treatment leads to the upregulation of glycolysis. A metabolic switch from mitochondrial oxidative phosphorylation to glycolysis occurred during mitotic arrest may have persist post-slippage [97]. Although the glycolytic dependency in mitotic-arrested cells is essential for their survival, it remains to be determined whether the enhanced glycolysis mediates cell fate post-slippage (Figure 33).

Critical to this highly glycolytic phenotype of antimitotic-treated cells is the significant upregulation of hexokinase 2 (HK2), an enzyme that catalyses the first step of glycolysis. HK2 is overexpressed in multiple cancer cells and involved in promoting cancer progression [180-182]. Our data revealed that anti-mitotic drugs induce significant increase in the expression of HK2 in multiple cancer cell lines (Figure 31). Hexokinase 2 is associated with mitochondrial and is implicated in cell survival [183]. Binding of HK2 to mitochondria has been shown to protect against loss of cell viability [184]. Although our preliminary data revealed that HK2 depletion by siRNA knockdown did not potentiate the cell death induced by Nocodazole, greater emphasis will be placed on determining whether HK2 mediates the post-slippage inflammation and the associated pro-tumorigenic effects. Recent study has also shown that high glycolytic activity of cancer cells contributes to chemotherapeutic resistance by modulating T cell-mediated antitumor immunity [185]. Several factors such as lactate and CXCL10 release by highly glycolytic tumors may be responsible for the impairment of antitumor immune response. Furthermore, it had been shown that the release of HK2 from mitochondria could triggers the activation and secretion of inflammasomes and IL-1β respectively.

Apart from mediating inflammatory response, the induction of glycolysis upon antimitotic drugs treatment may be essential for senescence transition. It has been reported that upon glucose starvation, HK2 binds and inhibits mTOR complex 1 (TORC1) resulting in the activation of autophagy

[186]. This suggest that the overexpression of HK2 in post-slippage cells could mediate the induction of autophagy and enable senescence. Therapy-induced senescence (TIS) cells generated from various anticancer agents exhibit increased glucose utilization coupled with high level of ATP and lactate production [99, 187]. In addition, blocking glycolysis with pharmacological inhibitors such as 2-DG (2-Deoxy-D-glucose) promotes the switch from senescence establishment to elimination by apoptosis. More work will be required to delineate the implications of HK2 in mediating cell fate post-slippage.

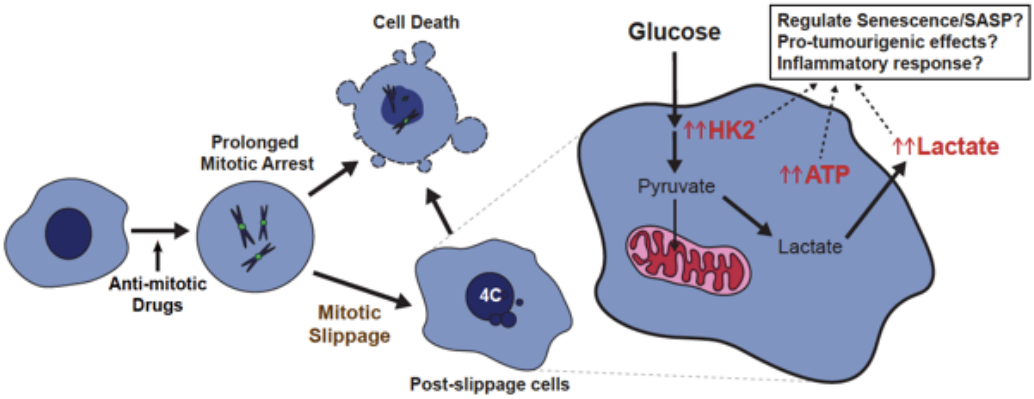

Figure 33. Proposed model depicting the potential effects of enhanced glycolysis in regulating post-slippage cell fate.

Antimitotic-treated post-slippage cells acquire an enhanced glycolytic phenotype through the upregulation of glycolytic gene, hexokinase 2 (HK2). Post-slippage cells displayed increased in ATP and lactate levels that may regulate senescence transition or pro-tumourigenic inflammation.

7. FUTURE DIRECTIONS

7.1 Crosstalk between post-slippage SASP and the tumour microenvironment

One major limitation of this study is the lack of preclinical validation on the efficacy of combination treatment (autophagy inhibitors and antimitotic therapies) where the host immune system is intact and taken into consideration. Tumour-immune system interaction has major implications on the prognosis of patients [188]. Multiple studies have reported the beneficial role of autophagy activation in promoting the elimination of tumour cells through modulation of the inflammatory response [132]. The autophagy-dependent inflammatory response is known to be bidirectional and context-dependent. Furthermore, SASP is highly heterogeneous and varies from cell type to cell type, with different components of SASP such as IL-1α and IL-1β, known to exert differential effects on mediating tumourigenesis [189]. Therefore, in order to fully enhance the efficacy of antimitotic therapies, it might not be sufficient to simply eliminate pro-tumourigenic SASP. Rather, the switch from pro-tumourigenic SASP into anti-tumorigenic SASP that provoke immunogenic cell death and clearance, will be desirable. This affirms the need to test the impact of mitotic slippage-induced SASP factors on the tumour microenvironment and host immune system in a spontaneous tumour model.

Within the established microenvironment, TAMs are considered one of the most abundant and crucial non-neoplastic cell types. TAMs is known to promote the growth, angiogenesis, and metastasis of a variety of cancers [13, 31, 32]. Numerous studies have demonstrated that the abundance of TAMs correlates with a poor prognosis coupled with accelerated tumour growth [11, 31, 32]. In the context of anti-mitotic drugs treatment, it has been recently reported by Olson et al. showing that the secreted factors from TAMs suppress the cytotoxic effects of Taxol by promoting early mitotic slippage [163]. Furthermore, TAM-derived cytokines such as IL-6, IL-1, IL-8 and TNF-α significantly contribute to proliferation, immunosuppression, and angiogenesis [32]. The differentiation of monocytes into polarised macrophage subsets such as M1-type tumour suppressive macrophage or M2-type tumour promoting macrophage (also known as TAM) depends on the exposure to different

cytokine milieu [190]. Thus, it will be of key interest to determine whether distinct post-slippage secretome could influence the polarisation of macrophages. To address this hypothesis, a preliminary experiment can be performed by incubating post-slippage derived CM onto THP-1 human monocytic cell line and assess M1/M2 polarisation. Instead of using CM, co-cultures of post-slippage senescent cells and THP-1 human monocytic cell line can also be established. Primary blood monocytes isolated from peripheral blood mononuclear cells (PBMCs) of healthy individuals can subsequently be used for further validation. The crosstalk between TAM and post-slippage cells via secreted factors could amplify the tumour-promoting effects and promote an immunosuppressive microenvironment.

The manifestation of secretory factors by post-slippage cells can also affect normal cells such as epithelial cells and fibroblasts. Indeed, it has been shown that senescence can be transmitted to normal human fibroblasts in a non-cell-autonomous manner [29, 191]. Furthermore, another study has recently shown that chemotherapeutic treatment induces senescence in normal cells and as such contributes to systemic side effects [37]. Thus, it is worth investigating whether secreted factors from the post-slippage context could reinforce senescence in normal cells that consequently potentiate the deleterious effects of post-slippage senescent cells.

7.2 **Deciphering signaling networks involved in post-slippage induced tumourigenesis**

Although this current work focuses on anti-mitotic drugs, it is anticipated that other classes of chemotherapeutic drugs may have similar roles in engendering non-cell-autonomous (paracrine) tumour progression. Hence, it will be of interest to identify and delineate signaling pathways and molecular mediators leading to SASP and pro-tumourigenic function post-slippage. One plausible upstream effectors of post-slippage senescence could arise from mitochondrial dysfunction. Many types of chemotherapy treatments including anti-mitotic drugs could induce mitochondrial dysfunction [192]. Consistent with other findings, post-slippage cells are shown to accumulate dysfunctional mitochondria (Figure 6). Defective mitochondria activate AMPK signaling and

protective autophagy to promote cellular survival [193]. Furthermore, it has been shown that compromised mitochondria can induce cellular senescence coupled with a distinct secretory phenotype [110]. In order to elucidate whether mitochondria are involved in regulating post-slippage senescence, we can utilize cells with depleted mtDNA by passaging cells with ethidium bromide (rho0 cells) or treating cells with electron transport chain inhibitors Rotenone or Antimycin A, and analyse their response to anti-mitotic drugs treatment. Delineating major signaling nodes along the "slippage-senescence-SASP-tumourigenesis" axis could potentially serve as beneficial therapeutic targets in combination with antimitotic drug therapy.

7.3 **Conclusion**

Anti-mitotic drugs are the most-commonly utilised class of chemotherapeutic agents administered as a first-line therapy [194]; however, the clinical success of antimitotic therapies is often impeded by acquired resistance. The cell fate following mitotic slippage, albeit representing a route of escape from mitotic arrest and mitotic cell death, has not been extensively studied. Here, for the first time, I showed that multinucleated post-slippage cells undergo senescence and elicits paracrine pro-tumourigenic effects, both *in vitro* and *in vivo*. The SASP factors secreted by post-slippage senescence cells promote migration, invasiveness and angiogenesis**.** Thus, the elimination of post-slippage cells is anticipated to be beneficial for the overall efficacy of antimitotic therapies. In search for effectors of post-slippage senescence, it was found that the pro-tumourigenic effects of SASP can be restrained by autophagy inhibition. It was further established that autophagy is responsible for the induction of post-slippage senescence, whereby its inhibition results in senescence bypass and subsequently led to cell death post-slippage.

I also found that discrete lipid biosynthesis pathways could contribute differentially to the regulation of post-slippage secretory factors. Modulating lipid biosynthesis in post-slippage cells by TOFA, amplified their pro-tumourigenic secretion profiles and accelerated the development of paracrine pro-tumorigenic behavior, particularly cell migration and invasiveness. Contrary to TOFA, treatment of post-slippage cells with C75, another drug targeting a different lipid biosynthesis pathway, abrogates the production of pro-tumorigenic factors and their associated effects in post-slippage cells. This suggests that discrete lipid biosynthesis pathways could contribute differentially to the regulation of pro-tumorigenic inflammation. The divergent effects of TOFA and C75 may be attributed to the opposing regulation of Malonyl-CoA, an intermediate in fatty acid synthesis that serves as mediator of fatty acid oxidation. Targeting lipid biosynthesis in post-slippage cells could reprogram its secretory profile that not only negates tumour-promoting effects, but may also promote anti-tumour inflammation for the clearance of tumour or post-slippage cells.

All in all, this study defined two major metabolic consequences that abrogate the tumour-promoting effects of antimitotic therapies; either by eliminating pro-tumourigenic senescent cells or by suppressing the secretion of the associated pro-tumorigenic factors. As such, understanding cell fate post-slippage provides opportunities for the development of novel therapeutic strategies to circumvent antimitotic drug resistance and enhance the treatment efficacy for cancer patients.

APPENDIX

Table 1. List of chemicals

Chemical	Concentration	Catalogue number	Company
Nocodazole (Noc)	100 ng/ml or 10 mpk	N3000	US Biological
Paclitaxel (PTX)	150 nM or 10 mpk	P1792A	US Biological
Thymidine	3 mM	T1895-25G	Sigma
ZM447439	2 μM	2458	Tocris
Monastrol	100 μM	1305	Tocris
Bafilomycin A1	10 nM or 25 nM	B1793	Sigma
Chloroquine	30 mpk	C6628	Sigma
Triascin C	1 - 4 μM	Ab141888	Abcam
TOFA	1 - 20 μg/mL	T6575	Sigma
C75	5 - 20 μM	C5490	Sigma
Orlistat	10 μM	O4139	Sigma

Table 2. List of primers

Gene	Sequence (5' to 3')
IL-8	Forward: GAGTGGACCACACTGCGCCA
	Reverse: TCCACAACCCTCTGCACCCAGT
IL-6	Forward: CCAGGAGCCCAGCTATGAAC
	Reverse: CCCAGGGAGAAGGCAACTG
BMP2	Forward: GGACATTCGGTCCTTGCGCCA
	Reverse: GGTCGACCTTTAGGAGACCGCAGT
IL-1α	Forward: AGTGCTGCTGAAGGAGATGCCTGA
	Reverse: CCCCTGCCAAGCACACCCAGTA
IL-1β	Forward: TGCACGCTCCGGGACTCACA
	Reverse: CATGGAGAACACCACTTGTTGCTCC
Fibronectin	Forward: GAGGGGACCTGCAGCCACA
	Reverse: TTCGCAACCTGCGGGAAAAA
ICAM1	Forward: GGCCCCCTACCAGCTCCAGA
	Reverse: GACTGGGAACAGCCCGTCCA
Vimentin	Forward: ACTACGTCCACCCGCACCTA
	Reverse: CAGCGAGAAGTCCACCGAGT
MMP-9	Forward: TTGACAGCGACAAGAAGTGG
	Reverse: GCCATTCACGTCGTCCTTA
Gapdh	Forward: GGTCGTATTGGGCGCCTGGTCACC
	Reverse: CACACCCATGACGAACATGGGGGC

Table 3. List of antibodies

Antigen	Antibody name	Catalogue number	Company
β-Actin	β-Actin (C4) Mouse mAb	sc-47778	Santa Cruz Biotechnology
P62	SQSTM1/P62 (D3) Mouse mAb	sc-28359	Santa Cruz Biotechnology
TP53	p53 (DO-1) Mouse mAb	sc-126	Santa Cruz Biotechnology
cyclin B1	cyclin B1 (H-433) Rabbit pAb	sc-752	Santa Cruz Biotechnology
cyclin D1	cyclin D1 (A-12) Mouse mAb	sc-8396	Santa Cruz Biotechnology
p-Histone H3	phospho-Histone H3 (Ser 10) Rabbit pAb	sc-8656-R	Santa Cruz Biotechnology
Mcl-1	Mcl-1 Antibody (S-19) Rabbit pAb	sc-819	Santa Cruz Biotechnology
ATG5	Atg5 (D5F5U) Rabbit mAb	#12994	Cell signaling technology
p-p70 S6 Kinase	Phospho-p70 S6 Kinase (Thr389) Rabbit pAb	#9205	Cell signaling technology
p70 S6 Kinase	p70 S6 Kinase Rabbit pAb	#9202	Cell signaling technology
AMPKα	AMPKα Rabbit pAb	#2532	Cell signaling technology
p-AMPKα	Phospho-AMPKα (Thr172) Rabbit pAb	#2531	Cell signaling technology
ULK1	ULK1 (D8H5) Rabbit mAb	#8054	Cell signaling technology
p-ULK1	Phospho-ULK1 (Ser757) Rabbit pAb	#6888	Cell signaling technology
p-Histone H2A.X	Phospho-Histone H2A.X (Ser139) Rabbit pAb	#2577	Cell signaling technology
p-Histone H3	Phospho-Histone H3 (Ser10) Rabbit pAb (Alexa Fluor® 488 Conjugate)	#9708	Cell signaling technology
Cleaved PARP	Cleaved PARP (Asp214)	#9541	Cell signaling

	Rabbit pAb		technology
p21	p21 Waf1/Cip1 (12D1) Rabbit mAb	#2947	Cell signaling technology
BubR1	BubR1 Mouse mAb	612503	BD Biosciences
LC3	LC3B Rabbit pAb	L7543	Sigma
GAPDH	GAPDH Mouse mAb	CB1001	Merck Millipore
Lamin B1	Lamin B1 Rabbit pAb	ab16048	Abcam
β-Catenin	β-Catenin Rabbit pAb	ab16051	Abcam
IL-8	IL-8/CXCL8 Mouse mAb	MAB208-100	R&D Systems
IL-1β	IL-1 beta /IL-1F2 Mouse mAb	MAB201-100	R&D Systems
IκBα	IκBα pAb	ab7217	Abcam
Phospho-IκBα	Phospho-IκBα mAb	9246	Cell signaling technology
Phospho-p65 (Ser536)	Phospho-NF-κB p65 (Ser536) pAb	3033	Cell signaling technology
p65 (D14E12)	NF-κB p65 (Ser536) pAb	8242	Cell signaling technology
Rabbit IgG	Donkey anti-Rabbit IgG-HRP	NA934	GE Health care life sciences
Mouse IgG	Sheep anti-Mouse IgG-HRP	NA931	GE Health care life sciences
Mouse IgG	Goat anti-Mouse IgG-Alexa Fluor 488	A-11001	Invitrogen
Mouse IgG	Goat anti-Mouse IgG-Alexa Fluor 594	A-11005	Invitrogen
Rabbit IgG	Goat anti-Rabbit IgG-Alexa Fluor 488	A-11008	Invitrogen
Rabbit IgG	Goat anti-Rabbit IgG-Alexa Fluor 594	A-11012	Invitrogen

Table 4. List of lipid hits from lipidomic

Compound	*p*	*p* (Corr)	FC (abs) Normalised
TG (54:1)	1.06E-43	4.31E-42	11.0
TG (52:1)	1.40E-45	1.14E-43	8.7
TG (60:1)	5.87E-38	4.75E-37	7.8
TG (56:1)	1.07E-38	9.64E-38	7.2
TG (52:0)	6.38E-32	2.15E-31	7.1
TG (58:1)	8.05E-40	1.09E-38	6.9
TG (56:2)	1.45E-39	1.68E-38	6.5
TG (50:0)	1.15E-32	4.23E-32	6.5
TG (54:2)	1.45E-36	9.81E-36	6.3
TG (50:1)	2.78E-40	4.50E-39	6.3
TG (60:2)	1.72E-39	1.74E-38	6.1
TG (58:2)	1.81E-40	3.67E-39	6.0
TG (62:2)	3.84E-36	2.37E-35	5.8
TG (62:1)	7.74E-32	2.51E-31	5.6
TG (48:1)	4.09E-36	2.37E-35	5.4
TG (48:0)	3.58E-37	2.63E-36	5.3
TG (52:2)	4.40E-33	2.05E-32	5.0
TG (56:3)	4.64E-34	2.35E-33	4.9
TG (46:0)	5.17E-41	1.40E-39	4.8
TG (58:3)	2.55E-31	7.96E-31	4.5
TG (60:3)	4.55E-33	2.05E-32	4.4
TG (62:3)	8.29E-33	3.53E-32	4.3
TG (50:2)	3.20E-32	1.13E-31	4.1
TG (56:4)	4.06E-28	9.13E-28	4.1
TG (54:3)	1.59E-29	4.04E-29	4.1
TG (58:0)	2.07E-25	3.57E-25	4.0
TG (46:1)	9.95E-33	3.84E-32	3.8
TG (52:3)	1.23E-25	2.26E-25	3.7
TG (54:0)	2.20E-26	4.23E-26	3.6
TG (48:2)	2.53E-27	5.26E-27	3.3
TG (44:0)	9.83E-28	2.10E-27	3.2
TG (50:3)	2.85E-20	3.61E-20	2.9
TG (47:1)	1.99E-24	3.23E-24	2.3
DG (36:1)	1.87E-28	4.32E-28	3.0
DG (34:1)	1.37E-25	2.46E-25	2.2
DG (32:0)	2.05E-26	4.05E-26	2.2
DG (36:2)	1.36E-24	2.24E-24	2.1
PC (P-36:1)	9.28E-28	2.03E-27	3.5
PC (36:1)	2.17E-30	5.85E-30	3.2
PC (P-36:0)	8.71E-24	1.31E-23	2.6
PC (P-32:0)	6.94E-27	1.40E-26	2.5

PC (38:3)	2.01E-23	2.97E-23	2.4
PC (34:0)	2.46E-20	3.16E-20	2.3
PC (P-38:3)	4.69E-24	7.45E-24	2.3
PC (38:2)	2.66E-22	3.78E-22	2.1
PC (28:0)	6.69E-29	1.64E-28	2.0
PE (P-36:5)	5.79E-31	1.68E-30	2.3
PE (37:0)	3.60E-20	4.48E-20	2.3
PE (P-38:3)	1.21E-25	2.26E-25	2.0

REFERENCES

1. Gascoigne, K.E. and S.S. Taylor, *How do anti-mitotic drugs kill cancer cells?* J Cell Sci, 2009. **122**(Pt 15): p. 2579-85.
2. Musacchio, A. and E.D. Salmon, *The spindle-assembly checkpoint in space and time.* Nat Rev Mol Cell Biol, 2007. **8**(5): p. 379-93.
3. Lara-Gonzalez, P., F.G. Westhorpe, and S.S. Taylor, *The spindle assembly checkpoint.* Curr Biol, 2012. **22**(22): p. R966-80.
4. Sinnott, R., et al., *Mechanisms promoting escape from mitotic stress-induced tumor cell death.* Cancer Res, 2014. **74**(14): p. 3857-69.
5. Gascoigne, K.E. and S.S. Taylor, *Cancer cells display profound intra- and interline variation following prolonged exposure to antimitotic drugs.* Cancer Cell, 2008. **14**(2): p. 111-22.
6. Orth, J.D., et al., *Analysis of mitosis and antimitotic drug responses in tumors by in vivo microscopy and single-cell pharmacodynamics.* Cancer Res, 2011. **71**(13): p. 4608-16.
7. Flores, M.L., et al., *Paclitaxel sensitivity of breast cancer cells requires efficient mitotic arrest and disruption of Bcl-xL/Bak interaction.* Breast Cancer Res Treat, 2012. **133**(3): p. 917-28.
8. Ma, H.T., et al., *Depletion of p31comet protein promotes sensitivity to antimitotic drugs.* J Biol Chem, 2012. **287**(25): p. 21561-9.
9. Fu, Y., et al., *Weakened spindle checkpoint with reduced BubR1 expression in paclitaxel-resistant ovarian carcinoma cell line SKOV3-TR30.* Gynecol Oncol, 2007. **105**(1): p. 66-73.
10. He, Y., et al., *Cell Division Cycle 6 Promotes Mitotic Slippage and Contributes to Drug Resistance in Paclitaxel-Treated Cancer Cells.* PLoS One, 2016. **11**(9): p. e0162633.
11. Munoz-Espin, D. and M. Serrano, *Cellular senescence: from physiology to pathology.* Nat Rev Mol Cell Biol, 2014. **15**(7): p. 482-96.
12. Wiley, C.D. and J. Campisi, *From Ancient Pathways to Aging Cells-Connecting Metabolism and Cellular Senescence.* Cell Metab, 2016. **23**(6): p. 1013-1021.
13. Hernandez-Segura, A., J. Nehme, and M. Demaria, *Hallmarks of Cellular Senescence.* Trends Cell Biol, 2018. **28**(6): p. 436-453.
14. Freund, A., et al., *Lamin B1 loss is a senescence-associated biomarker.* Mol Biol Cell, 2012. **23**(11): p. 2066-75.
15. Lin, S.P., et al., *RB maintains quiescence and prevents premature senescence through upregulation of DNMT1 in mesenchymal stromal cells.* Stem Cell Reports, 2014. **3**(6): p. 975-86.
16. Rajarajacholan, U.K., S. Thalappilly, and K. Riabowol, *The ING1a tumor suppressor regulates endocytosis to induce cellular senescence via the Rb-E2F pathway.* PLoS Biol, 2013. **11**(3): p. e1001502.
17. Stein, G.H., et al., *Differential roles for cyclin-dependent kinase inhibitors p21 and p16 in the mechanisms of senescence and differentiation in human fibroblasts.* Mol Cell Biol, 1999. **19**(3): p. 2109-17.
18. Waldman, T., K.W. Kinzler, and B. Vogelstein, *p21 is necessary for the p53-mediated G1 arrest in human cancer cells.* Cancer Res, 1995. **55**(22): p. 5187-90.

19. Yosef, R., et al., *p21 maintains senescent cell viability under persistent DNA damage response by restraining JNK and caspase signaling.* EMBO J, 2017. **36**(15): p. 2280-2295.
20. Serrano, M., et al., *Oncogenic ras provokes premature cell senescence associated with accumulation of p53 and p16INK4a.* Cell, 1997. **88**(5): p. 593-602.
21. Chen, Z., et al., *Crucial role of p53-dependent cellular senescence in suppression of Pten-deficient tumorigenesis.* Nature, 2005. **436**(7051): p. 725-30.
22. He, S. and N.E. Sharpless, *Senescence in Health and Disease.* Cell, 2017. **169**(6): p. 1000-1011.
23. Tato-Costa, J., et al., *Therapy-Induced Cellular Senescence Induces Epithelial-to-Mesenchymal Transition and Increases Invasiveness in Rectal Cancer.* Clin Colorectal Cancer, 2016. **15**(2): p. 170-178 e3.
24. Ewald, J.A., et al., *Therapy-induced senescence in cancer.* J Natl Cancer Inst, 2010. **102**(20): p. 1536-46.
25. Chang, B.D., et al., *Molecular determinants of terminal growth arrest induced in tumor cells by a chemotherapeutic agent.* Proc Natl Acad Sci U S A, 2002. **99**(1): p. 389-94.
26. Campisi, J. and F. d'Adda di Fagagna, *Cellular senescence: when bad things happen to good cells.* Nat Rev Mol Cell Biol, 2007. **8**(9): p. 729-40.
27. Perez-Mancera, P.A., A.R. Young, and M. Narita, *Inside and out: the activities of senescence in cancer.* Nat Rev Cancer, 2014. **14**(8): p. 547-58.
28. Toso, A., et al., *Enhancing chemotherapy efficacy in Pten-deficient prostate tumors by activating the senescence-associated antitumor immunity.* Cell Rep, 2014. **9**(1): p. 75-89.
29. Acosta, J.C., et al., *A complex secretory program orchestrated by the inflammasome controls paracrine senescence.* Nat Cell Biol, 2013. **15**(8): p. 978-90.
30. Wang, Q., et al., *Polyploidy road to therapy-induced cellular senescence and escape.* Int J Cancer, 2013. **132**(7): p. 1505-15.
31. Roberson, R.S., et al., *Escape from therapy-induced accelerated cellular senescence in p53-null lung cancer cells and in human lung cancers.* Cancer Res, 2005. **65**(7): p. 2795-803.
32. Davalos, A.R., et al., *Senescent cells as a source of inflammatory factors for tumor progression.* Cancer Metastasis Rev, 2010. **29**(2): p. 273-83.
33. Canino, C., et al., *SASP mediates chemoresistance and tumor-initiating-activity of mesothelioma cells.* Oncogene, 2012. **31**(26): p. 3148-63.
34. Krtolica, A., et al., *Senescent fibroblasts promote epithelial cell growth and tumorigenesis: a link between cancer and aging.* Proc Natl Acad Sci U S A, 2001. **98**(21): p. 12072-7.
35. Coppe, J.P., et al., *Senescence-associated secretory phenotypes reveal cell-nonautonomous functions of oncogenic RAS and the p53 tumor suppressor.* PLoS Biol, 2008. **6**(12): p. 2853-68.
36. Coppe, J.P., et al., *The senescence-associated secretory phenotype: the dark side of tumor suppression.* Annu Rev Pathol, 2010. **5**: p. 99-118.

37. Demaria, M., et al., *Cellular Senescence Promotes Adverse Effects of Chemotherapy and Cancer Relapse.* Cancer Discov, 2017. **7**(2): p. 165-176.
38. Levy, J.M.M., C.G. Towers, and A. Thorburn, *Targeting autophagy in cancer.* Nat Rev Cancer, 2017. **17**(9): p. 528-542.
39. He, C. and D.J. Klionsky, *Regulation mechanisms and signaling pathways of autophagy.* Annu Rev Genet, 2009. **43**: p. 67-93.
40. Wang, C.W. and D.J. Klionsky, *The molecular mechanism of autophagy.* Mol Med, 2003. **9**(3-4): p. 65-76.
41. Tanida, I., T. Ueno, and E. Kominami, *LC3 and Autophagy.* Methods Mol Biol, 2008. **445**: p. 77-88.
42. Mizushima, N. and T. Yoshimori, *How to interpret LC3 immunoblotting.* Autophagy, 2007. **3**(6): p. 542-5.
43. Bjorkoy, G., et al., *Monitoring autophagic degradation of p62/SQSTM1.* Methods Enzymol, 2009. **452**: p. 181-97.
44. Fang, L.M., et al., *Transcription factor EB is involved in autophagy-mediated chemoresistance to doxorubicin in human cancer cells.* Acta Pharmacol Sin, 2017. **38**(9): p. 1305-1316.
45. Xi, G., et al., *Autophagy inhibition promotes paclitaxel-induced apoptosis in cancer cells.* Cancer Lett, 2011. **307**(2): p. 141-8.
46. Ertmer, A., et al., *The anticancer drug imatinib induces cellular autophagy.* Leukemia, 2007. **21**(5): p. 936-42.
47. Chen, L., et al., *Autophagy inhibition contributes to the synergistic interaction between EGCG and doxorubicin to kill the hepatoma Hep3B cells.* PLoS One, 2014. **9**(1): p. e85771.
48. Pagotto, A., et al., *Autophagy inhibition reduces chemoresistance and tumorigenic potential of human ovarian cancer stem cells.* Cell Death Dis, 2017. **8**(7): p. e2943.
49. Wang, L., et al., *Autophagy mediates glucose starvation-induced glioblastoma cell quiescence and chemoresistance through coordinating cell metabolism, cell cycle, and survival.* Cell Death Dis, 2018. **9**(2): p. 213.
50. Hu, Y.L., et al., *Hypoxia-induced autophagy promotes tumor cell survival and adaptation to antiangiogenic treatment in glioblastoma.* Cancer Res, 2012. **72**(7): p. 1773-83.
51. Yang, Z.J., et al., *The role of autophagy in cancer: therapeutic implications.* Mol Cancer Ther, 2011. **10**(9): p. 1533-41.
52. Grasso, D. and M.I. Vaccaro, *Macroautophagy and the oncogene-induced senescence.* Front Endocrinol (Lausanne), 2014. **5**: p. 157.
53. Xiong, H.Y., et al., *Autophagic cell death induced by 5-FU in Bax or PUMA deficient human colon cancer cell.* Cancer Lett, 2010. **288**(1): p. 68-74.
54. Yonekawa, T. and A. Thorburn, *Autophagy and cell death.* Essays Biochem, 2013. **55**: p. 105-17.
55. Guo, W.J., et al., *Novel monofunctional platinum (II) complex Mono-Pt induces apoptosis-independent autophagic cell death in human ovarian carcinoma cells, distinct from cisplatin.* Autophagy, 2013. **9**(7): p. 996-1008.

56. Tai, W.T., et al., *Mcl-1-dependent activation of Beclin 1 mediates autophagic cell death induced by sorafenib and SC-59 in hepatocellular carcinoma cells.* Cell Death Dis, 2013. **4**: p. e485.
57. Sui, X., et al., *Autophagy and chemotherapy resistance: a promising therapeutic target for cancer treatment.* Cell Death Dis, 2013. **4**: p. e838.
58. Gewirtz, D.A., *Autophagy and senescence: a partnership in search of definition.* Autophagy, 2013. **9**(5): p. 808-12.
59. Kwon, Y., et al., *Autophagy Is Pro-Senescence When Seen in Close-Up, but Anti-Senescence in Long-Shot.* Mol Cells, 2017. **40**(9): p. 607-612.
60. Young, A.R., et al., *Autophagy mediates the mitotic senescence transition.* Genes Dev, 2009. **23**(7): p. 798-803.
61. Goehe, R.W., et al., *The autophagy-senescence connection in chemotherapy: must tumor cells (self) eat before they sleep?* J Pharmacol Exp Ther, 2012. **343**(3): p. 763-78.
62. White, E. and S.W. Lowe, *Eating to exit: autophagy-enabled senescence revealed.* Genes Dev, 2009. **23**(7): p. 784-7.
63. Huang, Y.H., et al., *Autophagy promotes radiation-induced senescence but inhibits bystander effects in human breast cancer cells.* Autophagy, 2014. **10**(7): p. 1212-28.
64. Amaravadi, R.K., et al., *Autophagy inhibition enhances therapy-induced apoptosis in a Myc-induced model of lymphoma.* J Clin Invest, 2007. **117**(2): p. 326-36.
65. Li, Z. and Y. Kang, *Lipid Metabolism Fuels Cancer's Spread.* Cell Metab, 2017. **25**(2): p. 228-230.
66. Menendez, J.A. and R. Lupu, *Fatty acid synthase and the lipogenic phenotype in cancer pathogenesis.* Nat Rev Cancer, 2007. **7**(10): p. 763-77.
67. Zaidi, N., J.V. Swinnen, and K. Smans, *ATP-citrate lyase: a key player in cancer metabolism.* Cancer Res, 2012. **72**(15): p. 3709-14.
68. Kuhajda, F.P., *Fatty acid synthase and cancer: new application of an old pathway.* Cancer Res, 2006. **66**(12): p. 5977-80.
69. Abramczyk, H., et al., *The role of lipid droplets and adipocytes in cancer. Raman imaging of cell cultures: MCF10A, MCF7, and MDA-MB-231 compared to adipocytes in cancerous human breast tissue.* Analyst, 2015. **140**(7): p. 2224-35.
70. Bozza, P.T. and J.P. Viola, *Lipid droplets in inflammation and cancer.* Prostaglandins Leukot Essent Fatty Acids, 2010. **82**(4-6): p. 243-50.
71. Accioly, M.T., et al., *Lipid bodies are reservoirs of cyclooxygenase-2 and sites of prostaglandin-E2 synthesis in colon cancer cells.* Cancer Res, 2008. **68**(6): p. 1732-40.
72. Boren, J. and K.M. Brindle, *Apoptosis-induced mitochondrial dysfunction causes cytoplasmic lipid droplet formation.* Cell Death Differ, 2012. **19**(9): p. 1561-70.
73. Zirath, H., et al., *MYC inhibition induces metabolic changes leading to accumulation of lipid droplets in tumor cells.* Proc Natl Acad Sci U S A, 2013. **110**(25): p. 10258-63.
74. Mehdizadeh, A., et al., *Common chemotherapeutic agents modulate fatty acid distribution in human hepatocellular carcinoma and colorectal cancer cells.* Bioimpacts, 2017. **7**(1): p. 31-39.

75. Barreto, R., et al., *Chemotherapy-related cachexia is associated with mitochondrial depletion and the activation of ERK1/2 and p38 MAPKs.* Oncotarget, 2016. **7**(28): p. 43442-43460.
76. Agmon, E. and B.R. Stockwell, *Lipid homeostasis and regulated cell death.* Curr Opin Chem Biol, 2017. **39**: p. 83-89.
77. Magtanong, L., P.J. Ko, and S.J. Dixon, *Emerging roles for lipids in non-apoptotic cell death.* Cell Death Differ, 2016. **23**(7): p. 1099-109.
78. Dixon, S.J., et al., *Human Haploid Cell Genetics Reveals Roles for Lipid Metabolism Genes in Nonapoptotic Cell Death.* ACS Chem Biol, 2015. **10**(7): p. 1604-9.
79. Pizer, E.S., et al., *Malonyl-coenzyme-A is a potential mediator of cytotoxicity induced by fatty-acid synthase inhibition in human breast cancer cells and xenografts.* Cancer Res, 2000. **60**(2): p. 213-8.
80. Flor, A.C., et al., *A signature of enhanced lipid metabolism, lipid peroxidation and aldehyde stress in therapy-induced senescence.* Cell Death Discov, 2017. **3**: p. 17075.
81. Flor, A.C., A.P. Doshi, and S.J. Kron, *Modulation of therapy-induced senescence by reactive lipid aldehydes.* Cell Death Discov, 2016. **2**.
82. Havas, K.M., et al., *Metabolic shifts in residual breast cancer drive tumor recurrence.* J Clin Invest, 2017. **127**(6): p. 2091-2105.
83. Viale, A., et al., *Oncogene ablation-resistant pancreatic cancer cells depend on mitochondrial function.* Nature, 2014. **514**(7524): p. 628-32.
84. Hanahan, D. and R.A. Weinberg, *Hallmarks of cancer: the next generation.* Cell, 2011. **144**(5): p. 646-74.
85. DeBerardinis, R.J., et al., *The biology of cancer: metabolic reprogramming fuels cell growth and proliferation.* Cell Metab, 2008. **7**(1): p. 11-20.
86. Vander Heiden, M.G., L.C. Cantley, and C.B. Thompson, *Understanding the Warburg effect: the metabolic requirements of cell proliferation.* Science, 2009. **324**(5930): p. 1029-33.
87. Lindholm, P., et al., *Influence of the blood glucose concentration on FDG uptake in cancer--a PET study.* J Nucl Med, 1993. **34**(1): p. 1-6.
88. Dang, C.V., et al., *Oncogenes in tumor metabolism, tumorigenesis, and apoptosis.* J Bioenerg Biomembr, 1997. **29**(4): p. 345-54.
89. Yu, L., et al., *The Glycolytic Switch in Tumors: How Many Players Are Involved?* J Cancer, 2017. **8**(17): p. 3430-3440.
90. Li, F.L., et al., *Acetylation accumulates PFKFB3 in cytoplasm to promote glycolysis and protects cells from cisplatin-induced apoptosis.* Nat Commun, 2018. **9**(1): p. 508.
91. Shen, H., et al., *Sensitization of Glioblastoma Cells to Irradiation by Modulating the Glucose Metabolism.* Mol Cancer Ther, 2015. **14**(8): p. 1794-804.
92. Wang, T., et al., *Glycolysis is essential for chemoresistance induced by transient receptor potential channel C5 in colorectal cancer.* BMC Cancer, 2018. **18**(1): p. 207.
93. Oronsky, B.T., et al., *Follow the ATP: tumor energy production: a perspective.* Anticancer Agents Med Chem, 2014. **14**(9): p. 1187-98.
94. Zhou, Y., et al., *Intracellular ATP levels are a pivotal determinant of chemoresistance in colon cancer cells.* Cancer Res, 2012. **72**(1): p. 304-14.

95. Longley, D.B. and P.G. Johnston, *Molecular mechanisms of drug resistance.* J Pathol, 2005. **205**(2): p. 275-92.
96. Phan, L.M., S.C. Yeung, and M.H. Lee, *Cancer metabolic reprogramming: importance, main features, and potentials for precise targeted anti-cancer therapies.* Cancer Biol Med, 2014. **11**(1): p. 1-19.
97. Domenech, E., et al., *AMPK and PFKFB3 mediate glycolysis and survival in response to mitophagy during mitotic arrest.* Nat Cell Biol, 2015. **17**(10): p. 1304-16.
98. Teichner, A., et al., *p31comet Promotes disassembly of the mitotic checkpoint complex in an ATP-dependent process.* Proc Natl Acad Sci U S A, 2011. **108**(8): p. 3187-92.
99. Dorr, J.R., et al., *Synthetic lethal metabolic targeting of cellular senescence in cancer therapy.* Nature, 2013. **501**(7467): p. 421-5.
100. Chen, J.Y., et al., *Additive effects of C(2)-ceramide on paclitaxel-induced premature senescence of human lung cancer cells.* Life Sci, 2010. **87**(11-12): p. 350-7.
101. Prencipe, M., et al., *Cellular senescence induced by aberrant MAD2 levels impacts on paclitaxel responsiveness in vitro.* Br J Cancer, 2009. **101**(11): p. 1900-8.
102. Shi, J., J.D. Orth, and T. Mitchison, *Cell type variation in responses to antimitotic drugs that target microtubules and kinesin-5.* Cancer Res, 2008. **68**(9): p. 3269-76.
103. Vogel, C., et al., *Crosstalk of the mitotic spindle assembly checkpoint with p53 to prevent polyploidy.* Oncogene, 2004. **23**(41): p. 6845-53.
104. Ganem, N.J. and D. Pellman, *Limiting the proliferation of polyploid cells.* Cell, 2007. **131**(3): p. 437-40.
105. Lee, B.Y., et al., *Senescence-associated beta-galactosidase is lysosomal beta-galactosidase.* Aging Cell, 2006. **5**(2): p. 187-95.
106. Yoshida, A., E.K. Lee, and J.A. Diehl, *Induction of Therapeutic Senescence in Vemurafenib-Resistant Melanoma by Extended Inhibition of CDK4/6.* Cancer Res, 2016. **76**(10): p. 2990-3002.
107. Sun, C., et al., *Reversible and adaptive resistance to BRAF(V600E) inhibition in melanoma.* Nature, 2014. **508**(7494): p. 118-22.
108. Broude, E.V., et al., *p21(Waf1/Cip1/Sdi1) mediates retinoblastoma protein degradation.* Oncogene, 2007. **26**(48): p. 6954-8.
109. Chicas, A., et al., *Dissecting the unique role of the retinoblastoma tumor suppressor during cellular senescence.* Cancer Cell, 2010. **17**(4): p. 376-87.
110. Wiley, C.D., et al., *Mitochondrial Dysfunction Induces Senescence with a Distinct Secretory Phenotype.* Cell Metab, 2016. **23**(2): p. 303-14.
111. Passos, J.F., et al., *Mitochondrial dysfunction accounts for the stochastic heterogeneity in telomere-dependent senescence.* PLoS Biol, 2007. **5**(5): p. e110.
112. Tai, H., et al., *Autophagy impairment with lysosomal and mitochondrial dysfunction is an important characteristic of oxidative stress-induced senescence.* Autophagy, 2017. **13**(1): p. 99-113.
113. Shokolenko, I., et al., *Oxidative stress induces degradation of mitochondrial DNA.* Nucleic Acids Res, 2009. **37**(8): p. 2539-48.
114. Brand, M.D. and D.G. Nicholls, *Assessing mitochondrial dysfunction in cells.* Biochem J, 2011. **435**(2): p. 297-312.

115. Crowley, L.C., M.E. Christensen, and N.J. Waterhouse, *Measuring Mitochondrial Transmembrane Potential by TMRE Staining.* Cold Spring Harb Protoc, 2016. **2016**(12).
116. Tchkonia, T., et al., *Cellular senescence and the senescent secretory phenotype: therapeutic opportunities.* J Clin Invest, 2013. **123**(3): p. 966-72.
117. Watanabe, S., et al., *Impact of senescence-associated secretory phenotype and its potential as a therapeutic target for senescence-associated diseases.* Cancer Sci, 2017. **108**(4): p. 563-569.
118. Xue, W., et al., *Senescence and tumour clearance is triggered by p53 restoration in murine liver carcinomas.* Nature, 2007. **445**(7128): p. 656-60.
119. Volk-Draper, L., et al., *Paclitaxel therapy promotes breast cancer metastasis in a TLR4-dependent manner.* Cancer Res, 2014. **74**(19): p. 5421-34.
120. Evdokimova, V., et al., *Reduced proliferation and enhanced migration: two sides of the same coin? Molecular mechanisms of metastatic progression by YB-1.* Cell Cycle, 2009. **8**(18): p. 2901-6.
121. Mizushima, N., T. Yoshimori, and B. Levine, *Methods in mammalian autophagy research.* Cell, 2010. **140**(3): p. 313-26.
122. Mizushima, N., et al., *A new protein conjugation system in human. The counterpart of the yeast Apg12p conjugation system essential for autophagy.* J Biol Chem, 1998. **273**(51): p. 33889-92.
123. Kim, J., et al., *AMPK and mTOR regulate autophagy through direct phosphorylation of Ulk1.* Nat Cell Biol, 2011. **13**(2): p. 132-41.
124. Meley, D., et al., *AMP-activated protein kinase and the regulation of autophagic proteolysis.* J Biol Chem, 2006. **281**(46): p. 34870-9.
125. Teng, Y., et al., *Evaluating human cancer cell metastasis in zebrafish.* BMC Cancer, 2013. **13**: p. 453.
126. Klionsky, D.J., et al., *Guidelines for the use and interpretation of assays for monitoring autophagy.* Autophagy, 2012. **8**(4): p. 445-544.
127. Dou, Z., et al., *Autophagy mediates degradation of nuclear lamina.* Nature, 2015. **527**(7576): p. 105-9.
128. Kang, C., et al., *The DNA damage response induces inflammation and senescence by inhibiting autophagy of GATA4.* Science, 2015. **349**(6255): p. aaa5612.
129. Zaffagnini, G. and S. Martens, *Mechanisms of Selective Autophagy.* J Mol Biol, 2016. **428**(9 Pt A): p. 1714-24.
130. Nacarelli, T. and C. Sell, *Targeting metabolism in cellular senescence, a role for intervention.* Mol Cell Endocrinol, 2017. **455**: p. 83-92.
131. Chude, C.I. and R.K. Amaravadi, *Targeting Autophagy in Cancer: Update on Clinical Trials and Novel Inhibitors.* Int J Mol Sci, 2017. **18**(6).
132. Galluzzi, L., et al., *Activating autophagy to potentiate immunogenic chemotherapy and radiation therapy.* Nat Rev Clin Oncol, 2017. **14**(4): p. 247-258.
133. Lee, C., et al., *Fasting cycles retard growth of tumors and sensitize a range of cancer cell types to chemotherapy.* Sci Transl Med, 2012. **4**(124): p. 124ra27.

134. Saleh, A.D., et al., *Caloric restriction augments radiation efficacy in breast cancer.* Cell Cycle, 2013. **12**(12): p. 1955-63.
135. O'Flanagan, C.H., et al., *When less may be more: calorie restriction and response to cancer therapy.* BMC Med, 2017. **15**(1): p. 106.
136. Morselli, E., et al., *Caloric restriction and resveratrol promote longevity through the Sirtuin-1-dependent induction of autophagy.* Cell Death Dis, 2010. **1**: p. e10.
137. Michaud, M., et al., *An autophagy-dependent anticancer immune response determines the efficacy of melanoma chemotherapy.* Oncoimmunology, 2014. **3**(7): p. e944047.
138. Shrihari, T.G., *Dual role of inflammatory mediators in cancer.* Ecancermedicalscience, 2017. **11**: p. 721.
139. Ostrand-Rosenberg, S., *Immune surveillance: a balance between protumor and antitumor immunity.* Curr Opin Genet Dev, 2008. **18**(1): p. 11-8.
140. Vegiopoulos, A., M. Rohm, and S. Herzig, *Adipose tissue: between the extremes.* EMBO J, 2017. **36**(14): p. 1999-2017.
141. Welte, M.A., et al., *Developmental regulation of vesicle transport in Drosophila embryos: forces and kinetics.* Cell, 1998. **92**(4): p. 547-57.
142. Kassan, A., et al., *Acyl-CoA synthetase 3 promotes lipid droplet biogenesis in ER microdomains.* J Cell Biol, 2013. **203**(6): p. 985-1001.
143. Poppelreuther, M., et al., *The N-terminal region of acyl-CoA synthetase 3 is essential for both the localization on lipid droplets and the function in fatty acid uptake.* J Lipid Res, 2012. **53**(5): p. 888-900.
144. Kapoor, T.M., et al., *Probing spindle assembly mechanisms with monastrol, a small molecule inhibitor of the mitotic kinesin, Eg5.* J Cell Biol, 2000. **150**(5): p. 975-88.
145. Bavetsias, V. and S. Linardopoulos, *Aurora Kinase Inhibitors: Current Status and Outlook.* Front Oncol, 2015. **5**: p. 278.
146. Zietkowski, D., et al., *Comparison of NMR lipid profiles in mitotic arrest and apoptosis as indicators of paclitaxel resistance in cervical cell lines.* Magn Reson Med, 2012. **68**(2): p. 369-77.
147. Bensaad, K., et al., *Fatty acid uptake and lipid storage induced by HIF-1alpha contribute to cell growth and survival after hypoxia-reoxygenation.* Cell Rep, 2014. **9**(1): p. 349-65.
148. Furuhashi, M. and G.S. Hotamisligil, *Fatty acid-binding proteins: role in metabolic diseases and potential as drug targets.* Nat Rev Drug Discov, 2008. **7**(6): p. 489-503.
149. Zhu, Y., Y. Zhou, and J. Shi, *Post-slippage multinucleation renders cytotoxic variation in anti-mitotic drugs that target the microtubules or mitotic spindle.* Cell Cycle, 2014. **13**(11): p. 1756-64.
150. Orth, J.D., et al., *Prolonged mitotic arrest triggers partial activation of apoptosis, resulting in DNA damage and p53 induction.* Mol Biol Cell, 2012. **23**(4): p. 567-76.
151. Cheng, B. and K. Crasta, *Consequences of mitotic slippage for antimicrotubule drug therapy.* Endocr Relat Cancer, 2017. **24**(9): p. T97-T106.
152. Hutti, J.E., et al., *Oncogenic PI3K mutations lead to NF-kappaB-dependent cytokine expression following growth factor deprivation.* Cancer Res, 2012. **72**(13): p. 3260-9.

153. Collins, T.S., L.F. Lee, and J.P. Ting, *Paclitaxel up-regulates interleukin-8 synthesis in human lung carcinoma through an NF-kappaB- and AP-1-dependent mechanism.* Cancer Immunol Immunother, 2000. **49**(2): p. 78-84.
154. DeNardo, D.G., et al., *Leukocyte complexity predicts breast cancer survival and functionally regulates response to chemotherapy.* Cancer Discov, 2011. **1**(1): p. 54-67.
155. Peng, J., et al., *Chemotherapy Induces Programmed Cell Death-Ligand 1 Overexpression via the Nuclear Factor-kappaB to Foster an Immunosuppressive Tumor Microenvironment in Ovarian Cancer.* Cancer Res, 2015. **75**(23): p. 5034-45.
156. Li, N., D.Y. Lizardo, and G.E. Atilla-Gokcumen, *Specific Triacylglycerols Accumulate via Increased Lipogenesis During 5-FU-Induced Apoptosis.* ACS Chem Biol, 2016. **11**(9): p. 2583-7.
157. Cooper, W.A., et al., *1H NMR visible lipids are induced by phosphonium salts and 5-fluorouracil in human breast cancer cells.* Magn Reson Med, 2001. **45**(6): p. 1001-10.
158. Deep, G. and I.R. Schlaepfer, *Aberrant Lipid Metabolism Promotes Prostate Cancer: Role in Cell Survival under Hypoxia and Extracellular Vesicles Biogenesis.* Int J Mol Sci, 2016. **17**(7).
159. Tabe, Y., et al., *Bone Marrow Adipocytes Facilitate Fatty Acid Oxidation Activating AMPK and a Transcriptional Network Supporting Survival of Acute Monocytic Leukemia Cells.* Cancer Res, 2017. **77**(6): p. 1453-1464.
160. Choi, J., Y.J. Cha, and J.S. Koo, *Adipocyte biology in breast cancer: From silent bystander to active facilitator.* Prog Lipid Res, 2018. **69**: p. 11-20.
161. Nieman, K.M., et al., *Adipocytes promote ovarian cancer metastasis and provide energy for rapid tumor growth.* Nat Med, 2011. **17**(11): p. 1498-503.
162. Atilla-Gokcumen, G.E., et al., *Dividing cells regulate their lipid composition and localization.* Cell, 2014. **156**(3): p. 428-39.
163. Olson, O.C., et al., *Tumor-Associated Macrophages Suppress the Cytotoxic Activity of Antimitotic Agents.* Cell Rep, 2017. **19**(1): p. 101-113.
164. Mitchison, T.J., et al., *Is inflammatory micronucleation the key to a successful anti-mitotic cancer drug?* Open Biol, 2017. **7**(11).
165. Jakhar, R., et al., *Autophagy Governs Pro-tumorigenic Effects of Mitotic Slippage-induced Senescence.* Mol Cancer Res, 2018.
166. Quijano, C., et al., *Oncogene-induced senescence results in marked metabolic and bioenergetic alterations.* Cell Cycle, 2012. **11**(7): p. 1383-92.
167. Warfel, J.D., et al., *Mitochondrial fat oxidation is essential for lipid-induced inflammation in skeletal muscle in mice.* Sci Rep, 2016. **6**: p. 37941.
168. Zhang, Q., et al., *Fatty acid oxidation contributes to IL-1beta secretion in M2 macrophages and promotes macrophage-mediated tumor cell migration.* Mol Immunol, 2018. **94**: p. 27-35.
169. Hossain, F., et al., *Inhibition of Fatty Acid Oxidation Modulates Immunosuppressive Functions of Myeloid-Derived Suppressor Cells*

and Enhances Cancer Therapies. Cancer Immunol Res, 2015. **3**(11): p. 1236-47.
170. McCune, S.A. and R.A. Harris, *Mechanism responsible for 5-(tetradecyloxy)-2-furoic acid inhibition of hepatic lipogenesis.* J Biol Chem, 1979. **254**(20): p. 10095-101.
171. Thupari, J.N., M.L. Pinn, and F.P. Kuhajda, *Fatty acid synthase inhibition in human breast cancer cells leads to malonyl-CoA-induced inhibition of fatty acid oxidation and cytotoxicity.* Biochem Biophys Res Commun, 2001. **285**(2): p. 217-23.
172. Hughes-Fulford, M., et al., *Arachidonic acid activates phosphatidylinositol 3-kinase signaling and induces gene expression in prostate cancer.* Cancer Res, 2006. **66**(3): p. 1427-33.
173. Jove, M., et al., *Palmitate-induced interleukin 6 production is mediated by protein kinase C and nuclear-factor kappaB activation and leads to glucose transporter 4 down-regulation in skeletal muscle cells.* Endocrinology, 2005. **146**(7): p. 3087-95.
174. Hu, M.B., et al., *High-fat diet-induced adipokine and cytokine alterations promote the progression of prostate cancer in vivo and in vitro.* Oncol Lett, 2018. **15**(2): p. 1607-1615.
175. Fanciulli, M., et al., *Energy metabolism of human LoVo colon carcinoma cells: correlation to drug resistance and influence of lonidamine.* Clin Cancer Res, 2000. **6**(4): p. 1590-7.
176. Peng, X., et al., *Autophagy promotes paclitaxel resistance of cervical cancer cells: involvement of Warburg effect activated hypoxia-induced factor 1-alpha-mediated signaling.* Cell Death Dis, 2014. **5**: p. e1367.
177. Bhattacharya, B., et al., *Increased drug resistance is associated with reduced glucose levels and an enhanced glycolysis phenotype.* Br J Pharmacol, 2014. **171**(13): p. 3255-67.
178. Liberti, M.V. and J.W. Locasale, *The Warburg Effect: How Does it Benefit Cancer Cells?* Trends Biochem Sci, 2016. **41**(3): p. 211-218.
179. TeSlaa, T. and M.A. Teitell, *Techniques to monitor glycolysis.* Methods Enzymol, 2014. **542**: p. 91-114.
180. Anderson, M., et al., *Hexokinase 2 promotes tumor growth and metastasis by regulating lactate production in pancreatic cancer.* Oncotarget, 2017. **8**(34): p. 56081-56094.
181. Wolf, A., et al., *Hexokinase 2 is a key mediator of aerobic glycolysis and promotes tumor growth in human glioblastoma multiforme.* J Exp Med, 2011. **208**(2): p. 313-26.
182. Patra, K.C., et al., *Hexokinase 2 is required for tumor initiation and maintenance and its systemic deletion is therapeutic in mouse models of cancer.* Cancer Cell, 2013. **24**(2): p. 213-228.
183. Pastorino, J.G., N. Shulga, and J.B. Hoek, *Mitochondrial binding of hexokinase II inhibits Bax-induced cytochrome c release and apoptosis.* J Biol Chem, 2002. **277**(9): p. 7610-8.
184. Pastorino, J.G., J.B. Hoek, and N. Shulga, *Activation of glycogen synthase kinase 3beta disrupts the binding of hexokinase II to mitochondria by phosphorylating voltage-dependent anion channel and potentiates chemotherapy-induced cytotoxicity.* Cancer Res, 2005. **65**(22): p. 10545-54.

185. Cascone, T., et al., *Increased Tumor Glycolysis Characterizes Immune Resistance to Adoptive T Cell Therapy.* Cell Metab, 2018. **27**(5): p. 977-987 e4.
186. Roberts, D.J., et al., *Hexokinase-II positively regulates glucose starvation-induced autophagy through TORC1 inhibition.* Mol Cell, 2014. **53**(4): p. 521-33.
187. Yao, G.D., et al., *Blocking the utilization of glucose induces the switch from senescence to apoptosis in pseudolaric acid B-treated human lung cancer cells in vitro.* Acta Pharmacol Sin, 2017. **38**(10): p. 1401-1411.
188. Fridman, W.H., et al., *The immune contexture in cancer prognosis and treatment.* Nat Rev Clin Oncol, 2017. **14**(12): p. 717-734.
189. Song, X., et al., *Differential effects of IL-1 alpha and IL-1 beta on tumorigenicity patterns and invasiveness.* J Immunol, 2003. **171**(12): p. 6448-56.
190. Ruffell, B., N.I. Affara, and L.M. Coussens, *Differential macrophage programming in the tumor microenvironment.* Trends Immunol, 2012. **33**(3): p. 119-26.
191. Kuilman, T. and D.S. Peeper, *Senescence-messaging secretome: SMS-ing cellular stress.* Nat Rev Cancer, 2009. **9**(2): p. 81-94.
192. Canta, A., E. Pozzi, and V.A. Carozzi, *Mitochondrial Dysfunction in Chemotherapy-Induced Peripheral Neuropathy (CIPN).* Toxics, 2015. **3**(2): p. 198-223.
193. Zhao, B., et al., *Mitochondrial dysfunction activates the AMPK signaling and autophagy to promote cell survival.* Genes Dis, 2016. **3**(1): p. 82-87.
194. Dumontet, C. and M.A. Jordan, *Microtubule-binding agents: a dynamic field of cancer therapeutics.* Nat Rev Drug Discov, 2010. **9**(10): p. 790-803.